MODELLING THE EFFECTS OF HALF CIRCULAR COMPLIANT LEGS ON THE KINEMATICS AND DYNAMICS OF A LEGGED ROBOT

A THESIS SUBMITTED TO
THE GRADUATE SCHOOL OF NATURAL AND APPLIED SCIENCES
OF
MIDDLE EAST TECHNICAL UNIVERSITY

BY

EGE SAYGINER

IN PARTIAL FULFILLMENT OF THE REQUIREMENTS
FOR
THE DEGREE OF MASTER OF SCIENCE
IN
ELECTRICAL AND ELECTRONICS ENGINEERING

MAY 2010

Approval of the thesis:

MODELLING THE EFFECTS OF HALF CIRCULAR COMPLIANT LEGS ON THE KINEMATICS AND DYNAMICS OF A LEGGED ROBOT

submitted by **EGE SAYGINER** in partial fulfillment of the requirements for the degree of **Master of Science in Electrical and Electronics Engineering Department, Middle East Technical University** by,

Prof. Dr. Canan Özgen
Dean, Graduate School of **Natural and Applied Sciences** _____

Prof. Dr. Ismet Erkmen
Head of Department, **Electrical and Electronics Engineering** _____

Assist. Prof. Dr. Afşar Saranlı
Supervisor, **Electrical and Electronics Engineering Dept., METU** _____

Assist. Prof. Dr. Yiğit Yazıcıoğlu
Co-supervisor, **Mechanical Engineering Dept., METU** _____

Examining Committee Members:

Prof. Dr. Kemal Leblebicioğlu
Electrical and Electronics Engineering Dept., METU _____

Assist. Prof. Dr. Afşar Saranlı
Electrical and Electronics Engineering Dept., METU _____

Prof. Dr. Aydan Erkmen
Electrical and Electronics Engineering Dept., METU _____

Assist. Prof. Dr. Gökhan Özgen
Mechanical Engineering Dept., METU _____

Assist. Prof. Dr. Çağatay Candan
Electrical and Electronics Engineering Dept., METU _____

Date: _____

I hereby declare that all information in this document has been obtained and presented in accordance with academic rules and ethical conduct. I also declare that, as required by these rules and conduct, I have fully cited and referenced all material and results that are not original to this work.

Name, Last Name: Ege Saygıner

Signature :

ABSTRACT

MODELLING THE EFFECTS OF HALF CIRCULAR COMPLIANT LEGS ON THE KINEMATICS AND DYNAMICS OF A LEGGED ROBOT

Saygıner, Ege
M.Sc., Department of Electrical and Electronics Engineering
Supervisor : Assist. Prof. Dr. Afşar Saranlı
Co-Supervisor : Assist. Prof. Dr. Yiğit Yazıcıoğlu

May 2010, 95 pages

RHex is an autonomous hexapedal robot capable of locomotion on rough terrain. Up to now, most modelling and simulation efforts on RHex were based on the linear leg assumption. These models disregarded what might be seen as the most characteristic feature of the latest iterations of this robot: the half circular legs. This thesis focuses on developing a more realistic model for this specially shaped compliant leg and studying its effects on the kinematics and dynamics of the resulting platform.

One important consequence of the half circular compliant leg is the resulting rolling motion. Due to rolling, the rest length of the leg changes and the leg-ground contact point moves. Another consequence is the varying stiffness of the legs due to the changing rest length. These effect the resulting behaviour of any platform using these legs. In the first part of the thesis we are studying the effects of the half circular leg morphology on the kinematics of RHex using a simple planar model. The rest of the studies within the scope of this thesis focuses on the effect of the half circular compliant legs on the dynamics of a single legged hopping platform with a point mass.

The formulation derived in this work is successfully integrated in a readily working but rather simple model of a single legged hopping system. We replace the equations of the straight leg in this model by the equations of the half circular compliant leg. Realistic results are obtained in the simulations and these results are compared to those obtained by the simpler constant stiffness straight leg model. This more realistic leg model brings us the opportunity to further study the effects of this leg morphology, in particular the positive effects of the resulting rolling motion on platform stability.

Keywords: Legged Robots, RHex, Half Circular Compliant Leg, Kinematic Modelling, SLIP

ÖZ

YARIM DAİRESEL ESNEK BACAKLARIN BACAKLI ROBOTLARIN KİNEMATİĞİ VE DİNAMİĞİ ÜZERİNE ETKİLERİNİN MODELLENMESİ

Saygıner, Ege
Yüksek Lisans, Elektrik ve Elektronik Mühendisliği Bölümü
Tez Yöneticisi : Yrd. Doç. Dr. Afşar Saranlı
Ortak Tez Yöneticisi : Yrd. Doç. Dr. Yiğit Yazıcıoğlu

Mayıs 2010, 95 sayfa

RHex, engebeli arazide hareket yeteneğine sahip altı bacaklı otonom bir robottur. Bugüne kadar RHex ile ilgili yapılmış olan modelleme ve simülasyon çalışmalarının çoğu düz bacak varsayımı üzerine kuruludur. Bu modeller, geliştirilmekte olan robotun en belirleyici özelliklerinden biri olan yarım dairesel bacakları gözardı eder. Bu tez, yarım dairesel esnek bacaklar için daha gerçekçi bir model geliştirmeye ve bu özel şekilli bacakların, ortaya çıkan robotik platformun kinematiği ve dinamiği üzerine etkilerini incelemeye odaklanır.

Yarım dairesel esnek bacak kullanılmasının önemli bir sonucu, ortaya çıkan yuvarlanma hareketidir. Yuvarlanmaya bağlı olarak, bacağın serbest haldeki uzunluğu değişir ve bacağın yere temas noktası yer değiştirir. Bir başka sonuç ise bacağın serbet haldeki uzunluğunun fonksiyonu olarak değişen esnekliğidir. Bunlar, yarım dairesel esnek bacakların kullanıldığı robotik platformların davranışını etkiler. Tezin ilk kısmında bu bacak şeklinin RHex'in kinematiği üzerine etkileri, basit düzlemsel bir model üzerinde incelenmektedir. Tezin sonraki kısımlarında ise bacağın değişken

esnekliğinin noktasal kütleli, tek bacaklı, zıplayan bir robotik platformun dinamiği üzerine etkileri incelenmektedir.

Bu çalışmada çıkarılan formüller, tek bacaklı zıplayan bir sistemin halihazırda çalışan, görece basit bir modeline başarıyla entegre edilmiştir. Bu modeldeki düz bacağa ait denklemler, yarım dairesel esnek bacağın denklemleri ile değiştirilmiştir. Simülasyonlarda gerçekçi sonuçlar elde edilmiş ve bu sonuçlar, görece daha basit olan sabit esneklikli düz bacak modelinin sonuçları ile karşılaştırılmıştır. Bu görece gerçekçi model, başta yuvarlanma hareketinin robotik platformun dengesine olumlu etkileri olmak üzere, bacak şeklinin etkilerinin daha ayrıntılı incelenmesine olanak tanır.

Anahtar Kelimeler: Bacaklı Robotlar, RHex, Yarım Dairesel Esnek Bacak, Kinematik Modelleme, SLIP

ACKNOWLEDGMENTS

I would like to thank my advisor Assist. Prof. Dr. Afşar Saranlı and my co-advisor Assist. Prof. Dr. Yiğit Yazıcıoğlu for their guidance throughout the whole three years of work. Their support and motivation was priceless. I would like to thank Assist. Prof. Dr. Uluç Saranlı who shared his valuable experience and ideas. I would like to thank Tülay Akbey and Yasemin Özkan Aydın for their friendly cooperation, collaboration and valuable support, and to Mert Ankaralı for his contributions. The SensoRHex research group in the direction of Assist. Prof. Dr. Afşar Saranlı and METU-ROLAB (Middle East Technical University Robotics and Autonomous Systems Laboratory) supplied an appropriate environment for realising this study.

TABLE OF CONTENTS

LIST OF TABLES

TABLES

LIST OF FIGURES

FIGURES

CHAPTER 1

INTRODUCTION

The interest in robotics started accelerating when man realized that the robot can replace himself in any kind of task that he does not have time, strength or courage to do. Since then, we have been designing and building a wide range of robots: from industrial robots which can do complex and repetitive tasks very fast to humanoids which can walk and talk. Maximizing the performance, power efficiency and automation in robotic systems have been the goal in many robotics studies. This is why animal locomotion is an interesting and valuable research topic for robotics.

We have been observing animals and also our own bodies in order to understand the dynamics of motion in natural mechanisms. Many researches are based on building mechanisms that operate just like the animals in nature, but this method mostly suffers from complexity. Building robots that is functionally similar to the natural mechanisms but mechanically simpler is the goal of many robotic studies now.

One example of the biologically inspired robots [1] is RHex which is designed to achieve mobility together with mechanical simplicity [2]. It is a hexapedal, autonomous mobile robot. It has six legs, each of which has one degree of freedom, and a rigid body about the size of a shoe box. RHex project has been continuing since 2001 by many research groups. The latest versions of RHex have half circular compliant legs. The compliance of the legs has an affect on the energy efficiency of the platform. Together with the half circularity of the legs, different kinematic and dynamic effects are introduced to the system.

This thesis focuses on modelling the half circular compliant legs of RHex. The effects of half circularity and compliance are implemented on a leg model in a MATLAB

simulation environment. The spring-like behaviour of the legs are studied, and a new leg model is introduced.

1.1 Motivation

Being energy efficient and mechanically simple is a great advantage in comparison of robots which serve the same purpose. Among the mobile robots that have been developed up to now, the hexapedal mobile robot RHex is distinguished with its outstanding performance in this comparison.

Modelling the half circular compliant legs of RHex is the main focus of this thesis. We are mainly motivated by the positive effects of rolling and compliance on dynamics of legged locomotion. We wanted to study this special leg geometry and its consequences on a realistic model in a MATLAB simulation environment.

The half circular leg which is the focus of this thesis contributes to the whole hexapedal system in many different ways. It has interesting dynamic behaviour, which can be used for the favour of efficiency and stability of locomotion [3] [4]. The compliance give the legs an additional degree of freedom and supplies a potential energy storage, and contributes to the power efficiency of the whole system in fast locomotion [5].

Although the half circular compliant legs have been used on RHex for some time, the modelling and simulation efforts regarding RHex have been assuming straight legs. Modelling the half circular compliant legs as straight legs with constant stiffness, linear springs is a rough approximation since the effects of half circularity are disregarded. The most fundamental result of half circularity is the rolling of the leg on the ground. Due to rolling, the leg-ground contact point moves. Secondly, the distance of the hip point from the leg-ground contact point changes due to rolling, in addition to the effect of compression. This means the effective length of the leg changes. And this results in the varying stiffness of the leg during motion. These effects cannot be modelled unless the true leg geometry is taken into account. The main contribution of this thesis is modelling the half circular compliant legs of RHex more accurately than the existing models.

1.2 The Scope of the Thesis

The following chapter presents the literature survey where detailed background information on RHex can be found. The chapter includes research about legged locomotion, biologically inspired robots, and modelling studies regarding legged mobile robots and RHex.

In Chapter 3, a planar kinematic model of RHex is presented. In this kinematic model, RHex is modelled as a two half circular legged planar robot. The aim of that model is to see the effects of the leg shape on the kinematics of the platform. In that chapter, the effects of compliance are disregarded for the sake of simplicity. Only the effects of half circularity are focused on. The kinematic relations derived in this chapter will be a basis for the following dynamic analysis chapters.

In Chapter 4, the simulation of the hybrid dynamic systems are explained. The spring loaded inverted pendulum (SLIP) model is introduced. Most importantly, the simulation environment that is used for testing our new leg model is introduced. This simulation environment was prepared for modelling the behaviour of a single linear legged hopping system before. The straight leg model is also explained and some example simulations with the linear leg are shown in this chapter.

In Chapter 5, the stiffness analysis of the half circular legs is presented. The force-deflection relation of the half circular compliant leg is derived using the Castigliano's Theorem. This derivation leads to an important contribution of this thesis: the leg stiffness as a function of the leg angle. This stiffness function will be replaced with the constant stiffness value in the previous straight legged model, in Chapter 6.

In Chapter 6, the new half circular compliant leg model introduced in Chapter 5 is verified on single legged planar robot simulations. The simulation environment used here is the same simulation environment as that of the previous straight-legged model, which was presented in Chapter 4. The simulation results with the half circular leg model are presented and discussed in this chapter.

The last chapter is the conclusion chapter.

CHAPTER 2

LITERATURE SURVEY

Legged robotics have become a wide and fruitful research area in the last decades. Among the other types of locomotion, legged locomotion is outstanding with many advantages. The nature also proves this fact, by having evolved legged systems which inspire us to adapt to our own mobile platforms. The type and number of legs in a robotic system is determined by the purpose of the robotic platform, and surface conditions. Most of the time, we encounter problems of optimizing variables like speed, power consumption, control complexity, weight and maneuverability. We design the system such that we obtain a suitable combination of these values according to the purpose of our platform.

Modelling and simulating these mobile platforms is also of great importance, in the sense that it supplies the necessary theoretical information of what we are physically building, and help foreseeing the relation between the system parameters and the observed behaviour without the need to do the experiments with the physical platform since those experiments are not always available and they are sometimes even risky.

2.1 Legged Locomotion

The wheel is the oldest and simplest solution found for man-made mobile platforms. Wheeled locomotion can be fast and energy efficient on flat and known surfaces. A wheel is usually driven by a motor if it is an actuated wheel and control of wheeled platforms is a simpler problem compared to the control of legged platforms. However in most of the areas where wheels are used, the surface is prepared for the wheel

like indoor surfaces, roads or rail roads. The outdoor surfaces suitable for wheels is limited. Wheels lack performance on rough terrain, where there are holes, rocks, or loose ground such as sand, as the case in a natural terrain [1].

Tracked locomotion can be a solution in the rough and loose ground where wheels are not useful. Tracked systems are powerful and competent in rough terrain, but they are heavy and they have high power consumption due to the large frictional forces between the palettes and the ground [6].

Legged robots stand out among the others with many advantages among the other types of locomotion. They can be successful on any kind of surface, in any environment, including the ones in which wheeled and tracked systems are used. One advantage is the ability to move on a wide range of surface types. They are much better in handling uneven terrain conditions, compared to wheeled or tracked systems [7], and they are capable of behaviours like running, jumping, and flipping which the others cannot achieve. This gives them dexterity and capability of a wide range of tasks. Additionally, the legs can be functional for purposes other than locomotion, like sensing the environment, or even pushing the obstacles away.

When we mention legged systems, we can talk about different kinds of gaits [7], [8], [9]. Number of legs, the shape of the legs, number of actuators per leg and types of actuation of the legs are the features of a robotic platform that determine its capabilities and the applicable gaits. Walking [10] [11] [12], running [13], [3], inclined surface climbing [14] [15], stair climbing [16] [17] [18], galloping [19], trotting [20] [21] and bounding [22] [23], are among the many types of gaits that the legged robots can achieve.

Gaits can be analysed under two main categories, statically stable gaits and dynamically stable gaits. In statically stable gaits, the mobile platform is in static equilibrium at every time instant. However in a dynamic gait the platform can lose the static equilibrium, that is the projection of center of mass of the platform on the horizontal plane can be outside the area enclosed by the leg-ground contact points [24], [25], [11]. As there are more legs on a mobile platform, it is easier to obtain statically stable gaits. For example, alternating tripod walking of a hexapedal robot is a quite stable gait, since there always at least three legs in contact with the ground and the center of

mass of the body is always above the triangle formed by the contact points. Genghis, a six legged autonomous walking robot performs statically stable gaits [26], where a passive walker is a good example to systems performing dynamic gaits [24]. A passive walker is a bipedal robot that can walk down a small slope without any actuation, by the as a consequence of its dynamics. RHex, which is the subject to modelling studies in this thesis, is a hexapedal mobile robot that can achieve both statically stable and dynamically stable gaits successfully on rough terrain [2].

We also encounter examples of hybrid locomotion systems in the literature. In [27], a system with both wheels and legs is presented, as an attempt to combine the ability to walk through rough terrain by using the legs and fast locomotion with wheels, when necessary. In [28], suction elements are incorporated to a tracked system, in order to have climbing ability. In [29], articulated mobility mechanisms are used in addition to wheels, in order to achieve self-righting which a wheeled system is not capable of. However, having different types of locomotion mechanisms on a single platform increases the mechanical complexity as well as control complexity. Being successful on more kinds of surfaces and being able to do many more different tasks is desirable however they come hand in hand with more actuation, more weight and more energy consumption, in addition to control and computational difficulties.

2.2 Biologically Inspired Robots

Biologically inspired robots are mostly legged robots, since leg is used by most of the land animals for locomotion. We do not see any wheeled or tracked animals, so obviously the legged systems are "chosen" by the nature to be the most successful locomotion type on land, in terms of speed, energy efficiency and design simplicity. Frogs, cockroaches, spiders, humans, cheetahs, horses and many others are among the fast and power efficient natural mechanisms that we know. All of them has different mechanisms, in terms of leg morphology, number of legs, and other leg parameters like compliance, and each of them is useful in a particular environment and surface condition. Biomechanical studies plays an important role in the field of legged robotics, since they help us understand how the nature solved the problem of locomotion [30] [31] [32] [33] [34] [35]. Gait analysis studies are an important part of the biomechanical

studies. To understand the dynamics of different gaits, there has been studies on humans [36] [37] [38] as well as animals [39] [40] [41] [42] [43] [44].

When the animals are observed during running which is a fully dynamic gait, it is found that the center of mass of the body follows a familiar trajectory: it acts like a spring loaded inverted pendulum (SLIP) [1] [45]. This implies that the animals and humans try to coordinate their muscles so as to obtain an energy efficient dynamic behaviour. The muscle coordination is done such that the muscles act like springs during locomotion and this is found to be serving the fundamental principle dynamic locomotion of animals: conservation of energy [46] [41]. Moreover, the corresponding spring constant of the legs is changed in order to gain adaptability to different types of surfaces [47] and to different speeds. There is biological evidence on the effect of compliance control on speed and performance [48] [49] [50].

Another important feature of the walking and running mechanisms is the curved feet, and the resulting rolling motion of the feet. A certain amount of curvature of foot increases the stability and energy efficiency of walking [10] [4]. In [51] it is shown that the rolling motion of the human feet has considerable effect on the energy efficiency of motion.

As understood from the biomechanical studies, nature has found its own solutions for fast and power efficient locomotion of mobile and autonomous systems on different terrain conditions. Being inspired of this, the field of legged robotics has learned and adapted a lot from the nature. We see examples of animals being inspiration to many robotics studies in the literature [1], [35] [52] [53] [54] [55] [56]. Some robotics studies try to mimic the nature and try to make robots that operate exactly like animals. Even artificial muscles have been built [57] [58] and implemented on robotic platforms [59] [60]. Some other studies are focused on designing systems that are functionally compatible with animals and humans in locomotion, but they do not need to be mechanically similar. This is advantageous for mechanical simplicity of the robot designs [61]. Observing nature, scientists have already learned that compliance of the legs have great effect on stability of the gaits, energy efficiency and speed so they have implemented compliance and observed improvements on the robotic platforms they have built [62] [63] [64] [65] [50]. Furthermore, it is observed that curved feet contribute

to stability and energy efficiency of the mobile platforms [4] [66]. So robots with rolling feet have also been designed and built and this contribution is verified on these robotic platforms [3] [10]. Even the ankle is implemented on some robotic systems, in order to achieve stronger stability [5] [67] [68] [10]. Eventually it is seen that as we try to improve the design, we get closer to the natural mechanisms and mechanical complexity increases. So we always have to compromise between mechanical simplicity and performance.

Each robotic platform has its own goal which determine the important features of the design. The goal can be moving on rough terrain, going up and down the stairs, going as fast as possible on a certain type of surface, or being able to walk through various sized obstacles. For example Rise [69] [15] is a biologically inspired hexapedal robot designed for climbing. Having two actuators per leg, it can climb up and down various types of surfaces without using suction elements or magnets in order to create adhesion or shear forces. The aim of the robot is being strong, rather than being fast. One of the most famous quadrupedal robot designs is Scout [14], which has compliant legs and can achieve dynamically stable gaits. Scout is capable of walking [70], running [63], bounding [71], trotting [21], and step climbing [17].

In reaching maximum speeds (body length/second) with maximized dexterity and robustness, six legged systems are found to be quite successful. On the other hand, many types of gaits can be applied to hexapedal systems [1]. Having six legs is advantageous in terms of being able to achieve both statically stable and dynamically stable gaits. RHex is an example to hexapedal robots, being capable of many types of gaits like walking, running [13], bounding [22], pronking [72], stair climbing [18], etc.

Being able to achieve different types of gaits give the adaptability to different types of terrains. And this brings the problem of gait transitions during locomotion. This is an important problem in legged robots, and studied on different robotic platforms [20] [73] [9].

Leg number and the leg structure plays an important role in the performance of the robotic systems mentioned above. Obviously the complexity of the system increases as the number of legs and the number of joints per leg increases. Each additional degree of freedom (DOF) inevitably brings complexity, calculation inaccuracy, and

possible source of failure to the system. From this perspective, imitating the nature in designing articulated robotic legs may not be the best solution to a legged robot locomotion problem.

The half circular compliant leg is the most characteristic feature of the hexapedal robotic platform RHex, since it is very simple and light, actuated with only one motor, and contributing the energy efficiency of the whole platform with its compliant nature resulting from both its material and geometry. The legs of RHex are attached to the body with one revolute joint, driven by a brushless DC motor and each leg is individually controlled. This gives the capability of many different gaits to RHex and 1-DOF legs make it easier to handle the gait control problems. Also, the advantages of compliance [74] and half circular feet [18] contribute to the dynamic stability of RHex's locomotion. In a recent study, a tunable stiffness leg is presented for RHex [75] and the effects of variable stiffness on the dynamic stability of RHex is shown in [76].

2.3 Modelling and Simulation Studies for Legged Robots

Observing the nature gives an idea about how animals and humans achieve dynamic locomotion. The experiments and measurements made with animals and humans are valuable in the sense that they show how physical laws act during the dynamic motion of a natural legged platform. For example in [77] the galloping gait of a horse is analysed and it is discussed under which circumstances a robot will achieve a similar behavior. In [35] dynamic motion of animals, especially insects are analysed and formulated. In [78] a mathematical model of the human body is presented and used for calculating the center of mass, the moment and moment of inertia of the body in different positions. In [79] dynamics of human gait is investigated in different gaits. A detailed kinematic and dynamic analysis of the human body is presented. In [80] very complex mechanisms with many DOF's like animals or humans are examined and the dynamics of these mobile systems are reduced to simpler templates and anchors which are a little more detailed than templates. The use of these templates and anchors in modelling studies are explained.

In most of the modelling studies of dynamic motion of mobile platforms we encounter

spring-mass models [1] [81]. Not only the natural dynamic motion of animals and humans, but also that of compliant legged mobile robots fit this model. SLIP models are successful in explaining dynamically stable and periodic gaits in two dimensions [82] [83]. In [84], three SLIP inspired models of three dynamic systems are studied. In [85] we see examples of dynamic simulations of legged robots, where the equations of motion are derived from the physical model and solved for the simulation of running motion. Dynamic simulations are useful for foreseeing the effects of certain system parameters on the resulting motion. And they can also be used to solve real life problems, for example the design of a gait controller [86] [87].

It is not easy to model a complex system successfully without making simplifications and approximations. More realistic models have less simplifications and approximations but they have more computational complexity. Both simple and realistic models are desirable [86]. The assumptions and approximations should be made carefully. For example in [88] the effect of leg mass on the models of running gaits in biological and robotic systems is investigated and although it is common to neglect the leg mass, it is found to be important in certain gaits. Modelling the leg-ground contacts as point contact in dynamically stable legged systems is also a very common approximation. However the bigger contact area and rolling motion of the feet were shown in some studies as in [4].

There has been studies for modelling the half circular compliant legged system RHex before: In [89] the leg is modeled as rigid rods, and this model was sufficient to analyse and control the flipping behaviour of RHex. In [90] this model was extended by taking the coulomb fricton forces at the contact points into account. In [2], the legs are modelled as linear springs. In [91], SLIP behaviour is observed in the dynamic motion of RHex. In [92] the bipedal SLIP template is introduced, and the model with one point mass and two linear spring legs is presented. In [93], a kinematic model of planar RHex was presented, taking the half circularity of the legs into account but assuming rigid legs. In a recent study [94] the leg is modelled as a hybrid mechanism composed of a rigid part and a curved part, connected by a torsional spring.

2.4 Relevance of the Literature to the Subject of This Thesis and More on RHex

The aim of this thesis is to model the effects of half circular leg geometry and also compliance of the legs, on kinematic and dynamic behaviour of the six legged platform SensoRHex. The SensoRHex project, as a new iteration of RHex, has been continuing with the collaboration of Middle East Technical University and Bilkent University, being funded by TUBITAK since 2006. In addition to improving the design and building the new hexapedal platform, modelling and simulation studies are also going on in the scope of this project.

A hexapedal robot is a convenient platform for studying and analysing both kinematics of the platform and dynamics of locomotion, since various statically stable and dynamically stable gaits are applicable [13] [22] [72] [18]. The effect of compliance on the dynamics of RHex have been shown in [91]. The effect of variable leg stiffness on the dynamics of RHex have been shown in [76] and it is proven that by tuning the stiffness, we can improve the performance of RHex.

The half circular compliant leg is found to be the most successful one [18] among the other leg iterations [13] [2]. Their performance is due to not only mechanical simplicity, ease of control and light weight but also contribution to energy efficient and stable locomotion, owing to their compliant nature. The compliant legs of RHex were usually modelled as linear springs in the previous modelling studies of RHex. In fact, curvature and rolling motion of the feet, which were neglected in the previous leg models contribute to energy efficiency and stability [4] [3]. The half circular geometry has an important effect on the compliance of the legs as well.

Being motivated by all these previous studies regarding the hexapedal robotic platform RHex, the aim of this thesis is to come up with a more accurate leg model, and go into the details of the kinematics and dynamics of motion with the new leg model. We think that the half circular compliant legs of RHex play an important role on RHex's performance and they should be modelled as accurately as possible in order to be understood better. A leg model taking both the geometry and variable compliance into account will help the dynamic behaviour of the whole platform be analysed more

successfully and this can even lead to different or improved leg designs, according to the needs of the future robotic platforms that will be built using compliant legs.

CHAPTER 3

A PLANAR KINEMATIC MODEL OF RHEX WITH HALF CIRCULAR LEGS

Understanding the kinematics of a system is essential for understanding the dynamics of the system. The physical system is firstly conceptualized in the kinematic analysis therefore it is not possible to do dynamic analysis, work on control strategies, or design improvements of a physical system without doing an appropriate kinematic analysis. Assumptions and approximations made in the kinematic analysis set the basis for the following dynamic analysis part of the research, therefore it is very important to set a strong basis of kinematics before any kind of further calculation.

The kinematic model presented in this chapter is the first step towards the ultimate goal of obtaining a full dynamic model of the RHex platform. In the previous modelling studies related to RHex, the kinematics of the system was over simplified. The legs were assumed to be linear and have constant length. As a result, effects of rolling motion in stance phase was ignored. The motivation of the study presented in this chapter is the need to develop a new planar kinematic model for RHex considering a more accurate leg shape and its effects on the system.

In the analysis presented in this chapter, the focus of attention will be on the rolling motion and its results on the two legged planar model. The "standing up behaviour", which can be defined as raising the body from the ground to a higher position only by rotating the legs, is observed. In this behaviour, both of the legs are in contact with the ground and the body is always in static equilibrium. The governing kinematic equations will be used to solve an example task problem.

In the following sections, the model assumptions and approximations will be presented. Then the system variables will be introduced and the geometric relations between them will be explained. Then the governing kinematic equation sets will be derived from them. These kinematic equations will be solved using MATLAB in order to solve the kinematics of a given system with two half circular rigid legs. At the end of this chapter, the model will be illustrated using an animation prepared in MATLAB, with an example problem.

3.1 Model Assumptions

First of all, for the model presented here is a planar model, like the models that will be presented later in this thesis. This means we are ignoring the lateral components of the forces. The system is assumed to be symmetric about the sagittal plane. Therefore, a leg pair which is symmetric about the sagittal plane in the real hexapedal platform is represented by a single leg in this model.

Secondly, only for this chapter the legs are assumed to be rigid. The compliance of the legs, deflection due to compliance and all kinds of dynamic effects will be ignored. In this chapter we are aiming to see the effects of the half circularity on the kinematics of the platform. Therefore first we wanted to separate it from the compliance effect, and observe the effect of rolling motion only. When the leg is rolling on the ground, the effective leg length (the distance between the hip point and the leg-ground contact point) changes only due to rolling. The effect of compliance will be introduced from the following chapter on.

The system is in static equilibrium all the time. The two legs are always in contact with the ground, that is, they are in "stance" phase. The standing up behaviour can be done only with this condition. In the standing up behaviour, the legs are rotated when both of them are touching the ground, and with the effect of rolling, the effective leg lengths change. Therefore it is possible to move the body center of mass up or down by rotating the legs only.

The leg shape is assumed to be a perfect half circle all the time, although in the real case due to the compliant nature the leg shape might change. In this model and in

the rest of the thesis, the leg radius is assumed to be the same at every point on the leg.

The legs are perfect half circles and the ground is a horizontal line, so the leg-ground contact is approximated as a point contact. The rolling is without slippage, so the system is a one degree of freedom system, when both legs are on the ground (double stance phase). This means in double stance phase, if we change a single variable and if we know the amount of change, it is possible to calculate the change in the rest of the variables that define the system.

3.2 Kinematic Formulation

In this section, a two dimensional kinematic analysis of the RHex platform is presented. The kinematic model presented here is shown to be useful not only as a basis for the dynamic analysis, but also independently useful in an example task behaviour.

Second important assumption made is the sagittal symmetry of the platform and behaviour modelled in this study. If the robotic platform is moving on a flat surface doing a sagittal plane symmetric motion, and if the yaw and roll angles are not of interest, then the presented two dimensional model is sufficient for the current analysis. Assuming the robot is symmetric with respect to the sagittal plane, the model developed is in 2-D.

Understanding the geometric relations and variables regarding a single leg is essential before constructing the kinematic model so this will be the topic of the following subsection.

3.2.1 Geometric Relations Regarding a Single Half Circular Leg

The last and most successful iteration of leg shapes was found to be the half circular leg for RHex. The leg is attached to the body from one end of the half circle and is rotated by a brushless DC motor, about an axis perpendicular to plane of the half circle. In a standard walking or running gait, each of the six legs make full rotations without changing direction, so that the robot can move forward on the ground smoothly.

Smoothly here means keeping the body height and forward velocity within certain intervals. This is only one of the advantages of the half circular leg geometry.

In some instances the legs are rotated in only a limited angular span. Standing up behaviour is such an example and it is defined as changing the state of the robotic platform from a state in which the body is lying on the ground, to a state in which it is standing up on the legs. It will be seen later in this chapter that the standing up behaviour is a very good illustration for another functional advantage of the half circular legs and also for the presented kinematic analysis.

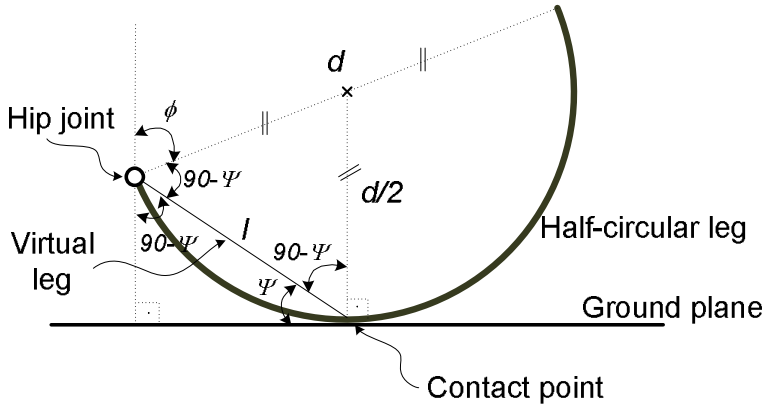

Figure 3.1: The half circular leg and the related variables for the kinematic analysis

The half circular leg and the variables related to the leg are shown in Figure 3.1. We can fully define a circle with two points and the radius. Therefore the hip point, the contact point and the leg radius are a good combination of variables that need to be known in order to be able to draw the half circular leg. The hip point is where the leg is attached to the body, and the contact point is where the leg touches the ground. These variables can obviously be replaced with another combination of independent variables which are related to the original combination geometrically. Another way we can draw it is if we know the hip point coordinates and the angular position of the leg, knowing that it is in contact with the ground which means it is tangent to the horizontal axis.

Among the variables regarding the leg, we are mostly interested in l, which is the effective leg length. It is the length of the virtual line drawn from the hip point to

the leg-ground contact point. The hip point is a common point on the body and the leg. So we can calculate its position at any time if we know the body position and orientation. However, due to rolling, the contact point is not attached to anywhere. It is an instantaneous point, defined by the tangent of the horizontal ground line to the leg at any instant. So the contact point moves along the ground during the rolling motion in stance.

In the previous models of RHex, this line was assumed to be the linear and constant length spring which represents the leg. In those models, this line was attached to the ground with a revolute joint in stance phase so the contact point was a point fixed to the ground during the whole stance phase. In this study this line is called "the virtual leg" and neither the length of this line nor the horizontal component of the position of contact point is constant during rolling. The length of the virtual leg is:

$$l = d \cdot \sin(\psi) = d \cdot \sin(\phi/2) \tag{3.1}$$

where d is the diameter of the leg and ϕ is the leg angle with respect to the ground, measured from a vertical line fixed at the hip.

The virtual leg angle ψ is defined as the angle of the virtual leg with respect to the ground, measured from the horizontal axis and again from the geometric relations ψ is related to ϕ simply as:

$$\psi = \phi/2 \tag{3.2}$$

As the leg rolls, the effective arc length, which is the length of the arc beginning from the hip until the leg-ground contact point also changes. This length is instantaneously equal to

$$l_{arc} = \phi \cdot r. \tag{3.3}$$

where r is the leg radius.

The amount of change in the horizontal position of the contact point during rolling in

a time interval Δt in stance phase is equal to the difference between the effective arc lengths at the beginning and at the end of that interval. If ϕ_0 is the leg angle with respect to the ground at time t_0 and ϕ_1 is the leg angle with respect to the ground at time t_1, then in the time interval $\Delta t = t_1 - t_0$, the horizontal component of the contact point changes as much as Δl_{arc} :

$$\Delta l_{arc} = \phi_1 \cdot r - \phi_0 \cdot r. \tag{3.4}$$

This concludes the helpful relations within a single leg, that will be used in the next subsection. Before going into the planar kinematic model of RHex, it is important to emphasize that the virtual leg is the core of the leg model presented in this study; because once we find the position of the end points of this line using the kinematic equations, then we do not have to consider the shape of the leg after this point and continue the calculations assuming that the leg is instantaneously equal to this line.

3.2.2 The Planar Kinematic Model of RHex

In this section, the planar model of RHex based on the half circular leg geometry is presented. Under the sagittal symmetry assumption, considering the front and rear leg pairs are in contact with the ground with no slippage, the system is a one degree of freedom system. The two legged planar model together with the variables is shown in Figure 3.2. The kinematic equations of this mechanism can be obtained using the loop closure method. The loop closure method gives two equations in each of the two coordinates in 2-D, and these equations are written in terms of the variables seen in the figure.

When the front and rear leg pairs of RHex are in contact with the ground, regardless of the middle leg pair, the two dimensional view of the system in sagittal plane is a one degree of freedom mechanism in which the four links are the front leg, the body, the rear leg, and the ground. In this case, the middle leg pair is redundant and if it is known that the middle leg pair is also in stance mode, than its position can simply be calculated using basic geometry. In other words, the angular position of the middle leg is dependent on the other variables and not necessarily should be considered as

one of the variables in the equations governing the one degree of freedom system, since the rear and front legs touching the ground fully defines our problem kinematically in the sagittal plane.

This two dimensional and one degree of freedom mechanism has some characteristic features. Namely, the two legs do not have a constant leg length but the leg length is a function of the leg angle as seen in the previous subsection. Also, the leg and the ground pair form a rolling contact pair. Due to the different rolling amounts of the two legs, the length of the ground link also changes. The system at hand has two revolute joints (at the hips), two rolling contact pairs, and four links, three of which do not have a constant length. Therefore, we have a quite complex system with many variables.

In Figure 3.2 and in Table 3.1 all the variables defining our system are shown.

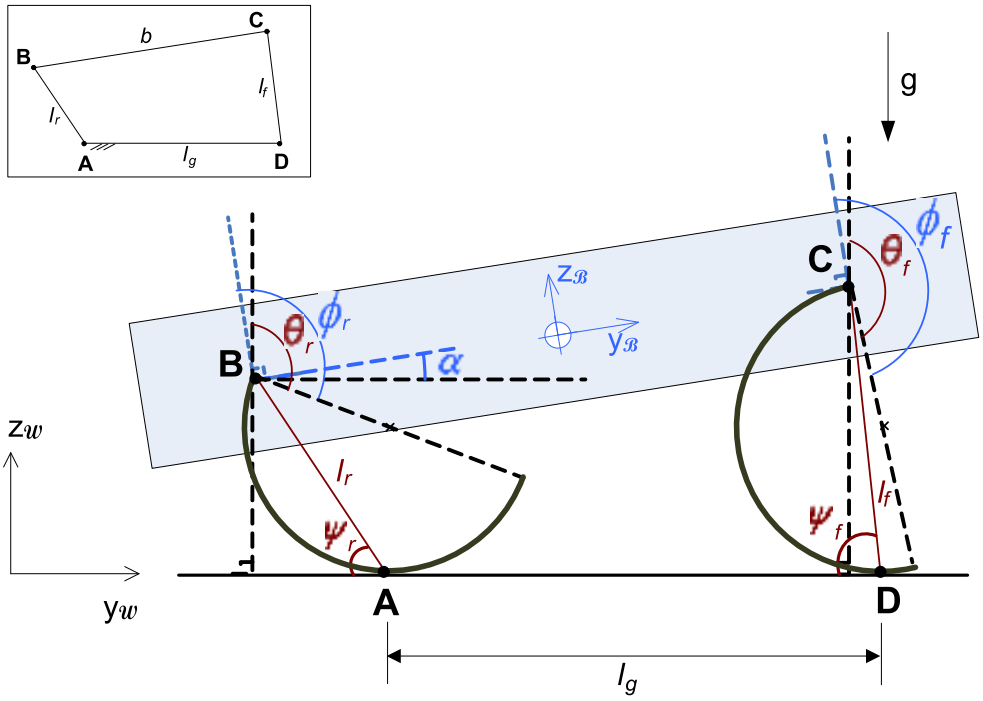

Figure 3.2: The new planar kinematic model developed for RHex. The robot is simplified to a four-link mechanism described by the quadrangle ABCD which is shown on the upper left corner.

With all the variables and their relations in mind, we can write the kinematic equations now.

Table 3.1: The Variables and The Indices Used in the Planar Kinematic Model of RHex

ϕ	Leg angles with respect to $z_{\mathcal{B}}$ in CW direction
θ	Leg angles with respect to $z_{\mathcal{W}}$ in CW direction
ψ	Angle of virtual link with respect to $-y_{\mathcal{W}}$
l_r	Virtual rear link length
l_f	Virtual front link length
l_g	The distance between the rear and front leg-ground contact points
d	Leg diameter
f	As index: Front leg
r	As index: Rear leg
$\mathcal{W}$	World frame
$\mathcal{B}$	Body frame

First of all, the angular position of the leg can be defined by either of the two variables: θ which is the angle of the leg with respect to the ground, measured from the vertical axis, or ϕ which is the angle of the leg with respect to the body, measured from a vertical axis attached to the body at the hip. Given the body angle α, these two can be interchangeable because the relation between these two variables and the body angle is simply:

$$\phi = \theta + \alpha. \tag{3.5}$$

θ, the leg angle with respect to the body is an essential element of the equations since it is the variable that is controlled by the motors. However using the other leg angle ϕ, has the advantage of giving us the angular position with respect to the world coordinates.

So this relation is employed in this mechanism to obtain the two of the kinematic relations, Equation 3.6 and Equation 3.7 for the front leg and for the rear leg, respectively.

$$\phi_{r_0} = \theta_{r_0} + \alpha_0 \tag{3.6}$$

$$\phi_{f_0} = \theta_{f_0} + \alpha_0 \tag{3.7}$$

And also the relation between the leg angle with respect to the ground and the leg angle with respect to the body was known so for each of the two legs we have:

$$\theta_{r_0} = 2\psi_{r_0} \tag{3.8}$$

$$\theta_{f_0} = 2\psi_{f_0} \tag{3.9}$$

The body angle (α) is related to the leg angle (θ_r) and again for the two legs:

$$\phi_{r_0} = \theta_{r_0} + \alpha_0 \tag{3.10}$$

$$\phi_{f_0} = \theta_{f_0} + \alpha_0 \tag{3.11}$$

The loop closure equations in $y-$ and $z-$ directions are the last two equations needed:

$$l_{r_0} \cdot \sin(\psi_{r_0}) + b \cdot \sin(\alpha_0) - l_{f_0} \cdot \sin(\psi_{f_0}) = 0 \tag{3.12}$$

$$l_{r_0} \cdot \cos(\pi - \psi_{r_0}) + b \cdot \cos(\alpha_0) + l_{f_0} \cdot \cos(\psi_{f_0}) = l_{g_0} \tag{3.13}$$

These eight equations are all we can derive from the ten variables that we have defined. This means, if we set any two of the ten variables at the beginning, then we can solve for the whole configuration at the starting instant of the simulation. For example we can set ψ_r and ψ_f, this will fix the initial configuration of the mechanism. Therefore before determining the initial configuration of the mechanism, we have two variables to set, which means the system is 2-DOF but only at the very beginning, while determining the initial configuration.

This is more understandable if we imagine we are holding a two half circular legged system as in Figure 3.2 in the air and suppose we want to put it on the ground. First we can put one of the legs on the ground, and we see that the second leg can be put on the ground not in a single way, but we have another DOF to determine.

Once we set the two initial variables, we can solve for the rest of the ten variables by using this first equation set of eight equations (Equations 3.6-3.13). Now that we have the whole initial configuration solved, the system is one degree of freedom from this

moment on. This means given the initial configuration, by changing only one variable in the system, the other nine variables can be solved for by using another set of nine equations which will be presented soon.

This whole process of determining the initial configuration with two inputs, then consequently having a one degree of freedom system, and solving this one degree of freedom system with a second set of equation is summarized in Figure 3.3.

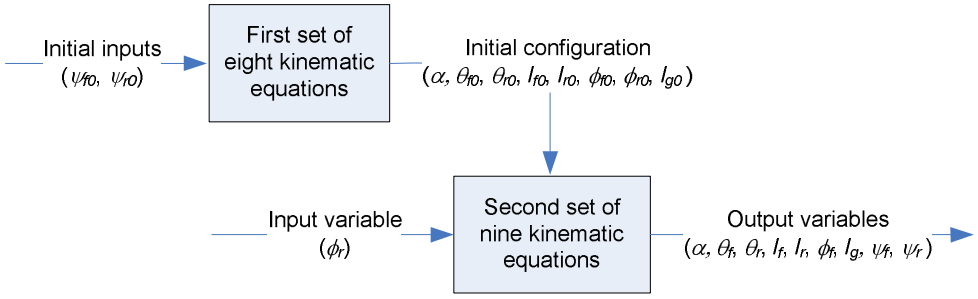

Figure 3.3: The solution procedure of the kinematic equations in the developed model.

As for the second set of equations, they are mostly obtained using the first set of equations. This step of the problem is defined as follows: we know the initial values of all ten variables from the first step. And we change one of the variables by a known amount. We are asked to solve for the new values of the other nine variables, in the new configuration of the mechanism. So what we need is the kinematic equations relating the old values and the known input to the new values of the variables, and these nine equations are shown below:

$$\theta_{r_1} - \theta_{r_0} = 2\psi_{r_1} - 2\psi_{r_0} \tag{3.14}$$

$$\theta_{f_1} - \theta_{f_0} = 2\psi_{f_1} - 2\psi_{f_0} \tag{3.15}$$

$$l_{r_1} - l_{r_0} = d \cdot \sin(\psi_{r_1}) - d \cdot \sin(\psi_{r_0}) \tag{3.16}$$

$$l_{f_1} - l_{f_0} = d \cdot \sin(\psi_{f_1}) - d \cdot \sin(\psi_{f_0}) \tag{3.17}$$

$$\phi_{r_1} - \phi_{r_0} = \theta_{r_1} + \alpha_1 - \theta_{r_0} - \alpha_0 \tag{3.18}$$

$$\phi_{f_1} - \phi_{f_0} = \theta_{f_1} + \alpha_1 - \theta_{f_0} - \alpha_0 \tag{3.19}$$

$$l_{r_1} \cdot \sin(\psi_{r_1}) + b \cdot \sin(\alpha_1) - l_{f_1} \cdot \sin(\psi_{f_1}) = 0 \tag{3.20}$$

$$l_{g_0} - d \cdot (\psi_{r_1} - \psi_{r_0}) + d \cdot (\psi_{f_1} - \psi_{f_0}) = l_{g_1} \tag{3.21}$$

$$\begin{aligned} l_{g_1} - l_{g_0} = {} & l_{r_1} \cdot \cos(\pi - \psi_{r_1}) + b \cdot \cos(\alpha_1) + l_{f_1} \cdot \cos(\psi_{f_1}) \\ & -l_{r_0} \cdot \cos(\pi - \psi_{r_0}) - b \cdot \cos(\alpha_0) - l_{f_0} \cdot \cos(\psi_{f_0}) \end{aligned} \tag{3.22}$$

Equations 3.14 - 3.23 are derived from the first set of kinematic equations: They are only relating the initial values of the variables to the new values. At this step, since we have already solved the first step, we know the initial values of the variables. The last equation of the second equation set comes from the relation between the rolling amounts of the two legs. The rolling amount of one leg was related to the change in the leg angle (ϕ) in Equation 3.4. Equation 3.23 is based on this relation, considering both of the legs.

As a result, now we have two equation sets with which we can set the initial configuration of the mechanism, and later determine the new configurations based on the change of a single variable. Once one link is fixed to the ground in the first step with the first set of eight equations, then the mechanism is a one degree of freedom mechanism. The use of this model will be better explained in the next part, when the example problem is presented and then solved using this formulation.

3.3 Case Study: Laser Scanning Problem

The use of the kinematic analysis presented above is shown in an example problem in this section. In order to be able to demonstrate the model that was developed, an example task in a realistic scenario was made: The robot is supposed to make a

vertical scanning motion with a laser scanner mounted on the body. The scanning will be done when the robot is standing, not walking. The desired angular span of the scanner thus the body is given. The rear leg will be rotated by an amount which we will find out using the formulation, so that the body angle will sweep the desired angle range. The desired motion is illustrated by the snapshots taken from the animation in Figure 3.4.

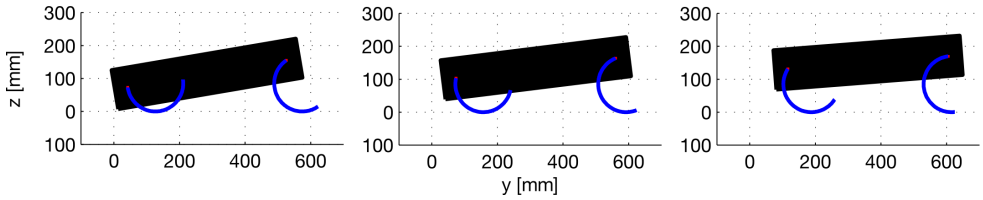

Figure 3.4: The snapshots from the animation, for the desired angle range being $5^o - 10^o$ and the selected initial leg angles being $\psi_{r_0} = 45^o$ and $\psi_{f_0} = 75^o$.

This body angle change can be achieved in stance mode only by using the advantage of half circular leg geometry, and this example illustrates the use of this model and also the multi-functionality of the half circular legs very well.

3.4 Simulations

The simulations were prepared in MATLAB which is found to be a very convenient environment for solving the kinematic equations presented previously. The kinematic equations were implemented in MATLAB codes and they were solved for obtaining results for the example task. The two equation sets were solved separately, so the example task was divided into two steps: First determining an initial configuration, and then beginning from this configuration, obtaining the achievable consecutive configurations.

In the simulations, we have set the robot to many different initial conditions. As explained in the previous sections, for setting the initial configuration, the system needs two input variables which were chosen to be ψ_r and ψ_f. For each combination of ψ_r and ψ_f, a corresponding initial configuration was obtained using the first kinematic equation set.

Then each initial configuration is employed in the second kinematic equation set together with an input variable which was chosen to be the rear leg angle (ϕ_r), in order to obtain the possible configurations that can be achieved with that initial configuration. The output variable was chosen to be the body angle (α) since the definition of the problem was to sweep a certain body angle range. For each initial configuration, the simulation was run twice: first increasing the input variable ϕ_r to its upper limit and then decreasing it to its lower limit. The upper and lower limits were determined by the physical system. The upper limit for the leg angle is when the length of the virtual leg is at its maximum, so the virtual leg is perpendicular to the ground. The lower limit for the leg angle ϕ_r is when the body touches the ground. So for each initial configuration, the robot was moved between these two states and the corresponding maximum and the minimum body angles that can be achieved by that leg angle pair set at the beginning was calculated. Since the problem asks to find a suitable leg angle input to the system with the goal of scanning a certain body angle range, the result of this simulation gives allowable initial leg angle pair, and the rear angle values that have to be set during the scanning motion.

3.5 Results

The maximum and minimum body angles that can be achieved by setting the leg angles ψ_r and ψ_f to different values is shown in Figure 3.5. Each of the legs angles was changed from 30^o to 90^o by increments of 10^o and the corresponding body angle to each combination is plotted. In this figure, two surfaces are seen. The upper surface is the surface formed by the maximum values of the body angle for each initial leg angle pair. The lower surface is formed by the minimum points or the body angle range corresponding to each initial leg angle pair. This figure shows the achievable body angle intervals for each initial leg angle pair, and it is useful for finding a convenient initial leg angle pair for the desired body angle range. The angle pairs where the desired body angle range is within the corresponding maximum and minimum values, are the pairs that we are looking for.

The desired body angle range is selected as 5^o - 10^o and the surface plot was scanned to find an initial leg angle pair whose corresponding minimum and maximum body

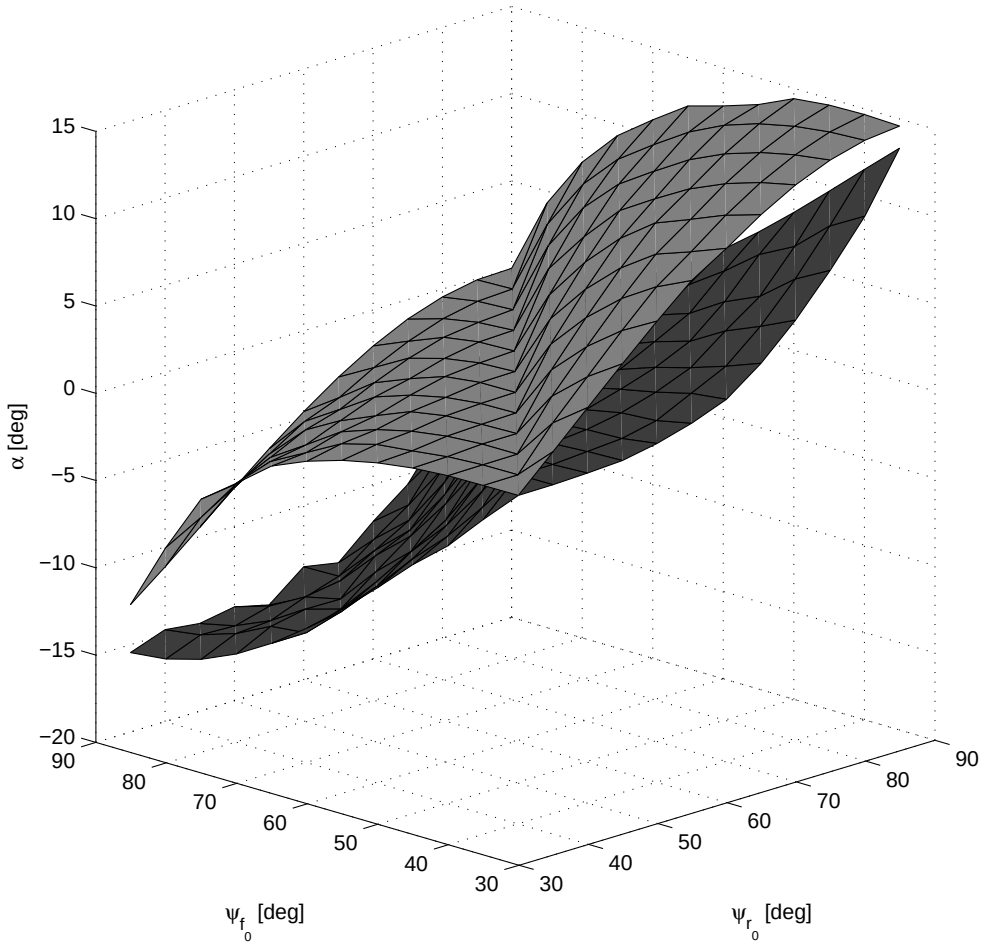

Figure 3.5: The surfaces formed by the maximum and the minimum achievable values of the body angle α, as a function of the two initial leg angles ψ_{f_0} and ψ_{r_0}.

angles include this interval. In Figure 3.6 the allowable pairs are shown with white. This figure means any of these white initial leg pairs allows us to scan the desired body angle range.

Any of them could have been picked for the second step of the analysis, in order to scan the desired angle and find out what values the rear leg should be set to. For this example, the $\psi_{r_0} = 45^o$ and $\psi_{f_0} = 75^o$ is selected. The corresponding initial configuration is calculated in first step of the analysis. Then using the second equation set the necessary leg angle range corresponding to the desired body angle range is found, and the configurations resulting from this leg angle change is animated as seen in Figure 3.4.

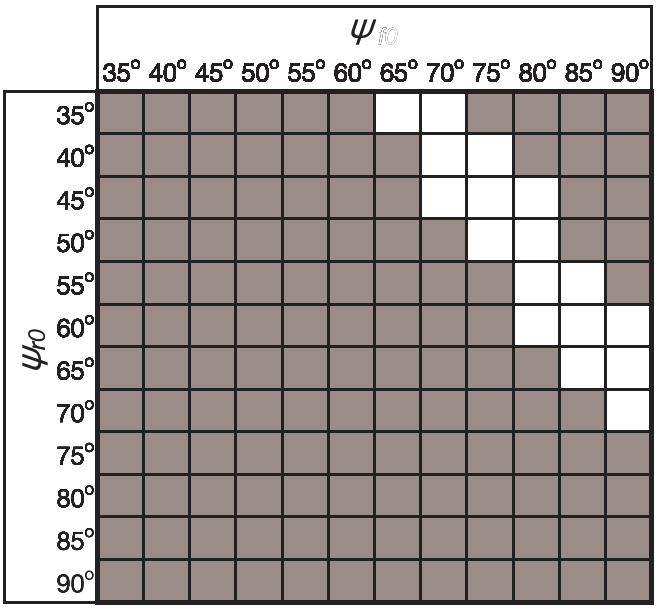

Figure 3.6: The allowable pairs of leg angles ψ_0 are seen in white, the desired angle range being $5^o - 10^o$.

During this simulation, the relation between the rear leg angle ϕ_r and the body angle α is also plotted and shown in Figure 3.7.

3.6 Discussion

Without being able to define the rolling motion, one has to assume that when in contact with the ground (stance phase), the leg is attached to the ground with a revolute joint. This means after the leg touches the ground, until the next the flight phase the leg-ground contact point does not change. Additionally, the change in the effective leg length due to the half circular and eccentric nature of the legs has to be ignored. In order to have a better accuracy compared to the models at hand, these effects of the leg geometry were successfully calculated and implemented in this model.

The model developed here is proven to be favourable not only as a basis for the dynamic analysis, but also in problems regarding the kinematics of the system. In the simulations, the planar kinematic model of RHex with two half circular rigid legs is shown to be working successfully. The example sensor scanning task was a very

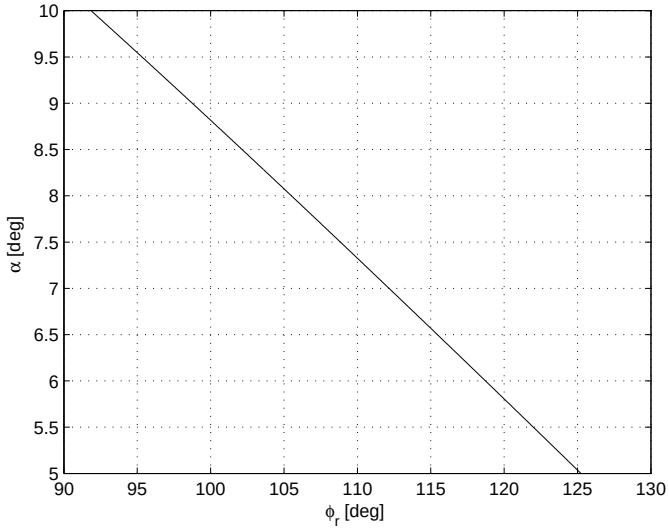

Figure 3.7: The body angle α as a function of the control input ϕ_r.

good example and a realistic scenario for clarifying how the model is useful in itself. This example not only showed the use of the kinematic model, but also demonstrated another function of the half circular legs, besides locomotion.

An interesting behaviour of the system was observed in the results of the simulations: The initial angular configuration of the body alone determines the range that can be covered being either positive or negative. If the body pitch angle α in the initial configuration is negative, it stays negative during the rest of the motion, and the same is valid for the positive initial body pitch angle. For the pairs on the diagonal of the feasibility map in Fig. 3.6 where ψ_{r_0} and ψ_{f_0} are equal to each other, the body pitch angle is equal to zero (i.e., the body is horizontal with respect to the ground) and it does not change at all during the change in the control input, just as expected.

As a result, this formulation sets the basis for any further kinematic analysis that can be done with RHex. It can be extended to any number of legs easily, or using a similar method, the 3-D model can be kinematically analysed. It is important to note that the study presented in this chapter is essential for the following dynamic analysis, and even for the extension of that dynamic analysis to more complex systems in the future.

CHAPTER 4

DYNAMIC MODELLING AND SIMULATION OF SLIP LOCOMOTION

One of the main goals of this thesis is to model the dynamic behaviour of the half circular compliant leg of the robotic platform SensoRHex. To achieve this, we are going to present a single legged hopper simulation with a half circular compliant leg. This simulation will be based on a linear leg model developed using the Spring Loaded Inverted Pendulum (SLIP) template, which will be introduced in this chapter.

SLIP template has been widely used for modelling legged locomotion. It is a hybrid dynamic system like the single legged hopping system that we are modelling in this thesis. The focus of this chapter will be going into the detail of these concepts and presenting the existing straight legged model on a readily working SLIP simulation environment. In the following chapters, we are going to build our new half circular compliant legged model on this existing model presented in this chapter.

4.1 Hybrid Dynamic Systems

When we observe running animals, we see that their motion does not have a continuous dynamic behaviour, but the motion is composed of separate phases. This implies that the dynamics of a running animal can not be explained with only one set of dynamic equations, but the motion is governed by a different set of equations in each phase. This is what makes the running animal a hybrid dynamic system. For example in the case of jumping of a kangaroo, the state of the animal periodically changes between stance and flight phases. In the stance phase, the legs are in contact with the ground

and there is the gravity and the ground reaction forces acting on the body. In the flight phase, the body undergoes a ballistic motion under the effect of gravity only.

The simulation of a hybrid dynamic system should be able to handle the each phase's dynamic equations separately and it should allow the phase transitions. For example if we want to simulate a system having two phases i.e. stance and flight, then first we have to derive the dynamic equations for each phase. While integrating the governing differential equations, at each numerical integration step we have to check if the system is satisfying the phase transition conditions. (For the case of running of an animal or a human, the transition condition for changing the phase from flight to stance can be a foot touching the ground. And the transition condition from stance to flight can be the foot leaving the ground or in other words, ground reaction forces becoming zero.) If the transition conditions are satisfied at any instant, the integration should continue with the new phase's dynamic equations. At the end of each phase, the last state of that phase is taken as the initial state for the new phase's dynamic equations. This procedure (integration and checking of the phase transition conditions, and changing the phase if necessary) is done continuously in a time interval or until a limit condition is reached.

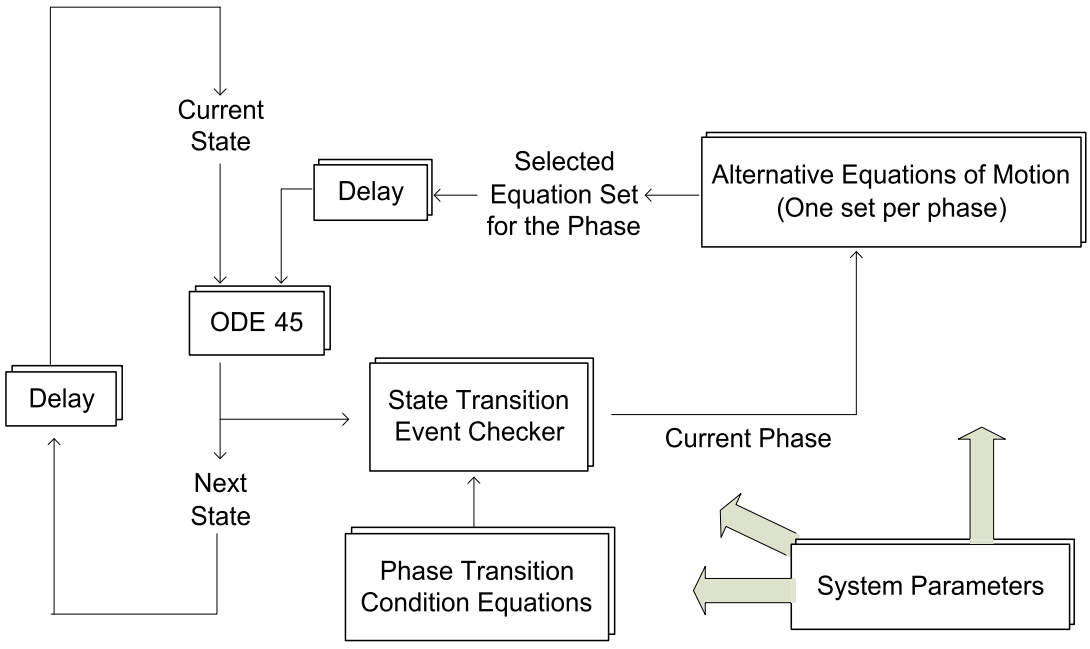

Figure 4.1: How the "hdss.m" MATLAB file works

In the following chapters, we will model and simulate a single legged hopper with a half circular compliant leg, which is also a hybrid dynamic system having two main phases: stance and flight. For applying the procedure explained above on this model, we will use a hybrid dynamic simulation framework called "Hybrid Dynamical System Specification" (HDSS) in which we can define different phases of a dynamic system, the dynamic equations of these phases, and the phase transition conditions. Given these and the initial conditions, hdss.m integrates the dynamic equations to obtain the new states at each step and catching the transition conditions to determine when to switch between phases. This framework was developed as part of our research group studies and Figure 4.1 summarizes the procedure.

4.2 SLIP Template

SLIP template is a popular model for modelling not only animal dynamic locomotion, but also dynamically running legged robots. This model is basically composed of a point mass bouncing on a massless linear spring (see Figure 4.2). For multi-legged creatures, slip behaviour means the behaviour of the center of mass is as if a virtual single leg was touching the ground [1]. When we look at the animals during running, we observe that the center of mass of the body follows a similar trajectory to that of the point mass in SLIP, and all the leg muscles are coordinated so as to obtain a proper equivalent spring constant to achieve this trajectory.

SLIP template was successfully used also for modelling the half circular compliant legged robotic platform RHex, based on the observation that the motion of RHex also resembles that of a SLIP system [91]. In this thesis, for modelling the half circular compliant leg we will use and modify an existing SLIP model of a one-legged hopper presented in [95]. The details of this model will be given in the following section.

4.2.1 Model Assumptions

An important assumption of the SLIP model is that the whole mass of the system is concentrated at the hip point. In other words, the leg has negligible mass compared to the body. The body is represented with a point mass and its moment of inertia

is assumed to be infinity. This means the body pitch is not affected by the torque applied at the body. This is why the moment of inertia of the body will not occur in the dynamic equations which will be presented in the next subsection.

Also, it is assumed that there is point contact and no slippage between the leg and the ground. Therefore, this contact point acts like a revolute joint between the leg and the ground, in stance phase.

4.2.2 Dynamic Equations

SLIP is an example to hybrid dynamic systems mentioned in the previous section, which means first of all it has separate phases with different dynamic equation sets. Secondly the phase transition conditions are defined using the system parameters and states. And lastly the dynamic equations are integrated in order to calculate the next step, given the current one. This is why SLIP template is very useful for modelling our one-legged hopper hybrid dynamic system.

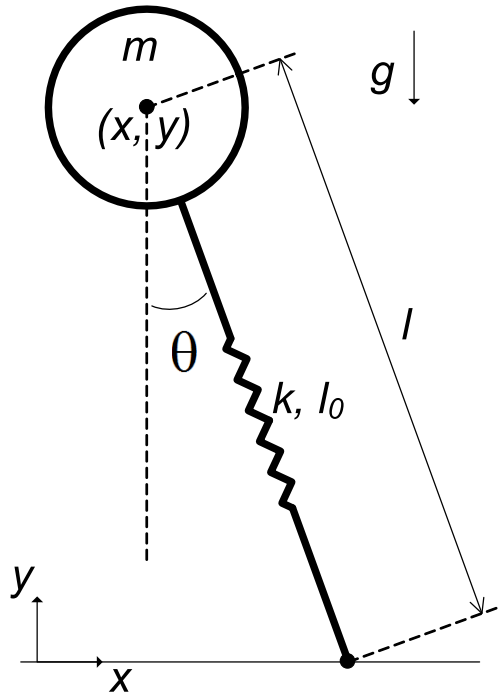

Figure 4.2: A Simple Spring Loaded Inverted Pendulum (SLIP) system and the related variables

There are two phases in SLIP motion: Flight and Stance. The transition between these phases are determined by the touch-down (from flight to stance) and lift-off (from stance to flight) events. In flight phase, the system is not in contact with the ground, and it is under the effect of gravity only. The spring is assumed to be massless so the body experiences projectile motion. The configuration of the system can be defined by the coordinates of the body center of mass only, so the equations of motion in cartesian coordinates are simply:

$$\ddot{x} = 0, \tag{4.1}$$

$$\ddot{y} = -g. \tag{4.2}$$

In stance phase, the system is in contact with the ground so also the ground reaction forces act on the system. In stance phase, the leg length l is a function of the ground reaction forces, the spring constant k and the undeformed leg length l_0, as the Hooke's Law states. The configuration of the system can be defined by the leg length l and the leg angle θ, as was done in [96]. The equations of motion for the stance phase are

$$\ddot{l} = l \cdot \dot{\theta}^2 - g \cdot \cos(\theta) + k \cdot (l_0 - l)/m, \tag{4.3}$$

$$\ddot{\theta} = \frac{g \cdot \sin(\theta) - 2 \cdot \dot{l} \cdot \dot{\theta}}{l}. \tag{4.4}$$

These equations are derived from the potential and kinetic energy equations:

$$PE = m \cdot g \cdot l \cdot \cos(\theta) + \frac{k \cdot (l_0 - l)^2}{2} \tag{4.5}$$

and

$$KE = \frac{m \cdot \dot{\theta}^2 \cdot l^2}{2} + \frac{m \cdot \dot{l}^2}{2}, \tag{4.6}$$

using the Lagrange method.

In order to fully define the motion of the system, these equations (4.1-4.2 for the flight phase and 4.3-4.4 for the stance phase) should be integrated, given the initial condi-

tions and the phase transition (touch-down and lift-off) conditions. In the following section, how this model is used for the existing straight leg model will be explained in detail.

It is important to note that in this thesis SLIP model is only a tool, and the existing linear legged SLIP model will be used as a successful test set-up for proving and visualizing the new half circular compliant leg model developed within the scope of this thesis.

4.3 The Existing Straight Leg Model

For the simulations of the half circular compliant leg model in this thesis, we are going to use an existing SLIP simulation environment presented in [95]. In this existing model, the leg is a straight leg and the spring representing the leg is a linear spring with a constant spring constant, as usual in a SLIP template. However, since the focus of this thesis is the effects of half circular leg shape, we will modify this model according to the half circularity of the leg and the varying stiffness of the spring representing the leg. This section is about the existing straight leg SLIP simulation of a single legged hopper. In the following chapters we will make a stiffness analysis of the half circular leg and integrate the equations regarding the half circular leg into the simulation environment presented here.

4.3.1 The System Variables and Equations of Motion

The existing straight leg model consists of a body of mass m_{body} and a toe of mass m_{toe} connected by a linear spring of stiffness k and undeflected length l_0 like the standard SLIP model explained in the previous section. The only difference of this model from the SLIP explained above is that the leg mass is placed as a separate point mass at the tip of the leg. The toe mass is necessary in the controlled simulation of the model, for being able to apply torque to the leg in order to bring it to the desired angular positions.

Since we also have a toe mass now, any configuration of this system can be defined by

four position variables: x_{hip}, y_{hip}, x_{toe}, y_{toe} and the four velocity variables which are their first derivatives. The first two of the four position variables give the position of the hip and the last two give the position of the toe. The state vector of the system is composed of these eight variables. The variables like the leg length (l) and the leg angle (θ) corresponding to the standard SLIP variables and their derivatives also can be derived as functions of these eight variables. Given an initial set of variables, the equations of motion of the system are integrated using the HDSS framework which was explained in Section 4.1, and the consecutive state vectors are obtained.

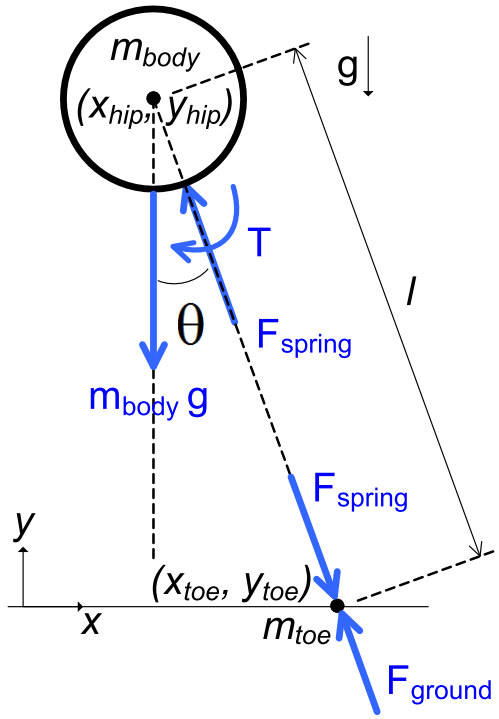

Figure 4.3: The free body diagram of the body and the toe, which the straight leg model consists of

In the existing model, there are two phases which were already mentioned: flight and stance. For each phase, the equations of motion are written in terms of the first derivatives of states of the system. The equations of motion are derived from the free body diagrams of the body and the leg are shown in Figure 4.3. For the flight phase, the equations of motion are:

$$\ddot{x}_{hip} = 0, \tag{4.7}$$

$$\ddot{y}_{hip} = -g, \tag{4.8}$$

$$\ddot{x}_{toe} = (\frac{T}{l} \cdot \cos(\theta) + F_{spring} \cdot \sin(\theta))/m_{toe}, \tag{4.9}$$

$$\ddot{y}_{toe} = (\frac{T}{l} \cdot \sin(\theta) + F_{spring} \cdot \cos(\theta))/m_{toe} - g. \tag{4.10}$$

As for the stance phase:

$$\ddot{x}_{hip} = (\frac{T}{l} \cdot \cos(\theta) + F_{spring} \cdot \sin(\theta))/m_{hip}, \tag{4.11}$$

$$\ddot{y}_{hip} = (\frac{T}{l} \cdot \sin(\theta) + F_{spring} \cdot \cos(\theta))/m_{hip} - g, \tag{4.12}$$

$$\ddot{x}_{toe} = 0, \tag{4.13}$$

$$\ddot{y}_{toe} = 0. \tag{4.14}$$

The MATLAB file "hdss.m" simply gives these equations of motion as input to MATLAB's integrator function "ode45", together with the phase transition conditions as summarized in Figure 4.1. Knowing the current state, the new states are obtained with this procedure. The simulation is also animated in MATLAB environment. In the next section, an example simulation will be presented.

4.3.2 Controlled Locomotion Simulations

In order to show the existing model is working, an example simulation is made using a simple controller presented in [97]. In this simulation, the controlled locomotion of the single straight legged hopper is observed. The motion reaches steady state with the selected controller which aims to keep the horizontal velocity at a desired value. The straight legged hopper achieves a stable hopping pattern with this controller, given the initial conditions and the system parameters. The snapshots from the animation showing the steady state hopping pattern can be seen in Figure 4.4. This pattern can also be observed from the hopping height and horizontal speed plots in Figure 4.5 and Figure 4.6. The controller used for the straight legged model here will be also used for simulating the controlled behaviour of the half circular leg model in Chapter 6.

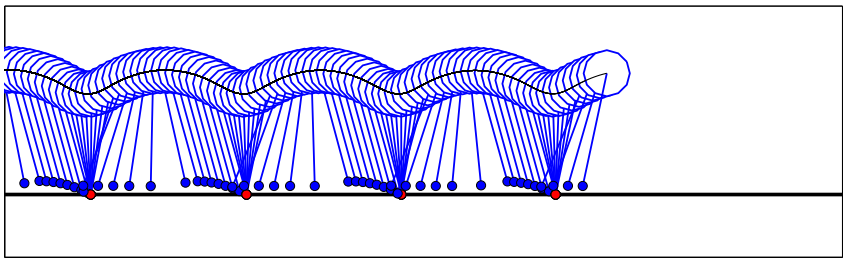

Figure 4.4: The animation of the controlled SLIP hopping at steady state

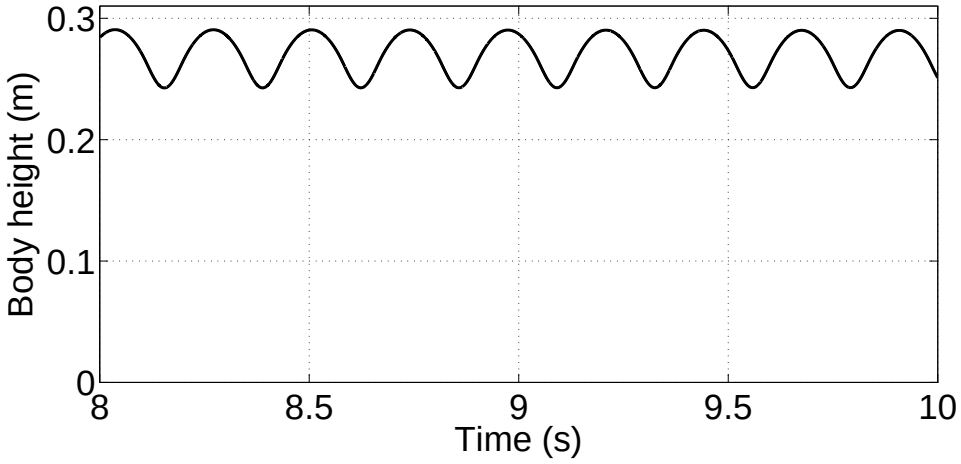

Figure 4.5: The controlled SLIP's steady state behaviour: Body height vs time

4.4 Concluding Remarks

In this thesis, this model is considered to be a successful simulation environment for plugging in our equations resulting from the half circularity of the leg. We are working on this model in order to extend it to a more accurate model which takes the half circularity into account. When the half circularity is introduced, the relationship between the ground reaction forces and the leg deflection will be re-defined and it will be derived as a function of the leg angle. Also, the contact point being a revolute joint

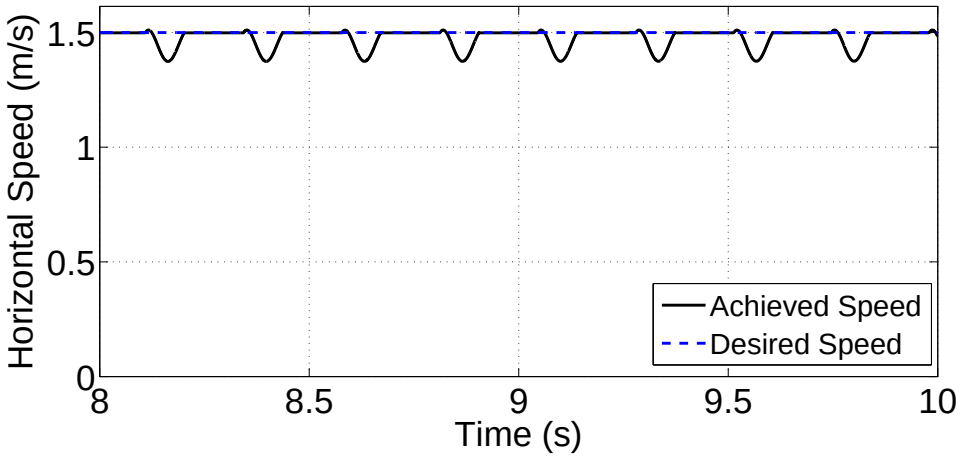

Figure 4.6: The controlled SLIP's steady state behaviour: Horizontal velocity vs time

fixed to the ground will not be valid any more and the rolling effect will be integrated in the equations. These improvements will be explained and discussed in the following chapters.

CHAPTER 5

STIFFNESS ANALYSIS OF THE HALF CIRCULAR COMPLIANT LEG

In the previous studies, the half circular compliant legs of RHex were modelled as linear and constant stiffness springs, as explained in the previous chapter. We claim that the constant stiffness assumption is too much simplification for the leg with this special morphology. The relation between the force and deflection can not be reduced to a constant; it should be changing as the leg angle changes. In this chapter, we are going to analyse the leg stiffness, and derive the relation between the ground reaction forces and the deflection in the leg, in order to be plugged in the half circular leg model in the following chapter.

In a linear spring, the force-deflection relation is given by the Hooke's Law as follows:

$$F = k \cdot \delta. \tag{5.1}$$

Here F is the axial force applied to the spring in Newtons, δ is the change in the length of the spring and k is the spring constant. The curved members, however, have different compliance behaviour than linear springs due to their geometry. Castigliano's Theorem is a useful tool for derivation of force-deflection relation in curved members. When we apply this theorem to the half circular compliant leg we will see that the ratio of the ground reaction force to the deflection is not simply a constant like the k in Equation 5.1, but it is a function of the point of application of the force on the leg, thus a function of the leg angle. So we can still consider the leg as a spring; but a spring whose stiffness is not a constant, instead, a function of θ. The stiffness equation

of the half circular compliant leg should look like:

$$F = k(\theta) \cdot \delta \tag{5.2}$$

In this chapter we are aiming to find $k(\theta)$, using the Castigliano's Theorem. In the following chapters this relation will be used in the simulation of the half circular compliant leg; the spring constant k in the existing linear leg model will be replaced by this relation.

5.1 Castigliano's Theorem

The Castigliano's Theorem is a useful tool for finding the force-deflection relation in a half circular compliant member under static loading [98]. The deflection of any point on the half circular member can be found using this theorem, given the external forces acting on the member. The method consists of two steps: The first step is finding the total strain energy of the system due to static loading, and the second step is taking the derivative of the total strain energy with respect to the force that is in the direction of the deflection we want to find.

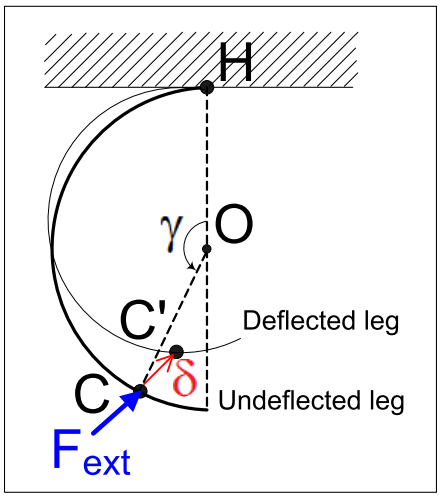

Figure 5.1: The relation between the external force F_{ext} applied at point C and the resulting deflection δ ($|\overline{CC'}|$) will be found by applying Castigliano's Theorem on the half circular member fixed to the ground at point H.

Suppose we have a half circular member as shown in Figure 5.1. The member is fixed to the ground at point H, no rotation or translation is allowed at this point. The force F_{ext} is acting on the body at a point on the leg, point C. $\overset{\frown}{HC}$ is an arc of angle γ and radius r. This force causes a deflection δ of the point C to point C'. Note that the force F_{ext} and the deflection δ are not necessarily in the same direction.

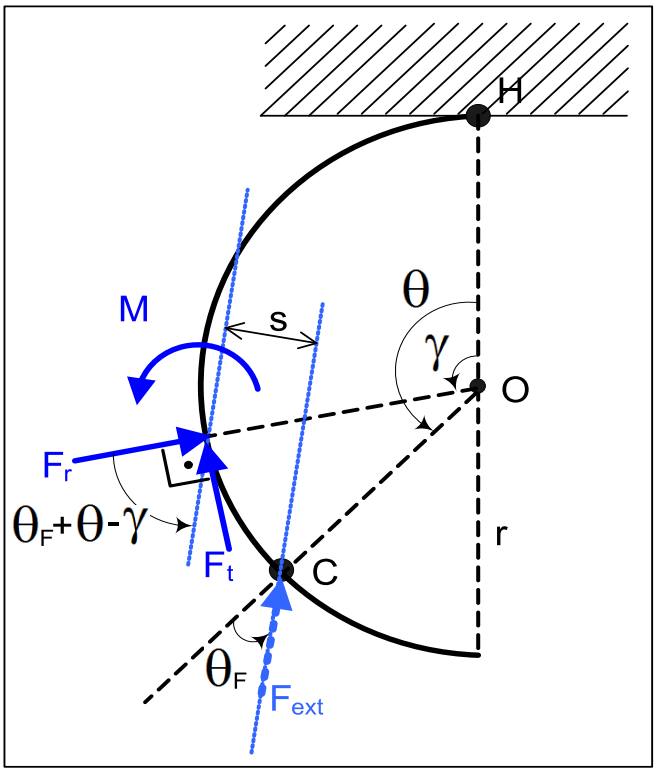

Figure 5.2: Cross sectional forces and moment (F_r, F_t and M) due to the external force F_{ext} which is applied at point C on the arc, with an angle of θ_F measured from the radial direction at point C.

In order to find the deflection to due to F_{ext} according to the theorem, we will first find the equivalent force components and moments throughout the arc $\overset{\frown}{HC}$, and then integrate them from point H to point C to find the total strain energy loaded in this arc. In Figure 5.2 the resulting cross sectional forces due to the applied external force are shown and they can be written in terms of F_{ext}, θ_F and θ as:

$$F_r = F_{ext} \cdot \cos(\theta_F + \theta - \gamma) \tag{5.3}$$

$$F_t = F_{ext} \cdot \sin(\theta_F + \theta - \gamma) \tag{5.4}$$

$$M = s \cdot F_{ext} \tag{5.5}$$

where γ is the integration variable. s is the distance between the axis of F_{ext} and an axis parallel to this and passing from the point at the cross section. It is derived from the geometric relations as:

$$s = 2 \cdot r \cdot \sin(\theta - \gamma) \cdot \cos(\theta_F + \frac{\theta - \gamma}{2}) \tag{5.6}$$

The strain energy terms due to these cross sectional forces are given by Castigliano's Theorem as:

$$U_1 = \int_0^\theta \frac{M^2 r \, d\gamma}{2EI}, \tag{5.7}$$

$$U_2 = \int_0^\theta \frac{F_t^2 r \, d\gamma}{2AE}, \tag{5.8}$$

$$U_3 = -\int_0^\theta \frac{M F_t \, d\gamma}{AE}, \tag{5.9}$$

$$U_4 = \int_0^\theta \frac{C F_r^2 r \, d\gamma}{2AG} \tag{5.10}$$

where r is the undeflected radius, E is the modulus of elasticity, I is the moment of inertia, A is the cross-sectional area, and G is the shear modulus of the leg. C is a constant related to the leg geometry. The total strain energy stored in the half circular member due to the external forces is simply the sum of those four components:

$$U = U_1 + U_2 + U_3 + U_4. \tag{5.11}$$

The first term is the most dominant term, therefore the total strain energy is often approximated as:

$$U \approx U_1 = \int_0^\theta \frac{M^2 r d\gamma}{2EI}. \tag{5.12}$$

Now that we have found the total strain energy stored in the half circular member, the second step for finding the deflection is to take the derivative of this energy. The deflection of point C in the direction of any force F applied at point C is simply:

$$\delta = \partial U / \partial F. \tag{5.13}$$

This method will be applied on the half circular compliant leg of RHex in the following section. The leg will be attached to the body and it will be in contact with the ground, the external forces being the ground reaction force.

5.2 Force - Deflection Relations in the Half Circular Compliant Leg

The deflection of the half circular compliant legs of RHex under static loading is investigated in this section. Castigliano's Theorem will be applied to the half circular compliant leg and the force-deflection relation will be derived. This relation will show that the stiffness is a function of the leg angle with respect to the ground, and this is one of the main improvements to the existing linear leg model.

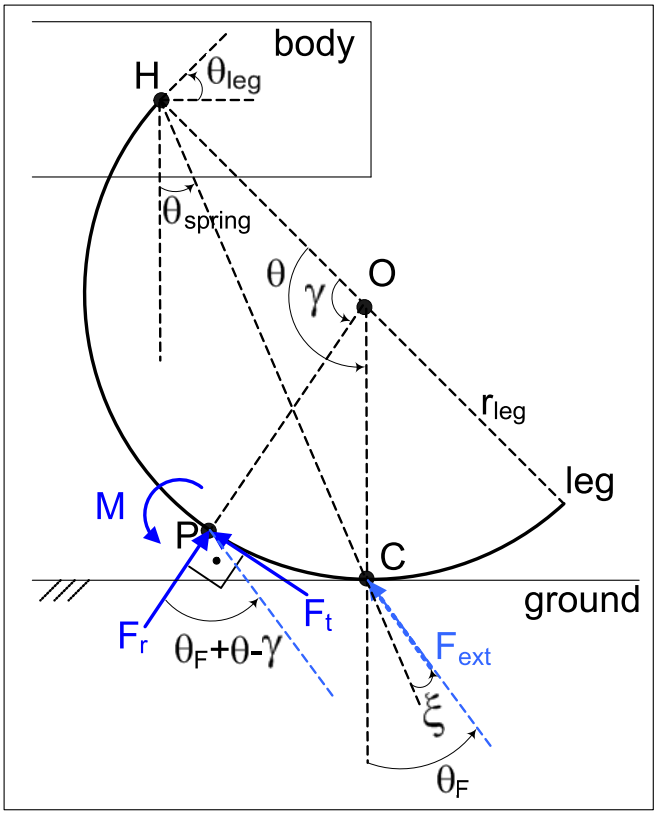

Figure 5.3: The half circular leg and the related variables for the deflection analysis

In order to apply Castigliano's Theorem to the leg, first we define the leg variables as seen in Figure 5.3. As seen in the figure, the leg is attached to the body at point H, and the angle of the leg with respect to the ground is measured at the hip. This angle, θ_{leg}, is the angle between the horizontal axis passing from point H and the tangent to the leg at point H.

Since we assume the leg is circular, the contact is the intersection of the leg circle and the tangent ground line. Point C is the leg-ground contact point. F_{ext} is the ground reaction force and it is applied at point C. By using Castigliano's Theorem, we will find the deflection of this point with respect to the hip point H.

It is important to note that in the case of a single legged hopping system, the ground reaction force acting on the leg causes deflection on the leg. However this deflection is not observed at the contact point C since the leg stays in contact with the ground. The deflection of the leg causes the hip point H to experience displacement. But here in this section we are only aiming to find the amount of deflection, given the external force. The displacements of points C and H will be discussed in the following chapter.

In order to find the total strain energy in the leg, we use the Equations 5.7 - 5.11. In these equations, we write every term in terms of the leg variables. First, we replace the terms F_r, F_t and M with their equivalent expressions presented in Equations 5.3 - 5.5 so that they are written in terms of F_{ext} and the angular variables regarding the leg.

There is one more geometric relation that we should integrate in the equations and that is

$$\theta = \pi - \theta_{leg}. \tag{5.14}$$

After combining these relations, we obtain the total strain energy stored in the leg as:

$$
\begin{aligned}
U_{leg} = &\int_0^{(\pi-\theta_{leg})} \frac{2r^3F_{ext}^2}{EI} \cdot \sin^2(\frac{\theta_{leg}+\gamma}{2} - \theta_F) \cdot d\gamma \\
&+ \int_0^{(\pi-\theta_{leg})} \frac{rF_{ext}^2}{2AE} \cdot \sin^2(\theta_F + \pi - \theta_{leg} - \gamma) \cdot d\gamma \\
&- \int_0^{(\pi-\theta_{leg})} \frac{2rF_{ext}^2}{AE} \cdot \sin(\theta_F + \pi - \theta_{leg} - \gamma) \cdot \sin^2(\frac{\theta_{leg}+\gamma}{2} - \theta_F) \cdot d\gamma \\
&+ \int_0^{(\pi-\theta_{leg})} \frac{CrF_{ext}^2}{2AG} \cdot \cos^2(\theta_F + \theta - \gamma) \cdot d\gamma.
\end{aligned} \tag{5.15}
$$

For obtaining the force-deflection relation from this equation, first the derivative $\partial U_{leg}/\partial F_{ext}$ is calculated. This equals to the deflection at the point where F_{ext} is applied. Then F_{ext}/δ is derived from this equation, and this equals to the force-deflection relation $k(\theta)$ which we were seeking in Equation 5.2.

$$
\begin{aligned}
k(\theta) = 2EIAG/(&-3r^3 sin(\pi-\theta)AG + 2r^3(\pi-\theta)AG + \\
&r^3 cos(\pi-\theta)(\pi-\theta)AG + 3rsin(\pi-\theta)IG - \\
&r(\pi-\theta)IG - 1.5rEIsin(\pi-\theta) + 1.5r(\pi-\theta)EI)
\end{aligned} \tag{5.16}
$$

Now we have the leg stiffness k as a function of the leg angle θ. We will use this equation in the following chapter, to replace the constant stiffness leg in the existing model with the half circular compliant leg.

5.3 Concluding Remarks

The legs are rolling on the ground during motion and the leg-ground contact point moves along the leg during rolling. This contact point is the integration limit in the energy equation in Castigliano's Theorem, because it is the point of application of the external forces. The contribution of this chapter is the calculation of the leg stiffness as a function of the leg angle. This equation will be used in Chapter 6, and it will replace the constant leg stiffness k of the previous leg model. As a result, the leg stiffness will not be a constant any more but it will be a function of the leg angle and the system parameters like the undeflected leg radius, etc.

CHAPTER 6

SLIP MODEL WITH VARIABLE STIFFNESS LEG

In this chapter, the new dynamic model of the half circular compliant leg is introduced. We took the readily working SLIP simulation environment presented in Chapter 4 as a testing environment for our new model. The leg is modelled as a spring as in the previous SLIP model, but the leg deflection is calculated in a different and more accurate way. The leg deflection is calculated with the Castigliano's Theorem with the procedure explained in Chapter 5. In the new model, the leg is not a constant stiffness spring any more, since the leg stiffness is a function of the leg angle. Within the scope of the work presented in this chapter, the leg stiffness variable in the SLIP equations is replaced with the new stiffness calculated for the half circular compliant leg. By doing this, the existing model is updated to a more accurate leg model.

Another improvement to the previous model is taking the rolling motion into account. In the previous model, the leg-ground contact was reduced to a single point throughout the whole stance phase. So the leg was assumed to rotate around a point fixed to the ground during the stance phase. However, using the kinematic relations derived in Chapter 3, the amount of rolling can now be calculated for the half circular leg. Calculating the horizontal position of the leg-ground contact point during rolling is integrated in the equations of the new model. The rolling effect makes the new leg model even more realistic.

In the following sections, the assumptions of this new leg model are explained, the equations governing the half circular compliant legged system are introduced, and simulations of the new leg model are presented.

6.1 Model Assumptions

The half circular compliant leg model presented in this thesis is considered to be a rather realistic model compared to the models with straight legs, which had to make a lot of assumptions and approximations. However, taking the leg geometry into account, we still had to make some assumptions and approximations in order to have a model that is quick and simple enough to be useful.

First of all, the motion is assumed to be symmetric with respect to the sagittal plane, therefore the model developed here is a planar model. This assumption is made throughout the whole study presented in this thesis.

Secondly, it is assumed that the force-deflection relation derived by the Castigliano's Theorem for the half circular beams is valid for our dynamic system with the half circular compliant leg. The deflection of the leg-ground contact point is calculated with this theorem and it is related to the ground reaction forces using the spring equation known as the Hooke's Law.

The fact that this compliant leg can be modelled as a spring which obeys the Hooke's Law is also a fundamental assumption. We assumed that the deformation of the leg during motion is perfectly elastic. Therefore, the leg returns to its initial shape after the loading is released from the leg. If we do not make this assumption, we have to calculate the residual stresses occurring in the leg and the plastic deformation. This would have make the model impractical, so this assumption had to be made for the sake of simplicity.

Another important assumption is that the leg preserves the half circularity during deflection. In the real case the shape of the deflected leg might be more similar to an ellipsoid, in which the radius is not constant throughout the leg. However, we need to make this half circularity assumption in order to position the leg, given the deflection of a point on the leg.

During the leg compression and decompression, the displacement of the leg-ground contact point with respect to the hip is assumed to be on the line connecting the hip and the leg-ground contact point. The assumed way of deflection is shown in

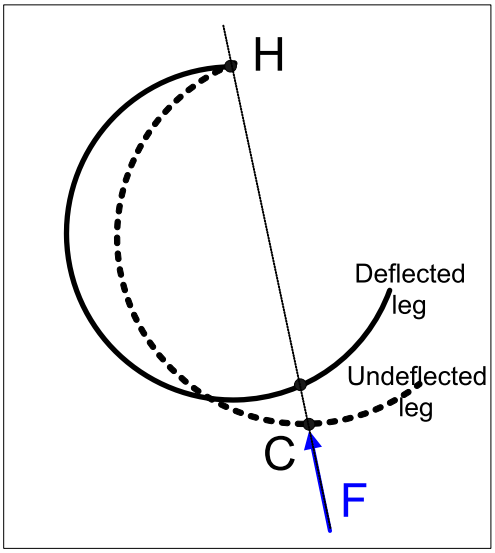

Figure 6.1: Direction of displacement of Point C is assumed to be towards the hip point, shown as Point H.

Figure 6.1. This is a very critical assumption since we use only the magnitude of the deflection that is calculated from the Castigliano's Theorem, and ignore the direction information. If we want to use also the direction of the displacement, then we would have to use more constraints, therefore more equations in the model. We had to make this assumption as result of a compromise between the simplicity and the accuracy of the model. This was explained in more detail in the previous section where the leg deflection was calculated.

As for the rolling motion, we assumed no slippage. Also, the contact of the leg and the ground is assumed to be point contact.

6.2 The Simulation Algorithm

To understand the simulation algorithm, it is necessary to be familiar with the simulation of hybrid dynamic systems, which was summarized in Section 4.1. As explained in Section 4.1, and shown in Figure 4.1, the hdss.m is a very useful framework prepared in MATLAB, for the simulation of motion of dynamic systems with phases following each other. Each phase has its own equations of motion, and the transition between two phases is defined by some events. Once the simulation is started with the initial

conditions, the hdss.m continuously checks for the transition conditions and change the phase flag if necessary, while integrating the equations of motion for the current phase for calculating the next state.

To summarize, the state vector is the set of variables that defines the whole system at any time instant. Equations of motion are the equations that are integrated for getting the new state vector. The phases are the parts of the motion having different equations of motion. In the following subsections, the simulation algorithm will be presented in more detail.

6.2.1 The Phases of the Motion

The motion of the single half circular compliant legged hopping system has three phases, while the single straight legged system had only two: stance and flight, as was seen in Chapter 4. The phases of the half circular compliant legged system are illustrated in Figure 6.2. As shown in this Figure, there are two critical variables that help us determine the phases: $y_{contact}$ and θ. $y_{contact}$ is defined as the minimum distance of the leg circle to the ground. We find it by drawing a tangent line that is parallel to the horizontal ground. The intersection of this tangent line with the leg gives the point that is defined as the "contact point". This contact point is on the leg half circle, only if the leg angle θ_{leg} is greater than zero, as can easily be seen in the figure. If θ_{leg} is negative, then the tangent point can not be on the leg, but the parallel horizontal line will intersect with the end point (toe) of the leg.

If the leg is in flight phase, θ_{leg} being positive or negative does not affect the dynamics of the system. However in stance phase, if θ_{leg} is greater than zero, it means that the leg is rolling on the ground. If it is negative, then it means that the leg is touching the ground with the toe, moreover, the leg is rotating around the toe since rolling is not possible on a single point. So in the simulation code, the calculation of the variables like the contact point, leg length, etc. depend on the phase of the system.

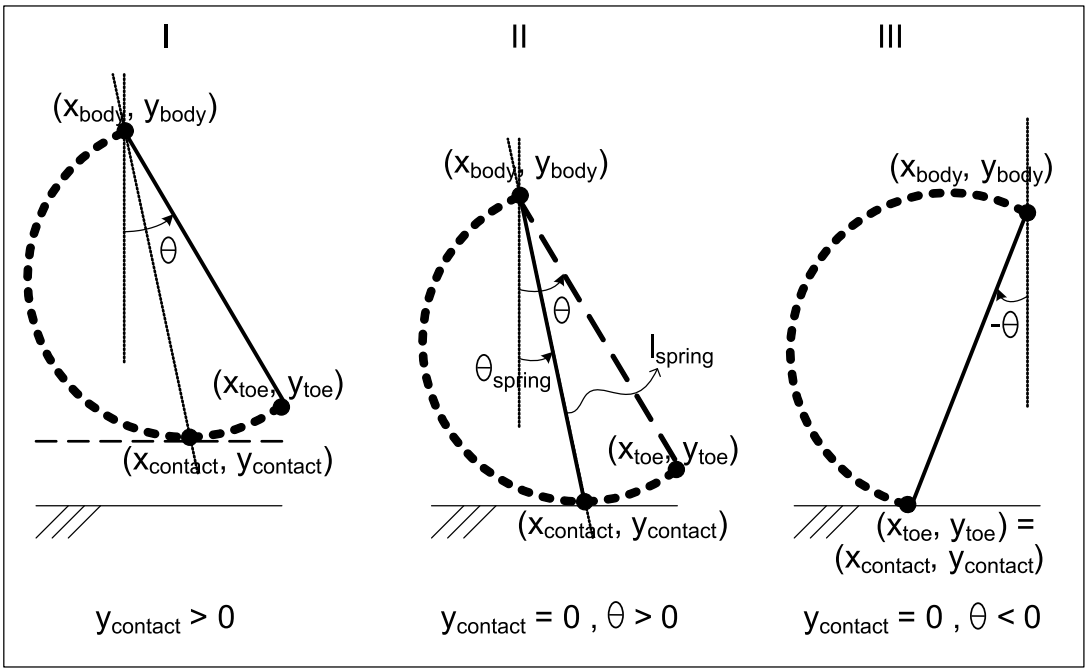

Figure 6.2: The three phases of the motion of the single half circular compliant legged hybrid dynamic system: I - Flight phase, II - Rolling stance phase and III - End point stance.

6.2.2 The User Inputs: The System Parameters and the Initial Conditions

System parameters are the physical properties of the system that are set at the beginning of the simulations, by the user. These are properties like the body mass, and the leg radius, that can be set to different values in different simulations in order to observe the effects of these parameters to the dynamics of the system. The values of the system parameters do not change during a simulation.

In the simulations, we chose as realistic parameters as possible, in order to get the closest results to the real behaviour. The size parameters related to the leg are given in Figure 6.3. A list of the system parameters can be found in Table 6.2.

The initial conditions that are set by the user are the desired initial position and velocity of the system, namely: x_{body}, y_{body}, $\dot{x}_{body}$, $\dot{y}_{body}$, θ_{leg}.

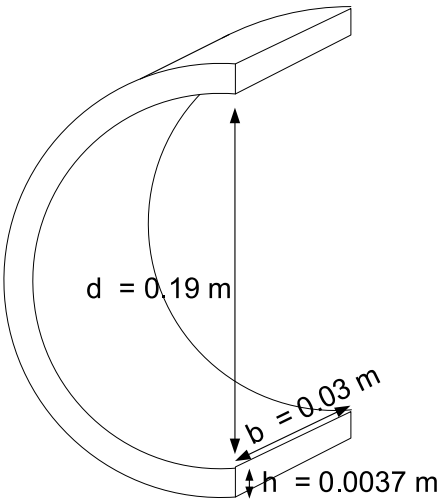

Figure 6.3: The size of the half circular compliant leg

6.2.3 The State Vector and The Equations of Motion

The state vector and the dynamic equations governing the system are the same as those of the straight leg model (Equations 4.7 - 4.11) presented in Chapter 4. However, while improving the straight leg model, we had to modify some of the existing variables, or create new variables for the new leg model. Although the equations of motion are the same, some of the variables in the equations calculating the new states were re-defined. As a result, only the force term in these equations was changed according to the new variables resulting from the half circularity and rolling motion.

The new force term is calculated using the new stiffness value of the leg, which was calculated in Chapter 5 from Castigliano's Theorem. In other words, the constant k_{spring} in the previous straight leg model was replaced with k_θ from Chapter 5.

Also, the horizontal position of the leg-ground contact point in stance phase was constant in the previous straight leg model. In the new model, we re-calculated the amount of translation of the leg-ground contact point at each step of the simulation and updated this position accordingly. The amount of translation of this point was calculated using the kinematic equations derived in Chapter 3, as:

$$\delta l = \delta\theta \cdot l_{spring} = \delta\theta \cdot r \cdot \sin(\theta). \tag{6.1}$$

6.3 Simulations

Simulations were done in a MATLAB simulation environment, as was done in Chapter 4. There was already a simulation code for the constant length and constant stiffness single leg, and the same environment was used in order to implement the new relations of the half circular compliant leg. In order to take the rolling and deflection into consideration, many more variables and many more relations had to be written in the existing algorithm. Finally a working MATLAB model was obtained and then some experiments were made in order to show that the model is realistic.

In Figure 6.4 some sample snapshots from a simulation are seen. The system is composed of a half circular compliant leg, and a point mass. The virtual leg, which in fact does not exist in the physical system is also illustrated in the figure, as a line connecting the body and the leg-ground contact point. The change in the body position, the leg angle and the leg radius are clearly seen in the snapshots.

The simulations were made in order to prove that the derived dynamic relations are correct. In the simulations the aim was first to have a realistic dynamic motion, together with all the deflection and rolling effects. For this, the one legged hopping system was thrown from a certain height to the ground, with various initial positions and velocities. The constants due to the material and the dimensions were selected as realistic as possible. Among the observed outputs were the body height, the body horizontal speed, and the energy change during the jump.

The following subsections will present different simulations made with different conditions. First a single jump with and without initial speed is observed. Then successive jumps are obtained with different initial conditions. Then a controller is added to the system in order to achieve a desired horizontal speed. Here, the controller in Chapter 4 is used. Next, the results obtained with the straight leg in Chapter 4 are compared with those obtained with the half circular compliant leg with similar system parameters and initial conditions. In the subsequent set of simulations, the initial condition sensitivity of the model is analysed, the behavioural change due to the modulus of elasticity is observed, and the model accuracy is tested with different leg angles.

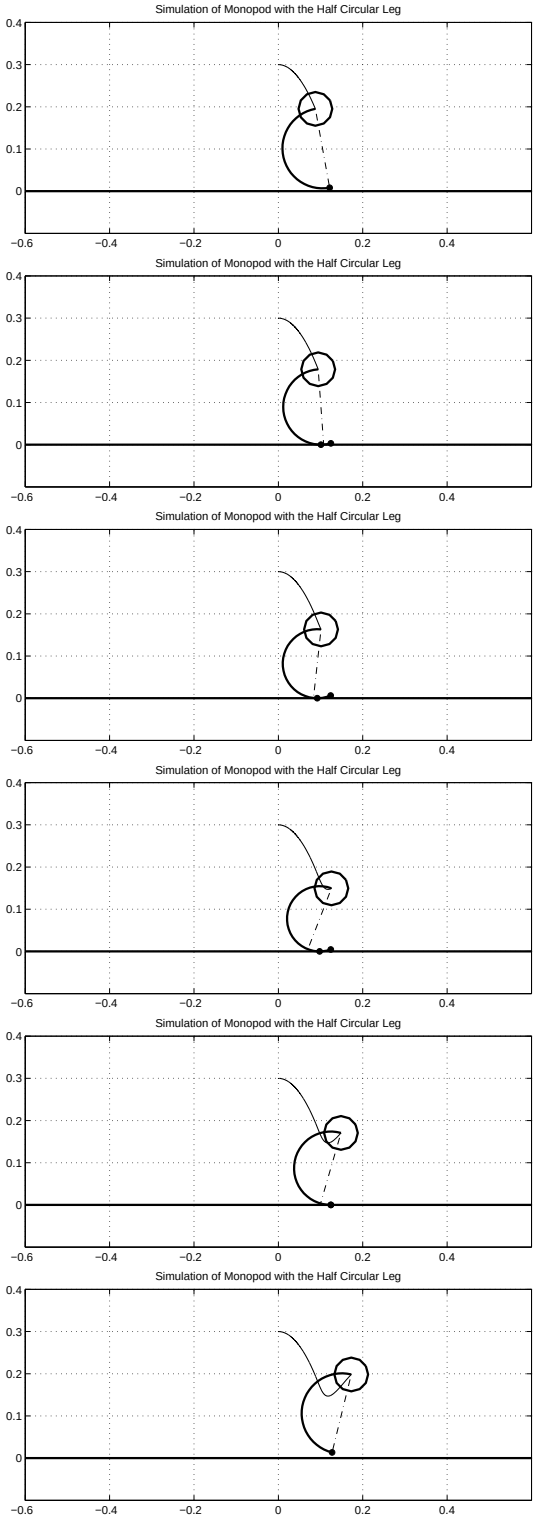

Figure 6.4: Sample snapshots taken from the MATLAB simulation environment, illustrating the change in the half circular compliant leg during stance phase of a jump

6.3.1 Single Jump

A single step of dynamic hopping, or a single jump, can be considered as the motion that is observed between the two successive highest body vertical positions. In this time interval, at first the body is in flight phase. It is thrown from a certain height and it starts to descend. As soon as it touches the ground the stance phase begins and the leg begins to compress. When the leg-ground reaction forces become high enough to lift the body up again, the decompression of the leg starts. When the leg reaches its rest length, it leaves the ground and goes into the flight phase again. The body ascends until the next peak of the body vertical position.

In Figure 6.5, the trajectories of the body in several single jump scenarios are plotted. In these plots, the body is thrown with different initial conditions and with different system parameters which are noted on the figure. The different values include the initial horizontal speed, the leg touch-down angle and the leg damping constant. In all these simulations, the horizontal position is 0 m, the initial height is 0.3 m and the initial vertical speed is 0 m/s. As for the system parameters, the geometric features of the leg are as seen in 6.3 and the modulus of elasticity (E) is taken as 22 GPa.

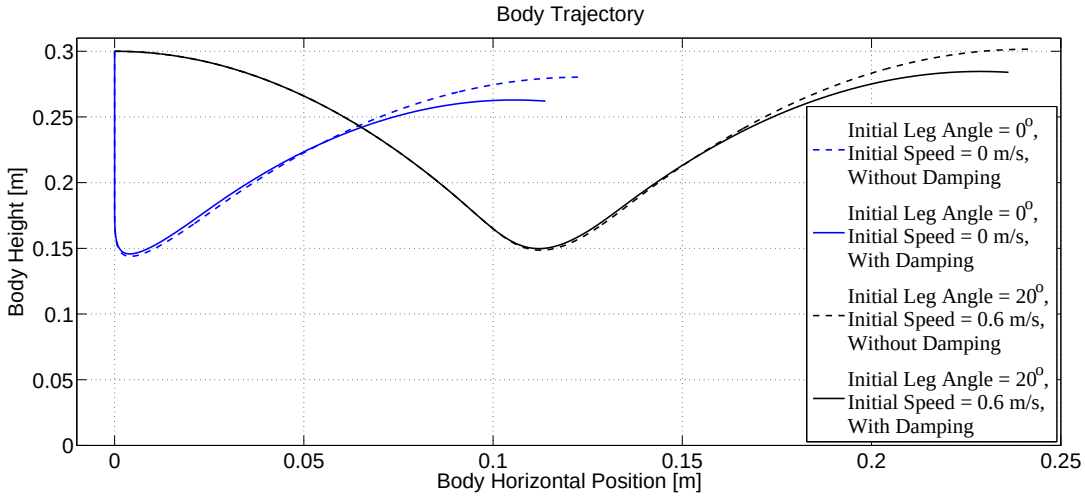

Figure 6.5: The single jump body trajectories are plotted for four scenarios which are noted on the figure legend. In the cases with damping, the damping coefficient d is taken as 3 Ns/m. The initial horizontal position for all four cases is 0 m, the initial height is 0.3 m and the initial vertical speed is 0 m/s.

In Figure 6.5 the trajectories of the jumps with 0 initial horizontal speed start with a vertical fall. The jumps with no damping can reach higher apex heights at the end of the single jump. This is because no energy is dissipated due to damping, so the system has more potential energy left, at the end of the jump.

For the same initial conditions and system parameters, the changes in the leg length are shown in Figures 6.6 - 6.9. It is clearly seen in all these figures that in the stance phase of the jump (between the touch-down and lift-off events) the leg length first decreases and then increases again. These occur when the leg stores the spring potential energy and transforms it back into kinetic energy.

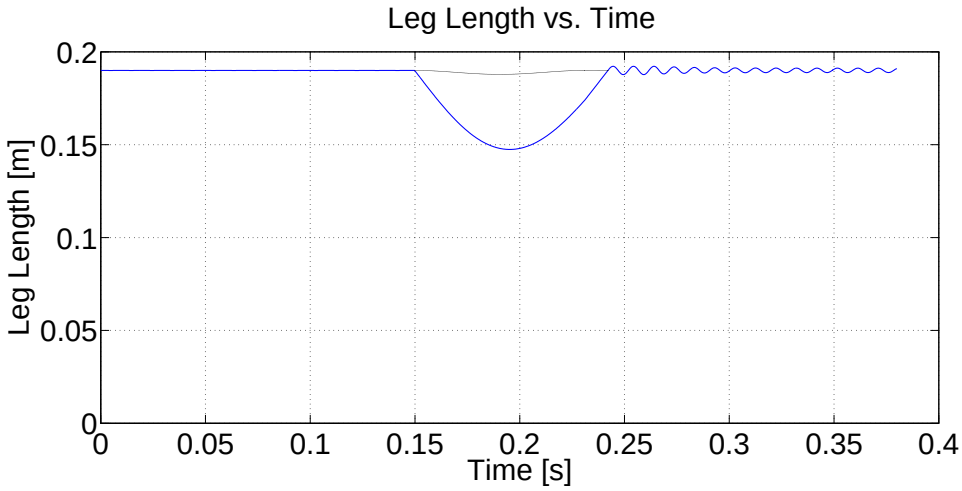

Figure 6.6: The leg length vs time of a system with the initial leg angle 0^o, the initial horizontal speed 0 m/s and the damping coefficient 0 Ns/m in a single jump is plotted. The other initial conditions and system parameters are the same as those of the other single jump simulations.

After the lift-off event, the fluctuations in leg length continues in the scenarios with the damping coefficient being zero. This is because the leg continues to behave like a spring in the flight phase and the small toe mass causes small fluctuations. These fluctuations are damped very quickly in the scenarios with non-zero damping coefficient, so they are not seen.

The leg length at lift-off is greater than the leg length at touch-down. This is because the leg experiences rolling between these two events. At the lift-off moment, the leg

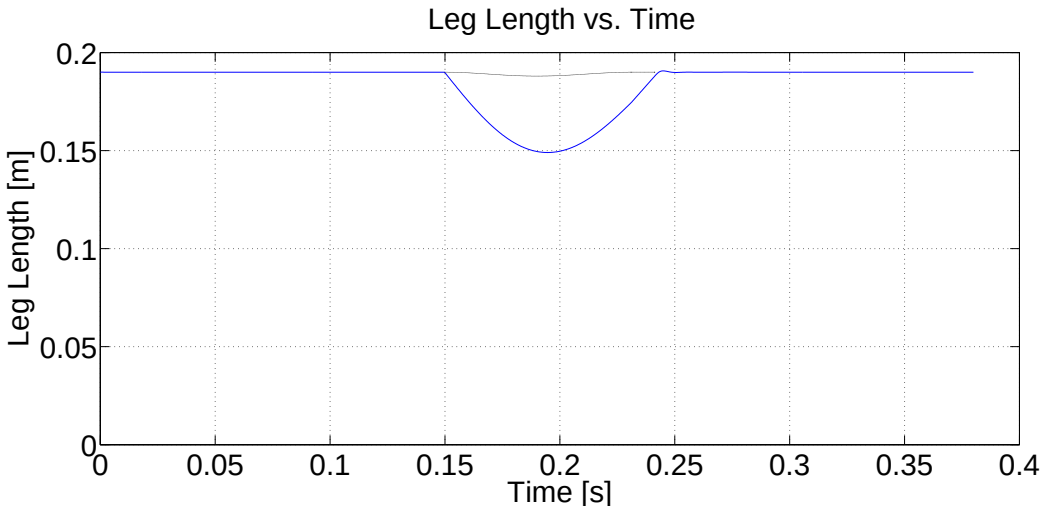

Figure 6.7: The leg length vs time of a system with the initial leg angle 0^o, the initial horizontal speed 0 m/s and the damping coefficient 3 Ns/m in a single jump is plotted. The other initial conditions and system parameters are the same as those of the other single jump simulations.

angle θ_{leg} is smaller, and the effective leg length is longer. This causes the leg stiffness to be smaller at touch-down, than in lift-off. Since the leg is shorter at touch-down, it is more stiff. This effect can be seen in Figure 6.10.

This figure presents the leg stiffness in the four scenarios mentioned before. In the cases with an initial horizontal speed of 0.6 m/s and leg angle of 20^o, the leg stiffness differences between the touch-down and lift-off are clear. The leg begins the stance phase with a shorter effective length so it is more stiff at the beginning of the stance phase. As it leaves the ground, the effective length has increased so the stiffness is smaller at the end of the stance phase. Between these two events, the stiffness increases and decreases again. This is because the leg stiffness is a function of the leg radius and the leg angle, as proven in Chapter 5. The leg radius first decreases and then increases during stance, due to the compression and decompression.

In the cases with zero initial speed and zero leg angle, the stiffness plot has another increasing part just before lift-off. This can be explained by the phases the leg goes through, within the stance phase. As explained before, the leg can be in three phases during motion: Flight, rolling stance and end point stance. In the stance mode, if the leg is touching the ground with its end point, then rolling cannot occur but the

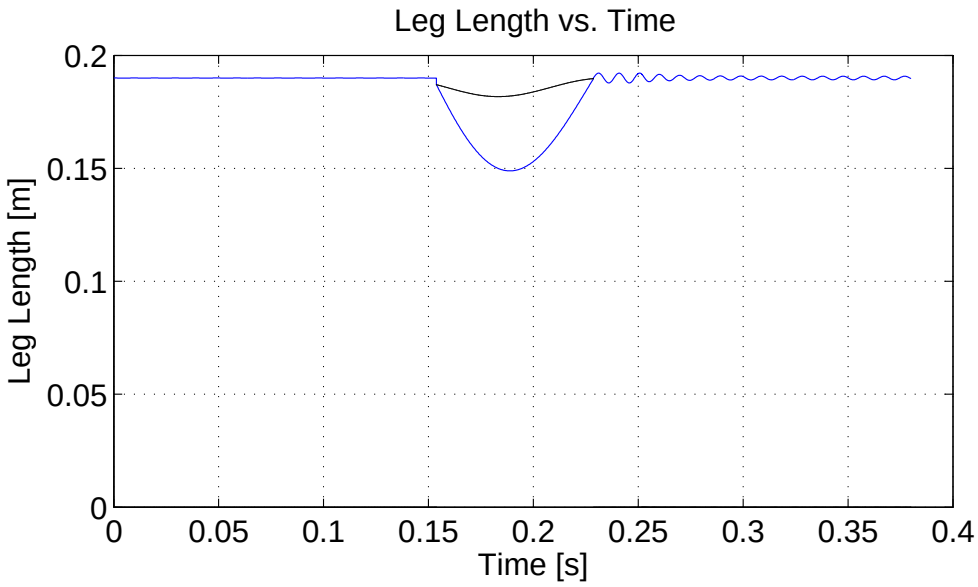

Figure 6.8: The leg length vs time of a system with the initial leg angle 20^o, the initial horizontal speed 0.6 m/s and the damping coefficient 0 Ns/m in a single jump is plotted. The other initial conditions and system parameters are the same as those of the other single jump simulations.

leg rotates around its end point. The increasing behaviour just before lift-off in the mentioned plot shows us that the leg has entered the end point stance phase before lift off. It is natural to observe this increase because the leg is in decompression just before lift-off and the stiffness is increasing due to the increase in the leg radius.

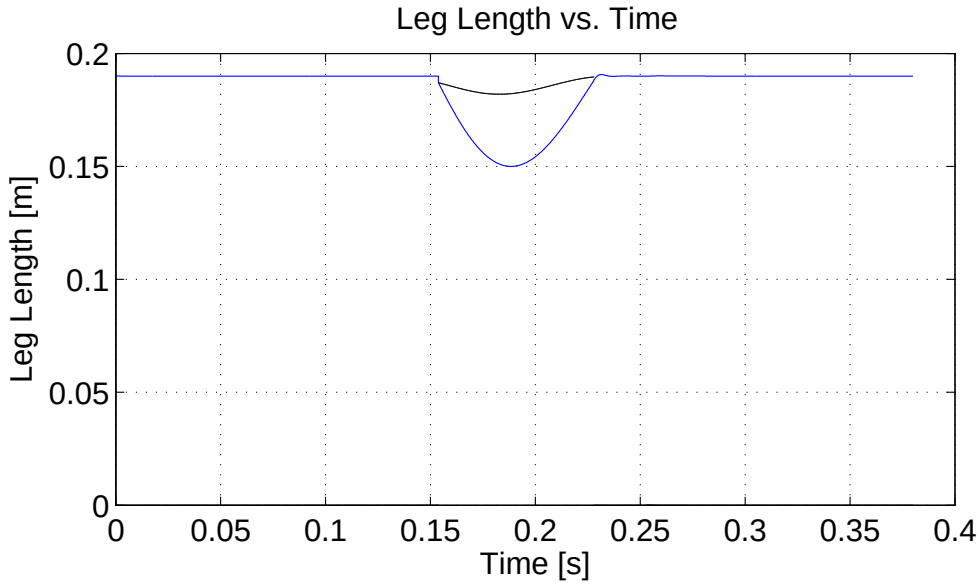

Figure 6.9: The leg length vs time of a system with the initial leg angle 20^o, the initial horizontal speed 0.6 m/s and the damping coefficient 3 Ns/m in a single jump is plotted. The other initial conditions and system parameters are the same as those of the other single jump simulations.

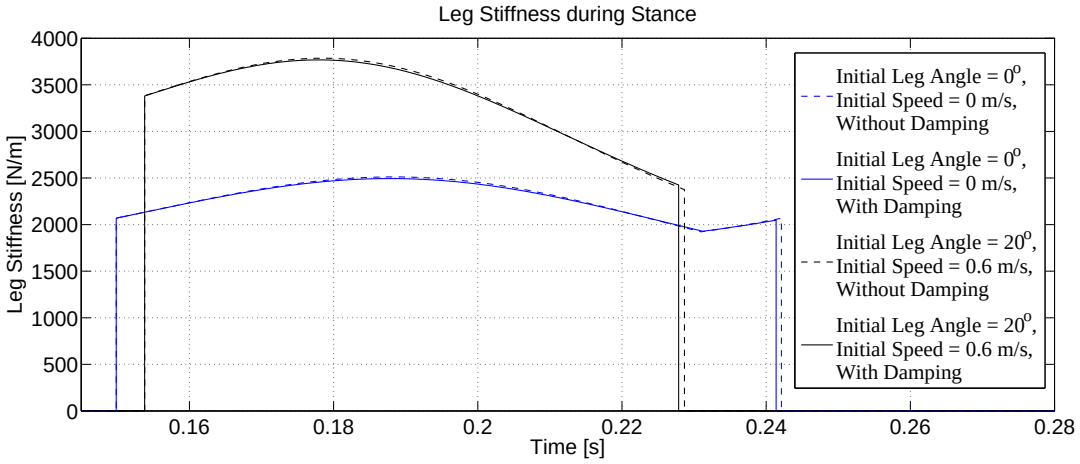

Figure 6.10: The leg stiffness vs time of a system in a single jump are plotted for the four scenarios which are noted on the figure legend. In the cases with damping, the damping coefficient d is taken as 3 Ns/m. The other initial conditions and system parameters are the same as those of the other single jump simulations.

6.3.2 Successive Jumps without a Controller

After analysing a single jump, we wonder about the changes in the observed variables during successive jumps. In the previous subsection, we stopped the simulation when the body height reached another peak value, in order to observe the variables like the body position, the leg length and the leg stiffness in a single jump. In this subsection we do not stop the simulation but leave the system free to move as long as it can. We can see the behaviour of the uncontrolled system this way. We observe body position, body horizontal speed and energy changes during successive jumps.

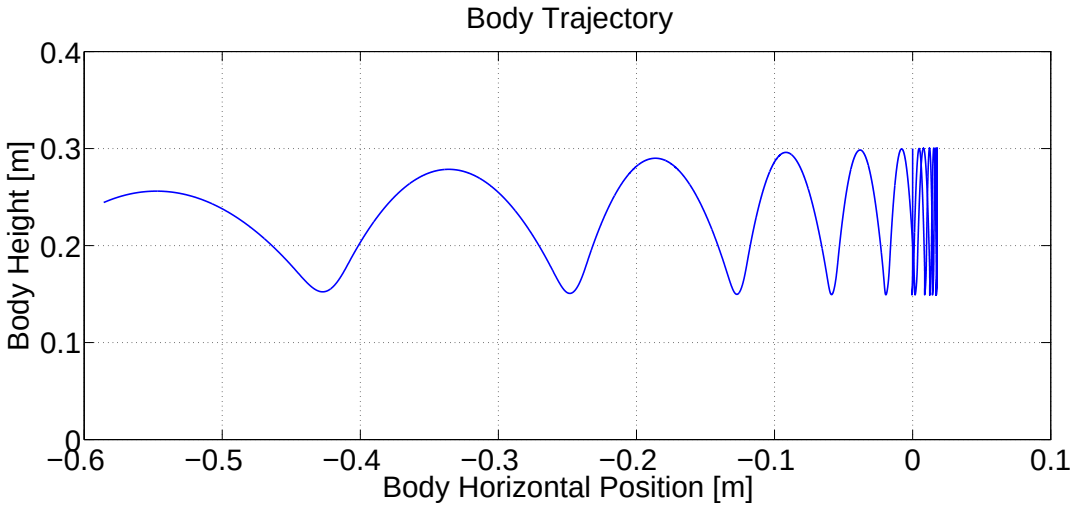

Figure 6.11: The body trajectory of a system experiencing several jumps without a controller. The initial horizontal speed is 0 m/s and the leg touch-down angle is 15^o. The damping coefficient is 0 Ns/m.

First let us choose the initial conditions as follows: the initial body horizontal position 0 m, the initial body height 0.3 m, the initial horizontal speed 0 m/s, the initial vertical speed 0 m/s and the touch-down angle 15^o. The body trajectory of a system with these initial conditions and no damping is plotted in Figure 6.11. As seen in the plot, the system jumps almost vertically for several times and then it gains negative horizontal speed and falls down after a while. The system is not symmetric; the leg length and the leg angle are different at touch-down and lift-off, as seen in the previous subsection. This is how the horizontal speed of the system can change after a while. If the leg angle is around 15^o, then it can jump vertically for a long time

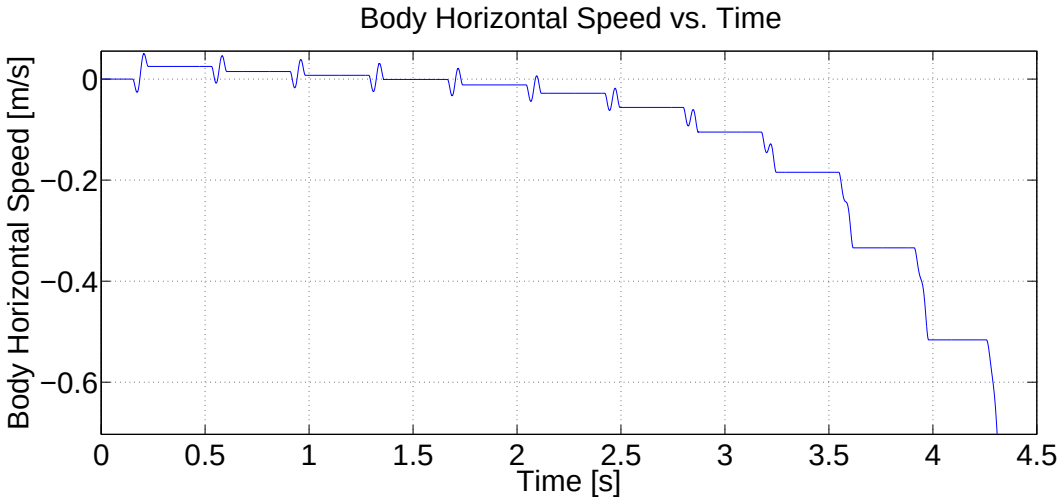

Figure 6.12: The horizontal speed of a system experiencing several jumps without a controller. The initial horizontal speed is 0 m/s and the leg touch-down angle is 15^o. The damping coefficient is 0 Ns/m.

before gaining horizontal speed in either direction. If it is smaller than 15^o then the system tends to gain positive horizontal speed. Otherwise, the system tends to gain negative horizontal speed. Once the horizontal speed starts increasing or decreasing, it gets faster and faster in subsequent jumps. This is clearly seen in the horizontal speed plot of the same simulation with these initial conditions, as presented in Figure 6.12.

The sum of potential and kinetic energies of this system is plotted in Figure 6.13. This system is not controlled, and no torque is applied on the legs during stance. So the sum of potential and kinetic energies is expected to stay constant during motion, except for the stance phases. In stance phase during compression, the total energy decreases because it is spent to load the spring-like leg with spring potential energy. The spring releases this energy in decompression, so the energy reaches somewhere near to its previous value at the end of the stance phase. The sharp falls on the total energy plot represent the stance phases. In Figure 6.13, we can see that the energy stays almost constant during the whole motion.

With the same initial conditions but with a damping coefficient of 3 Ns/m, the body

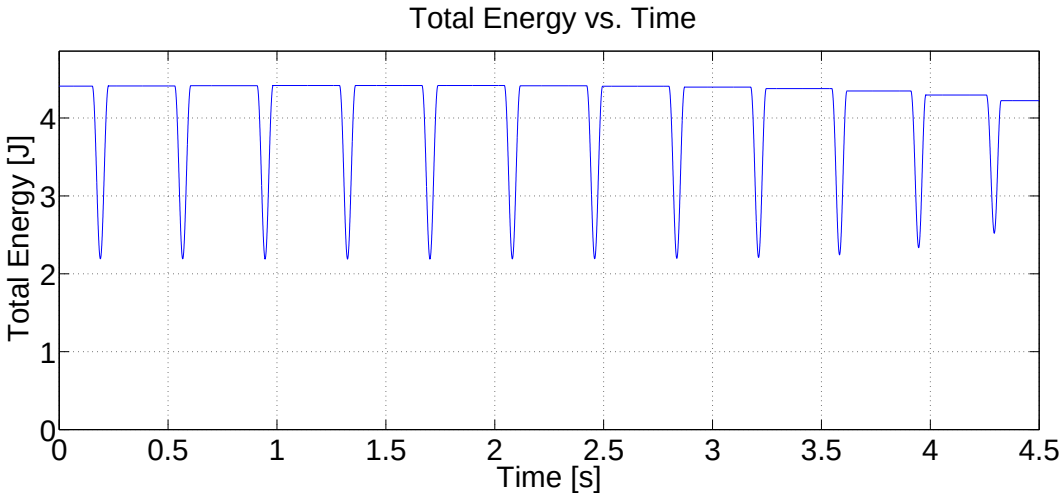

Figure 6.13: The sum of kinetic and potential energies of a system experiencing several jumps without a controller. The initial horizontal speed is 0 m/s and the leg touchdown angle is 15^o. The damping coefficient is 0 Ns/m.

trajectory would be like in Figure 6.14. The horizontal speed for this case is plotted in Figure 6.15, and the energy plot is shown in Figure 6.16. The damping causes the system to lose energy faster, as seen in the energy plot. This energy loss causes the system to reach lower apex heights at each jump, and causes it to fall down sooner than as was in the no damping case.

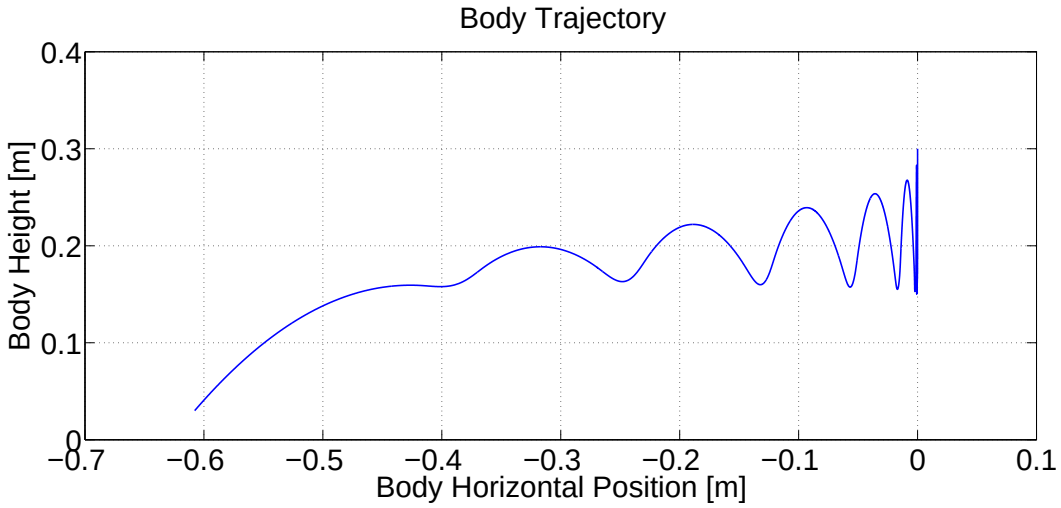

Figure 6.14: The body trajectory of a system experiencing several jumps without a controller. The initial horizontal speed is 0 m/s and the leg touch-down angle is 15^o. The damping coefficient is 3 Ns/m.

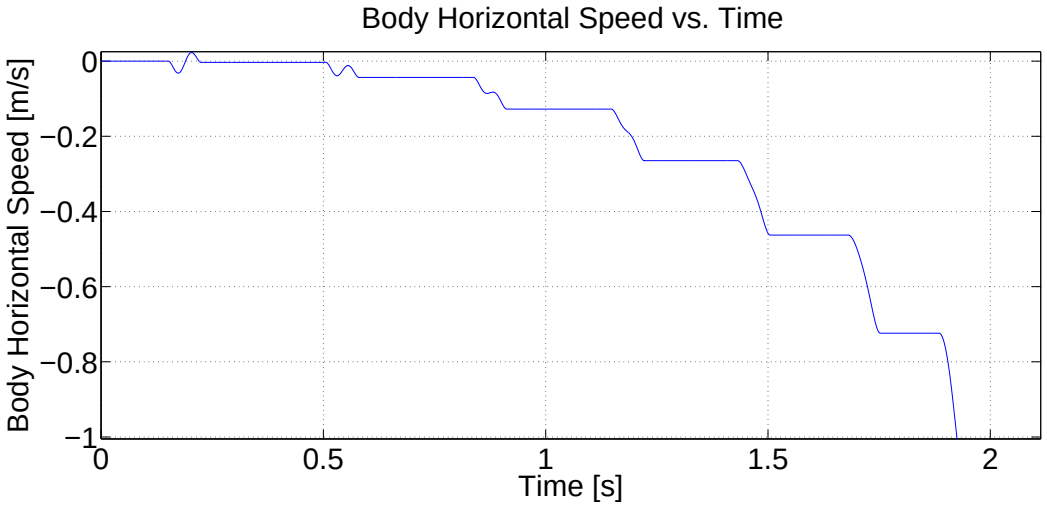

Figure 6.15: The horizontal speed of a system experiencing several jumps without a controller. The initial horizontal speed is 0 m/s and the leg touch-down angle is 15^o. The damping coefficient is 3 Ns/m.

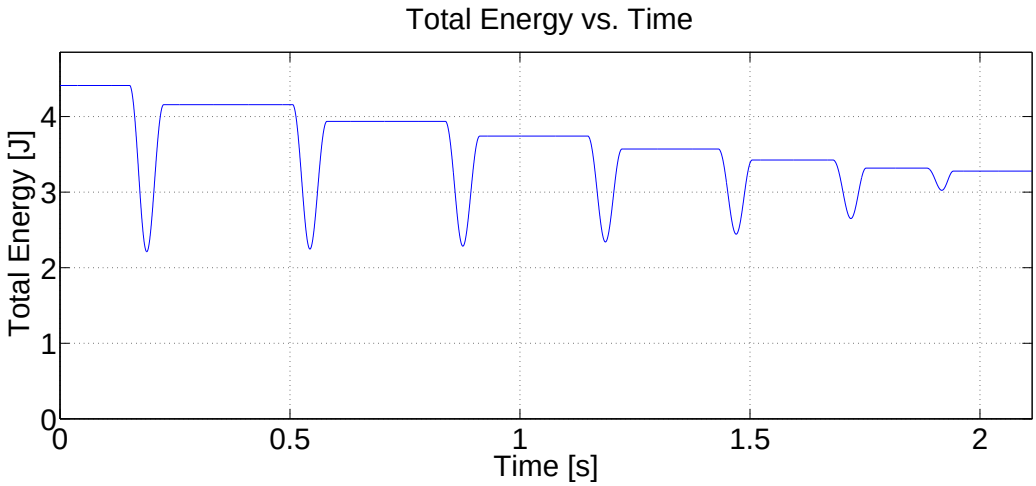

Figure 6.16: The sum of kinetic and potential energies of a system experiencing several jumps without a controller. The initial horizontal speed is 0 m/s and the leg touchdown angle is 15^o. The damping coefficient is 3 Ns/m.

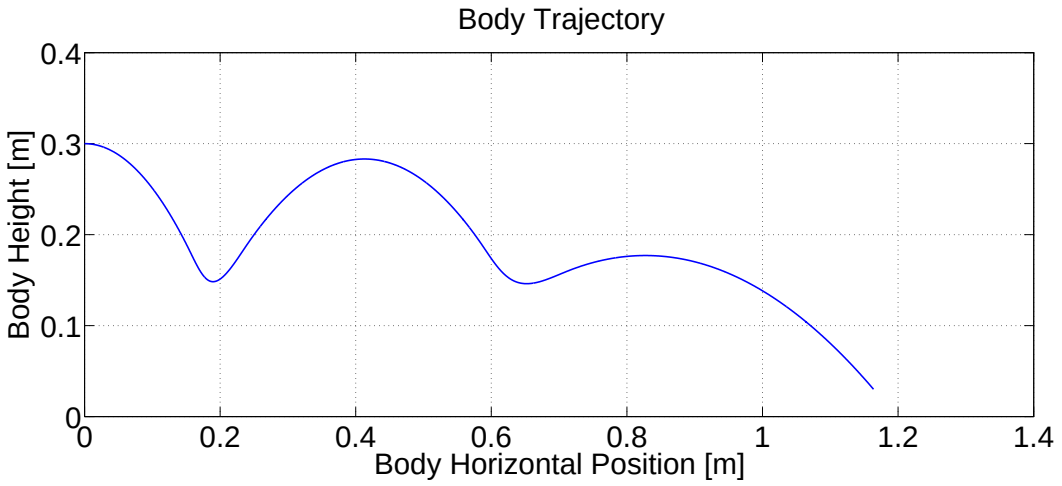

Figure 6.17: The body trajectory of a system experiencing several jumps without a controller. The initial horizontal speed is 1 m/s and the leg touch-down angle is 20^o. The damping coefficient is 0 Ns/m.

Now let us change the following initial conditions and keep the rest constant: the initial horizontal speed 1 m/s, the leg touch-down angle 20^o. The body trajectory for these new initial conditions and no damping is shown in Figure 6.17. The horizontal speed is plotted in Figure 6.18 and the sum of the potential and the kinetic energies is shown in Figure 6.19. In this case the horizontal speed is increasing at each jump, which means the kinetic energy is increasing. So the potential energy has to decrease, which leads to a decrease in the apex heights at each jump. As for the small increase in the total energy plot, it is because of the model inaccuracies. These inaccuracies are due to the assumptions made while deriving the dynamic equations and the stiffness relation. The effect of the model inaccuracies can be compensated by adding a small amount of damping to the system. The plots for the same initial conditions with damping coefficient being 3 Ns/m are shown in Figures 6.20 - 6.22. In the case with damping, the increase in the horizontal speed is slower. So the apex heights are higher for a longer time and the system experiences several more jumps in the damped case, compared to the no damping case.

In a perfect system, the total of the kinetic and potential energies of the body at

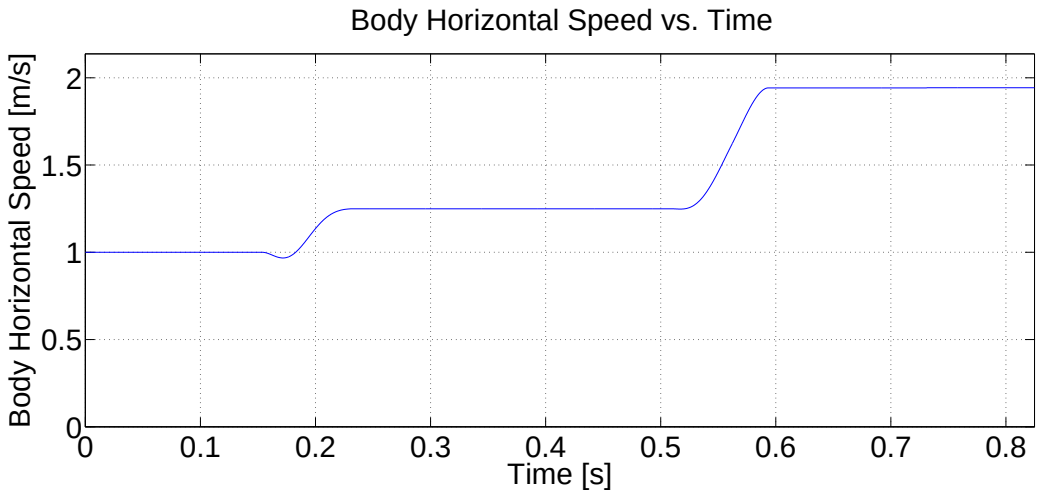

Figure 6.18: The horizontal speed of a system experiencing several jumps without a controller. The initial horizontal speed is 1 m/s and the leg touch-down angle is 20^o. The damping coefficient is 0 Ns/m.

all the flight phases in a simulation could have stayed the same. However we know that we have made a lot of assumptions in this model. Also, there are energy losses because of damping and energy gains because of the torques applied to the system. This is why the energy at the flight phases does not stay the same, but still have similar values in successive jumps.

Here it is important to note that there is no controller for pushing the system to a steady-state behaviour. However we need to bring the leg to the chosen touch-down angle after each jump. So a certain amount of torque is always applied at the leg, during the flight phase for getting the leg ready for the next touch-down with the desired angle. But this torque is a very small torque, since the toe mass is chosen to be very small compared to the body mass.

In all these plots presented in this subsection, the leg is uncontrolled, so it falls down after several jumps. But if it is controlled, then the motion can continue for a longer time. This is the case presented in the following subsection.

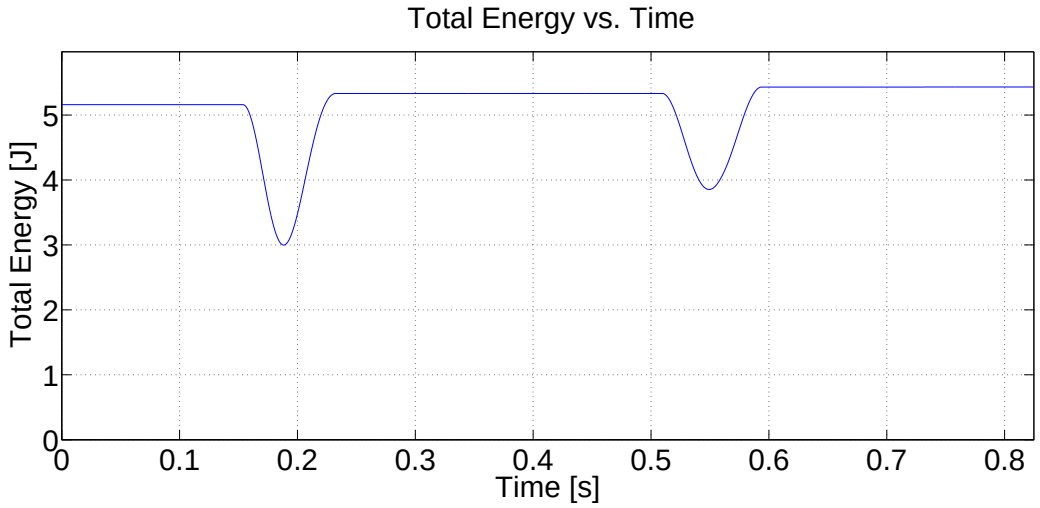

Figure 6.19: The sum of kinetic and potential energies of a system experiencing several jumps without a controller. The initial horizontal speed is 1 m/s and the leg touch-down angle is 20^o. The damping coefficient is 0 Ns/m.

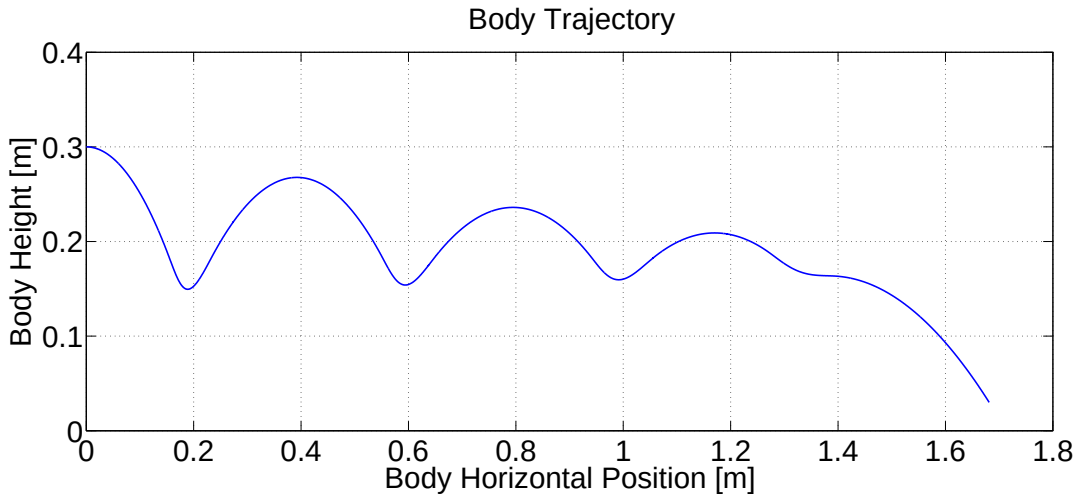

Figure 6.20: The body trajectory of a system experiencing several jumps without a controller. The initial horizontal speed is 1 m/s and the leg touch-down angle is 20^o. The damping coefficient is 3 Ns/m.

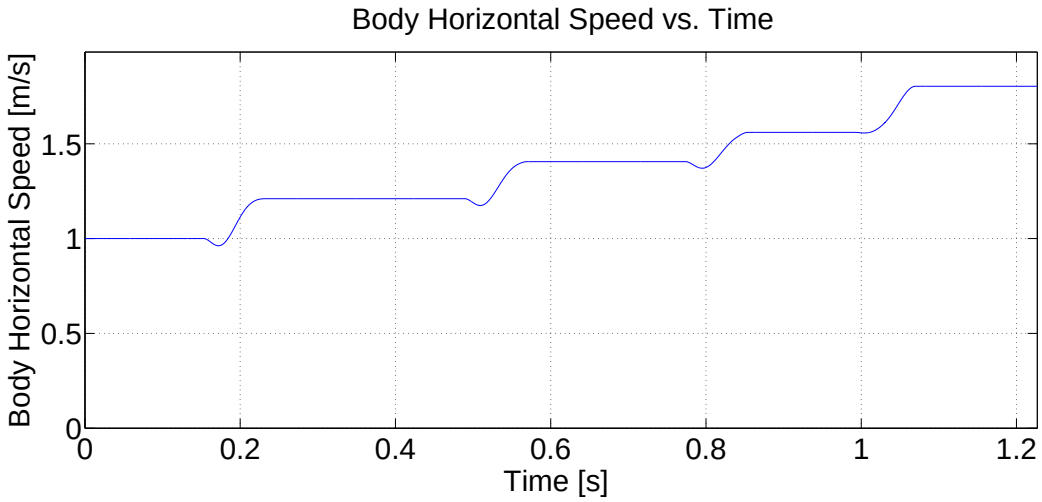

Figure 6.21: The horizontal speed of a system experiencing several jumps without a controller. The initial horizontal speed is 1 m/s and the leg touch-down angle is 20^o. The damping coefficient is 3 Ns/m.

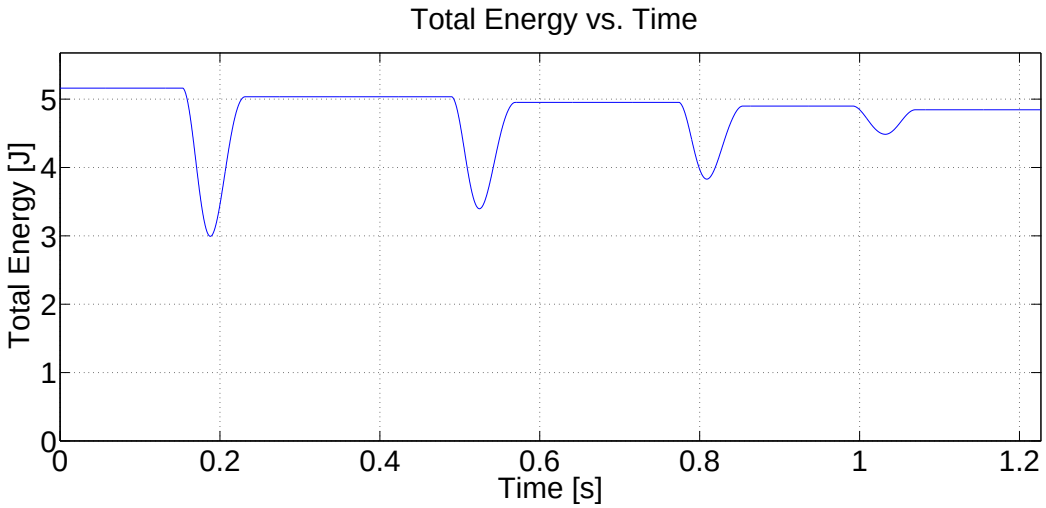

Figure 6.22: The sum of kinetic and potential energies of a system experiencing several jumps without a controller. The initial horizontal speed is 1 m/s and the leg touch-down angle is 20^o. The damping coefficient is 3 Ns/m.

6.3.3 Steady State Behaviour with a Controller

In the previous simulations we have seen the behaviour of a single legged hopping system which is thrown from a certain height. In this subsection we are going to integrate a controller to this system and observe the behaviour under the effect of this controller. The controller which is used here is the same as the one used in Chapter 4. It is a simple proportional controller which is designed to bring the system to a desired horizontal speed. It applies the necessary amount of torque to the legs during stance phase.

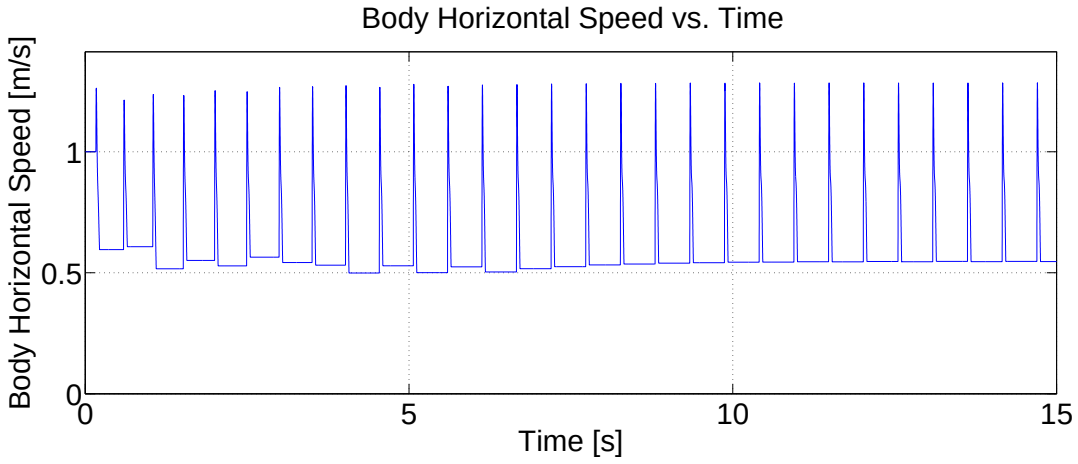

Figure 6.23: The horizontal speed vs time plot of a system with a simple proportional controller which aims to bring the horizontal speed to 1.8 m/s. The initial height is 0.3 m, the initial speed is 1 m/s, the leg touch-down angle is 40^o. The damping coefficient d = 0 Ns/m.

First let us choose the initial conditions as follows: The initial horizontal position 0 m, the initial height 0.3 m, the initial horizontal speed 1 m/s, the initial vertical speed 0 m/s and the leg touch-down angle 40^o. And let us choose the desired horizontal speed for the controller as 1.8 m/s. Figure 6.23 shows the horizontal speed vs time plot for this case without damping. As seen in the figure, the horizontal speed achieves a steady state value, although there is considerable amount of steady state error. The body height vs time plot for the same case is presented in Figure 6.24. Here we see that also the body height reaches a steady state value. So we expect to see the energy

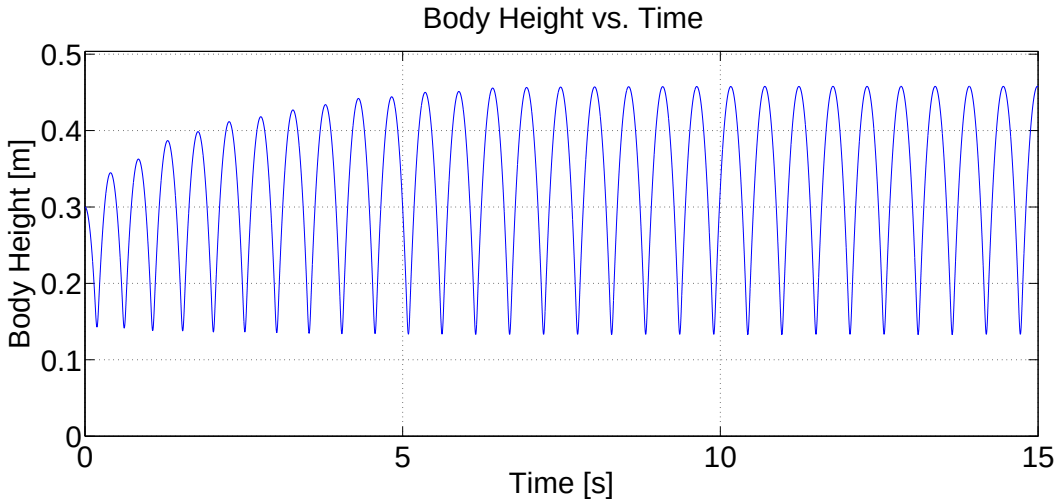

Figure 6.24: The body height vs time plot of a system with a simple proportional controller which aims to bring the horizontal speed to 1.8 m/s. The initial height is 0.3 m, the initial speed is 1 m/s, the leg touch-down angle is 40^o. The damping coefficient d = 0 Ns/m.

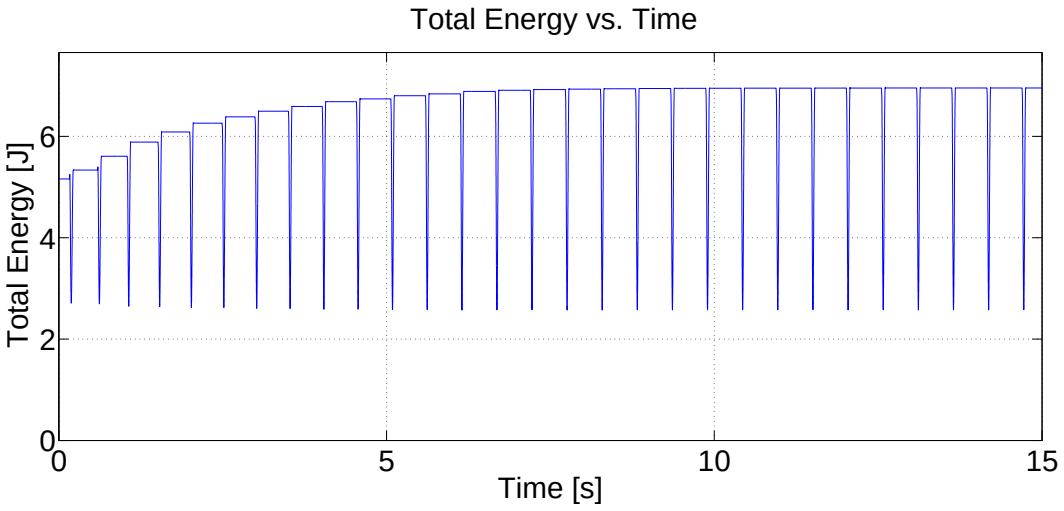

Figure 6.25: The sum of kinetic and potential energies vs time plot of a system with a simple proportional controller which aims to bring the horizontal speed to 1.8 m/s. The initial height is 0.3 m, the initial speed is 1 m/s, the leg touch-down angle is 40^o. The damping coefficient d = 0 Ns/m.

plot to reach a steady state value as well, since the energy is the sum of the kinetic and potential energies, which are calculated using the body speed and the body height respectively. The energy plot presented in Figure 6.25 confirms this guess.

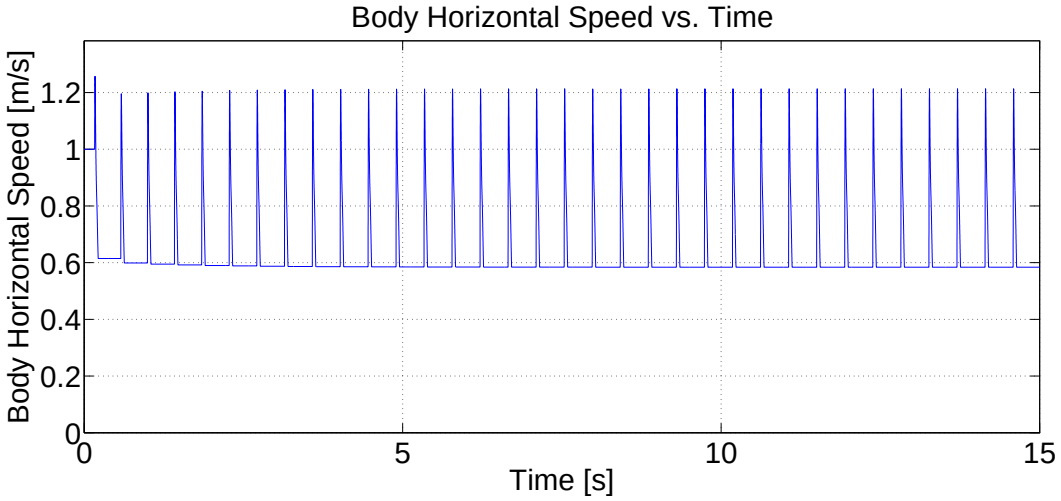

Figure 6.26: The horizontal speed vs time plot of a system with a simple proportional controller which aims to bring the horizontal speed to 1.8 m/s. The initial height is 0.3 m, the initial speed is 1 m/s, the leg touch-down angle is 40^o. The damping coefficient d = 3 Ns/m.

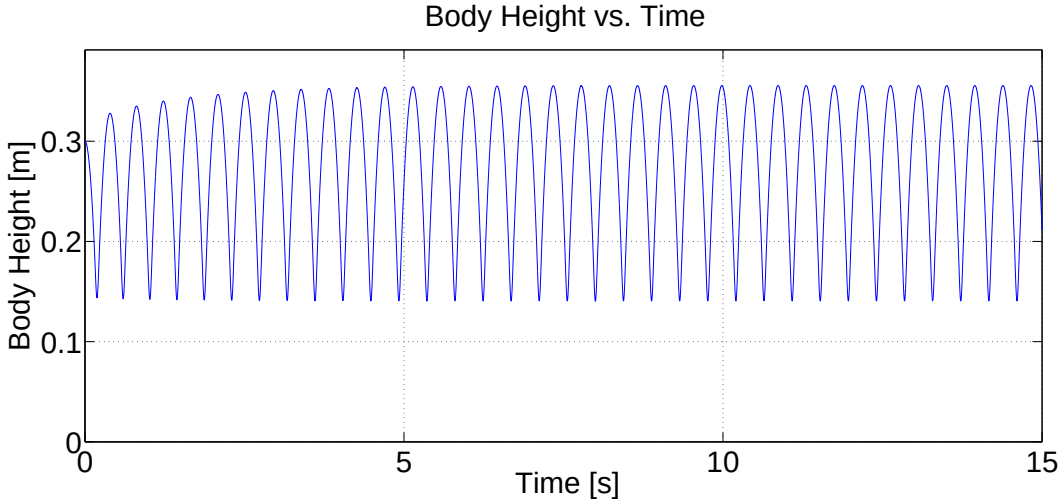

Figure 6.27: The body height vs time plot of a system with a simple proportional controller which aims to bring the horizontal speed to 1.8 m/s. The initial height is 0.3 m, the initial speed is 1 m/s, the leg touch-down angle is 40^o. The damping coefficient d = 3 Ns/m.

Setting the damping coefficient as 3 Ns/m, we obtain the horizontal speed vs time plot as in Figure 6.26. As seen in the figure, the damping does not increase the performance of the system in terms of reaching the desired horizontal speed very much. However, it makes the system reach the steady state value sooner. If we check the body height

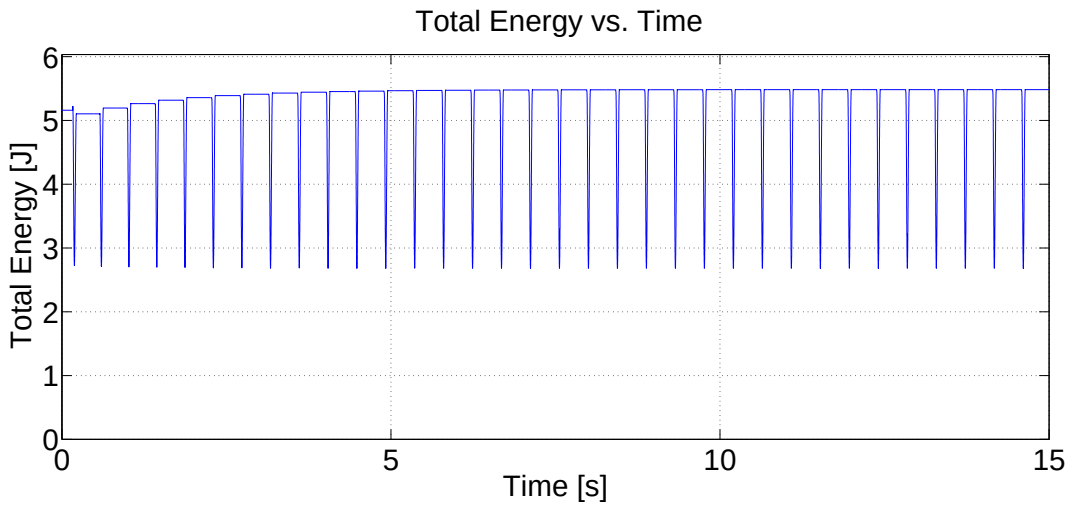

Figure 6.28: The sum of kinetic and potential energies vs time plot of a system with a simple proportional controller which aims to bring the horizontal speed to 1.8 m/s. The initial height is 0.3 m, the initial speed is 1 m/s, the leg touch-down angle is 40^o. The damping coefficient d = 3 Ns/m.

vs time plot in Figure 6.27, we see that the body height converges to a smaller value. This means the energy must be used more efficiently, so the steady state energy value should be less than the one in the no damping case. This is confirmed by the energy plot in Figure 6.28.

The controller was first used for the straight leg model and it was seen that it works for the straight leg model. In this subsection, we did not aim to find a successful controller for the half circular compliant leg model, but only wanted to see how this controller works for our new model. From the results, we can say that the controller which works well for the straight leg model still makes the half circular compliant leg reach a steady state. But the steady state error is very high, and some improvements on the controller is necessary, if the half circular compliant leg is desired to be controlled. These experiments were useful to prove that the new leg model is successfully working with a controller, and it can be used for controller design problems in the future.

6.3.4 Comparison of the Straight Leg and the Half Circular Compliant Leg Models

In this subsection, we aim to compare the two models: the straight leg model and the half circular leg model. For this, we use the same simulation environment and run simulations with both models, using the same initial conditions and similar system parameters.

Naturally, the system parameters of the two systems are not exactly the same. For example, the rest length of the spring in the straight leg model is a constant, since it uses a linear spring. However in the half circular compliant leg model, the rest length of the spring is a function of the leg angle, as proven in Chapter 5. Also, the leg stiffness is a constant in the straight leg model. However in the half circular leg model the leg stiffness is calculated from the leg angle, the leg radius and some more system parameters. These new system parameters include the modulus of elasticity, which does not exist in the straight leg model. So these are the examples to the differences between the parameters of the two systems. Despite the differences, it is possible to create similar simulation conditions for the two systems.

In the comparison simulations presented here, first the simulations with the half circular compliant leg were run. A leg stiffness vs time plot was obtained. The average of the leg stiffness values observed in this plot was used as the stiffness constant for the straight leg model, in the simulations corresponding to the same initial conditions. The same procedure was applied to the leg length, which was constant in the straight leg model but varying in the half circular compliant leg model. So similar system parameters were tried to be obtained this way.

The first comparison case has the following initial conditions: The initial horizontal position 0 m, the initial height 0.3 m, the initial horizontal speed 1 m/s, the initial vertical speed 0 m/s and the leg touch-down angle 40^o. The damping coefficient d = 0 Ns/m. The desired horizontal speed is 1.8 m/s, and the same controller is used for both models. The horizontal speed vs time plots for this case with both the half circular compliant leg and the straight leg are seen in Figure 6.29. As seen in the figure, the straight leg model reaches the desired horizontal speed, while the half circular leg

model reaches another horizontal speed value with a considerable steady state error. When we check the body height vs time plots for this case in Figure 6.30, we see that the half circular compliant leg model reaches a steady state body height value but the straight leg model does not. The body height of the straight leg model increases continuously, so we expect the energy plot to be increasing for the straight leg model as well. Figure 6.31 shows the comparison of the sum of kinetic and potential energies for the two models. As seen from these figures, the controller which brings the half circular compliant leg to a steady state body height cannot make it with the straight leg model, at least within the first 15 seconds of the simulation. However the same controller is successful at reaching the desired horizontal speed value for the straight leg model but results in considerable steady state error with the half circular compliant leg.

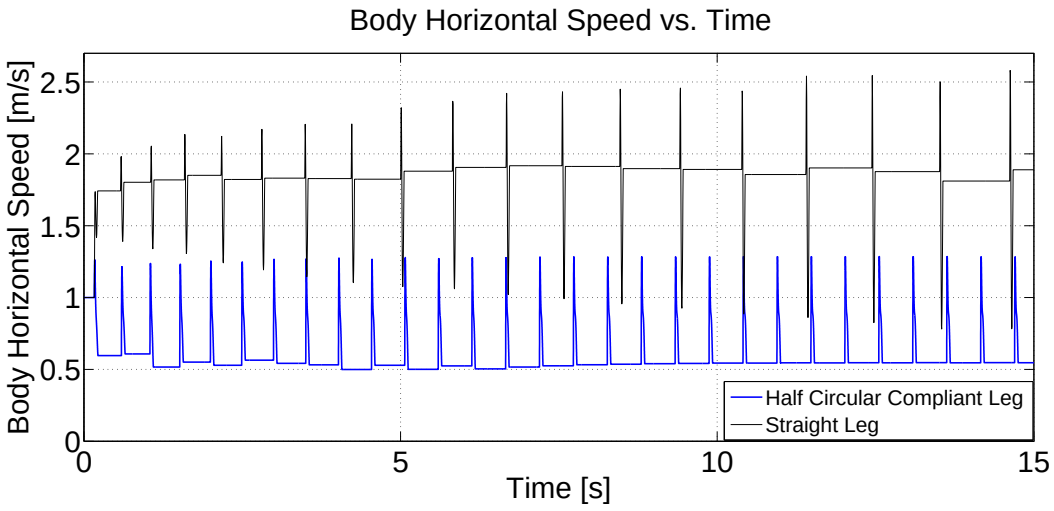

Figure 6.29: The horizontal speed vs time plot for the two models: The straight leg model and the half circular compliant leg model. The simulations are run with the same initial conditions and similar system parameters, and with the same controller which aims to bring the system to a desired horizontal speed of 1.8 m/s. The damping coefficient d = 0 Ns/m.

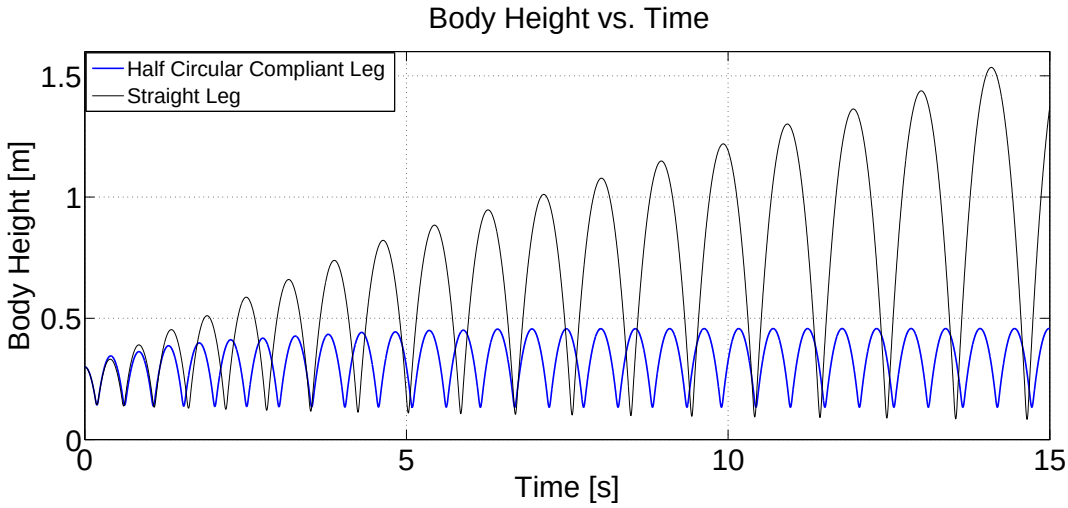

Figure 6.30: The body height vs time plot for the two models: The straight leg model and the half circular compliant leg model. The simulations are run with the same initial conditions and similar system parameters, and with the same controller which aims to bring the system to a desired horizontal speed of 1.8 m/s. The damping coefficient d = 0 Ns/m.

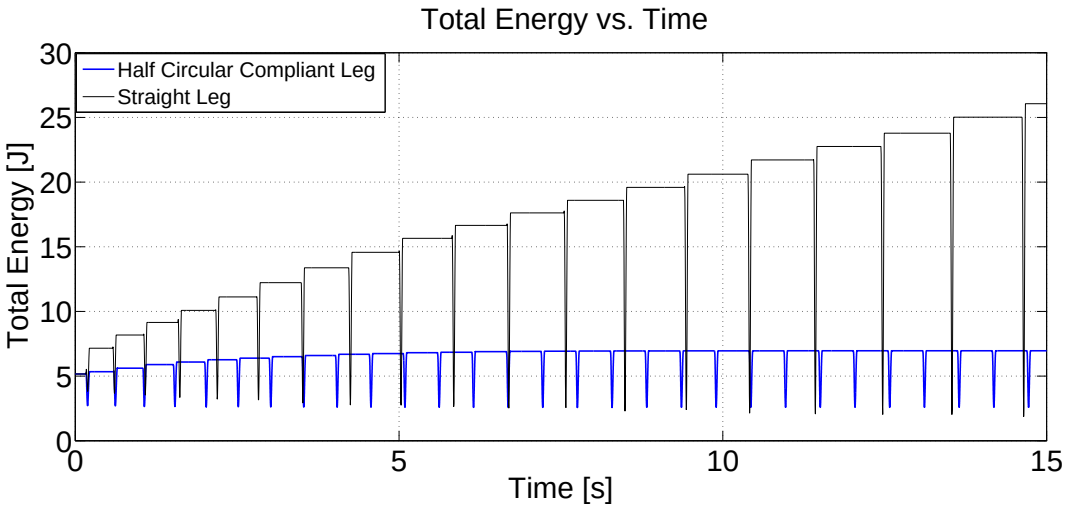

Figure 6.31: The sum of kinetic and potential energies vs time plot for the two models: The straight leg model and the half circular compliant leg model. The simulations are run with the same initial conditions and similar system parameters, and with the same controller which aims to bring the system to a desired horizontal speed of 1.8 m/s. The damping coefficient d = 0 Ns/m.

The same initial conditions and controller are used for another simulations, this time with the damping coefficient being 3 Ns/m. The results are seen in Figures 6.32 - 6.34. The results show that the same controller performs far better with the same system parameters with the straight leg, if there is damping in the system. The difference between the two models in the body height and the energy plots are less with damping. The straight leg model even seems to be converging to a steady state body height value. Also, the desired horizontal speeds are achieved sooner than in the case with no damping.

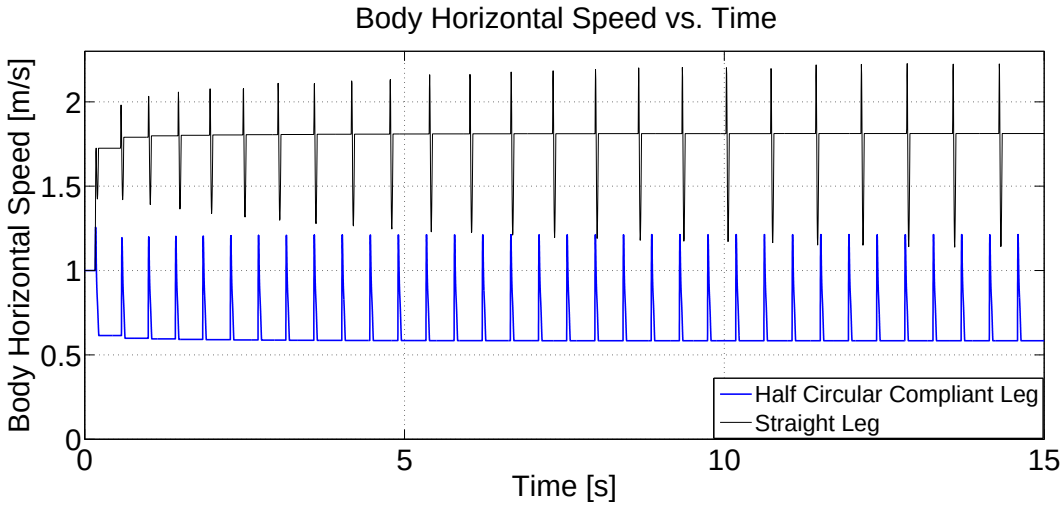

Figure 6.32: The horizontal speed vs time plot for the two models: The straight leg model and the half circular compliant leg model. The simulations are run with the same initial conditions and similar system parameters, and with the same controller which aims to bring the system to a desired horizontal speed of 1.8 m/s. The damping coefficient d = 3 Ns/m.

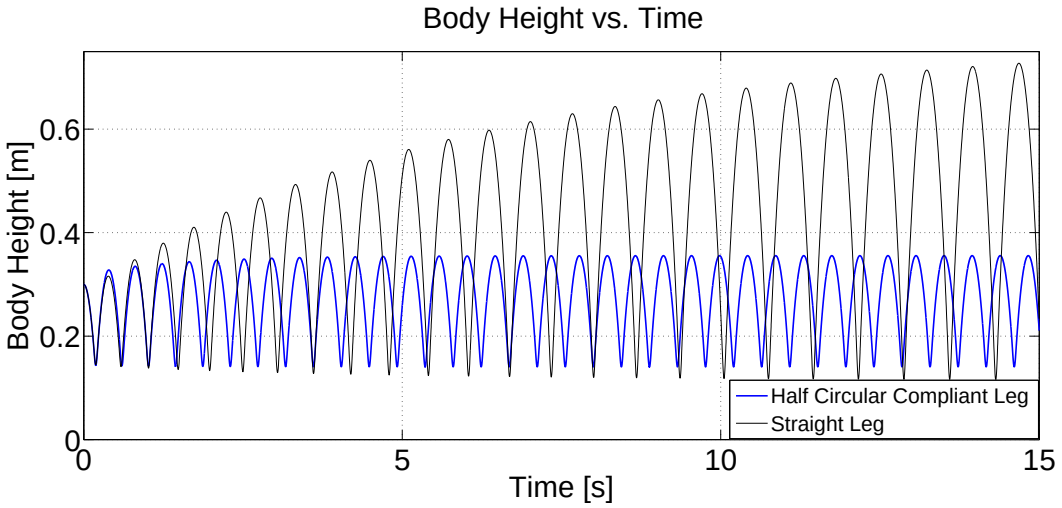

Figure 6.33: The body height vs time plot for the two models: The straight leg model and the half circular compliant leg model. The simulations are run with the same initial conditions and similar system parameters, and with the same controller which aims to bring the system to a desired horizontal speed of 1.8 m/s. The damping coefficient d = 3 Ns/m.

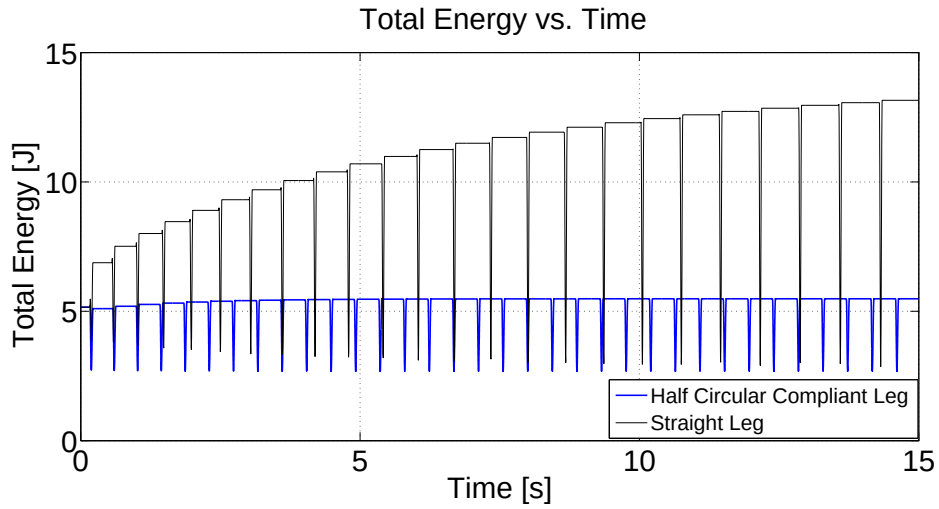

Figure 6.34: The sum of kinetic and potential energies vs time plot for the two models: The straight leg model and the half circular compliant leg model. The simulations are run with the same initial conditions and similar system parameters, and with the same controller which aims to bring the system to a desired horizontal speed of 1.8 m/s. The damping coefficient d = 3 Ns/m.

6.3.5 Initial Condition Sensitivity

In this subsection, we are going to investigate the dependence of the outputs to the initial conditions. For this, we are going to run the simulations many times with different initial conditions and we are going to observe if or when the system is reaching a steady state. This analysis will give us the sensitivity of the new model and the used controller to the initial conditions that are set at the beginning.

The controller that is used to simulate a steady state behaviour in the previous subsections aims to bring the single legged hopping system to a desired horizontal speed. So the time of convergence to the steady state horizontal speed will be the performance criterion in this analysis. The observed initial conditions are chosen to be the initial horizontal speed and the initial height of the body. These initial conditions are set to different values and the results are observed for each combination. The initial horizontal speed is set to 0.8, 0.9, 1.0, 1.1 and 1.2 m/s, and the initial body height is set to 0.20, 0.25, 0.30, 0.35, 0.40 m. So, 25 simulations are done in total. The results of these simulations, in terms of the convergence time, are listed in Table 6.1 for the no damping case and in Table 6.2 for the case with the damping coefficient being d = 6 Ns/m. As for the other system parameters and the initial conditions, they are kept as presented in the previous subsections before.

In order to measure the convergence times, the horizontal speed plots are analysed. The convergence time is the time it takes for the system to reach a horizontal speed value within a band around the steady state horizontal speed value with $\mp 1\%$ error. (In Table 6.1, the values marked with an asterisk are calculated according to the $\mp 2\%$ band because 1% accuracy could not be achieved although the system reached steady state.)

The convergence times presented in these tables are measured in order to see if the controller used in this study is sensitive to the initial conditions. The results show that in all combinations considered, the controller achieves to reach a steady state value. In the tested cases, no divergence is observed. The cases with damping reach the steady state sooner, as was observed in the previous subsections as well.

Table 6.1: Convergence Time [s] for 25 Simulations with the Half Circular Compliant Leg Model. (The damping coefficient d = 0 Ns/m)

		Initial Height [m]				
		0.20	**0.25**	**0.30**	**0.35**	**0.40**
Initial Horizontal Speed [m/s]	**0.8**	11.3	10.7	8.8	8.5	6.6
	0.9	10.3	10.7	9.4	8.0	6.6
	1	10.3	10.7	9.4	9.1	5.6
	1.1	11.4	10.7*	10.5*	8.1	8.3
	1.2	10.3	10.2*	8.9	8.1	4.0

Table 6.2: Convergence Time [s] for 25 Simulations with the Half Circular Compliant Leg Model. (The damping coefficient d = 6 Ns/m)

		Initial Height [m]				
		0.20	**0.25**	**0.30**	**0.35**	**0.40**
Initial Horizontal Speed [m/s]	**0.8**	2.4	2.0	0.2	2.3	3.2
	0.9	2.5	2.0	0.2	2.7	3.2
	1	2.5	1.6	1.0	2.7	3.2
	1.1	2.5	1.6	1.4	2.7	3.2
	1.2	2.5	1.3	1.4	2.7	3.6

6.3.6 Behavioural Change due to the Modulus of Elasticity

In this subsection, the effect of one system parameter on the behaviour of the half circular compliant legged system is observed. This is done by running several simulations, changing that parameter and keeping the rest of the system parameters and the initial conditions constant. This system parameter is chosen to be the modulus of elasticity, E.

The modulus of elasticity is chosen to be the observed parameter since it is directly related to the stiffness of the leg. In the calculation of the leg stiffness, the modulus of elasticity is an important constant. It is a constant related to the leg material. In the simulations until now, a reasonable and average modulus of elasticity value (22 GPa) was used. In an actual experiment set up, it is possible to use different legs having different modulus of elasticities. Therefore we would like to know how our new leg model reacts to the changes in this parameter.

Table 6.3: The Convergence Time [s] and the Stiffness Range [N/m] for Different Modulus of Elasticity [GPa] Values (without Damping)

Modulus of Elasticity (E) [GPa]	$t_{steadystate}$ **[s]**	k_{min} **-** k_{max} **[N/m]**
21.1	10.4	3400-6400
21.2	10.4	3400-6300
21.3	6.7	3400-6300
21.4	no convergence	-
21.5	8.9	3500-6600
21.6	12.5	3500-6600
21.7	9.9	3500-6500
21.8	8.9	3600-6800
21.9	8.9	3600-6800
22.0	9.4	3600-6800

In Table 6.3 the effect of the modulus of elasticity value on the convergence time and on the leg stiffness are seen, for the no damping case. The convergence time does not follow a significant pattern, so in the no damping case the modulus of elasticity seems to have no effect on the convergence time. However the leg stiffness value is directly related to the modulus of elasticity. In the last column of this table, the maximum and minimum leg stiffness values reached at steady state are shown. The increase in the leg stiffness values together with an increase in the modulus of elasticity is observed.

In Table 6.4, the same cases are simulated with a damping coefficient of 6 Ns/m. The convergence times are remarkably lower as a result of damping. But in this table, with the greater modulus of elasticity (therefore stiffness) values, smaller convergence times are observed. So the damping might be playing a role in making this effect more obvious. The positive effect of damping on the system stability was observed in the previous simulations as well.

Table 6.4: The Convergence Time [s] and the Stiffness Range [N/m] for Different Modulus of Elasticity [GPa] Values (with Damping)

Modulus of Elasticity (E) [GPa]	$t_{steadystate}$ **[s]**	k_{min} **-** k_{max} **[N/m]**
21.1	1.4	3600-6200
21.2	1.4	3600-6200
21.3	1.4	3600-6200
21.4	1.4	3700-6300
21.5	1.4	3700-6300
21.6	1.4	3700-6300
21.7	1.0	3700-6400
21.8	1.0	3700-6400
21.9	1.0	3800-6400
22.0	1.0	3800-6500

6.3.7 Model Accuracy Analysis due to the Leg Angle

In this thesis we are motivated to model the half circular compliant legs of RHex more accurately than the existing models. However, the half circular leg model also has some inaccuracies due to the assumptions and approximations made during calculations. We can understand this for example when we observe the change in the total energy of the system. The total energy of the system is calculated simply by summing the kinetic and potential energies. In a perfect model, the energy should be conserved if there is no source or loss of energy. The damping and the applied torque are the causes of energy change. A realistic energy plot is expected from a realistic model.

In this subsection, we are going to analyse the relationship between the energy plots, and the system accuracy. For this we are going to use the leg angle; for different leg angle values we are going to observe the energy plots and try to reach an opinion about the accuracy of the model. (The leg angle is measured at the hip point. It is the angle between the tangent line drawn at the hip point and the horizontal.)

For this purpose fifteen simulations are run in total, for the combinations of five leg angle values (25^o, 30^o, 35^o, 40^o, 45^o) and three damping coefficient values (0 Ns/m, 3 Ns/m, 6 Ns/m). Each simulation is run for a single jump with the same initial conditions and with no torque applied during stance. The initial energy values of all cases are the same, as the initial height and the initial speed are the same. At the end of the jump, when the body reaches the next apex height, the sum of potential and kinetic energies is calculated again and they are noted on Table 6.5 as the percentage of the initial energy.

If there is no damping we do not expect to see any change in the energy. However we see that all the values in the first column of Table 6.5 are slightly greater than 100%. So energy increase is observed in the cases with no damping. This must be because of the inaccuracies of the model. But this inaccuracy decreases as we go down the column. So we can say that as the leg angle increases, the energy plot is more realistic. This is reasonable, considering the derivation method of force-deflection relation which was explained in Chapter 5.

While deriving the force-deflection relation in Chapter 5, the potential energy was

integrated from the hip point of the leg, up to the leg-ground contact point. If the leg angle is smaller, then the leg-ground contact point is farther from the hip point. So the integration is done over a longer arc segment. This may cause more error accumulation, then it would for a larger leg angle value.

Table 6.5: The Effect of Leg Touch-Down Angle and Damping on the Energy Plots

		Damping Coefficient [Ns/m]		
		0	**3**	**6**
Leg Touch-Down Angle [o]	**25**	%103.12	%97.44	%92.55
	30	%102.88	%97.30	%92.48
	35	%102.61	%97.17	%92.40
	40	%102.30	%97.03	%92.38
	45	%101.97	%96.89	%92.38

In the second column in Table 6.5 the energy changes are listed for the five leg angle values when the damping coefficient is 3 Ns/m and the third column is for d = 6 Ns/m. In all the columns the energy percentage at the end of the jump is higher if the leg angle is smaller. Also, as the damping coefficient increases, the energy loss is higher as expected.

6.4 Discussions

The most important objective of this study is to make a more realistic dynamic model of the half circular compliant leg, compared to the previous models. For this purpose, some of the approximations made in the previous models were left out, and they were replaced with accurate calculations of the necessary variables. However it is not possible to eliminate all the approximations, and perfectly model the real world if we want to have a good and fast enough, achievable model. Especially together with the contributions of the half circular shape, even some additional approximations had to be made.

One of the most important approximations that keep the model from being perfect is the conservation of the half circular shape. At any time instant, the radius of the leg is assumed to be constant at each point along the length of the half circular leg. This means a perfect circle can be fit on the leg at any instant, even when

in compression. In the real case the leg shape can be more similar to an ellipse, while in compression. Rather than modelling the leg as a half circle, modelling it as an ellipse or another second degree polynomial could have been more realistic, but it would have meant putting additional variables in the equations and causing the need for finding new relations. This would have made the calculations harder, slower and more incomprehensible for the sake of only little more correction to this model. Fortunately, the current model and the MATLAB codes are appropriate for this possible improvement with a little more effort in the future.

The model presented in this study is a planar model since we assumed that the motion was symmetric with respect to the sagittal plane. With a planar model, we obviously cannot model the behaviours that are not symmetric with respect to the sagittal plane. However this study is considered to be a first step for a more detailed model that can possibly done in the future. In the kinematic model, the pitch angle was important but the yaw and roll angles were not of interest. In the dynamic analysis part, only a single legged robot was studied. In the future, when more legs are considered and when the lateral forces play important role, then this model can be extended to a 3-D model. The presented two dimensional model is sufficient for the current analysis.

The main contribution of this study was to simulate the half circular compliant leg more realistically than the previous linear leg model, by taking the varying leg length and the varying stiffness into account. For this, we derived the leg length and the leg stiffness as a function of the leg angle, separately in Chapter 3 and Chapter 5. The leg stiffness as a function of the leg angle $k(\theta)$ derived in this study is the main improvement after the previous model. However it is important to note that $k(\theta)$ is calculated using Castigliano's Theorem, by integration. The cross section forces are integrated from the hip point to the leg-ground contact point. What we observed from many simulations with different leg angles is that, as the contact point gets closer to the tip point of the leg, the errors in the integration in the leg force calculation accumulates. Therefore the model becomes less accurate due to the compliance being involved more. As the contact point gets closer to the hip point, the simulation results were more sensible, the energy plots were more realistic.

In general, the resulting motion in the simulations was as expected, there was almost

no error in phase transitions or almost no unrealistic or discontinuous behaviour. We can say that the model is qualitatively realistic. We can say it is quantitatively realistic as well, to some extent. This can be said by looking at the resulting plots of the important variables. However a more accurate verification can only be by making real life experiments with an actual robot having the same parameters as in the simulation. This is left as a future work, when such an experimental set-up is ready for the necessary experiments and measurements.

6.5 Concluding Remarks

The main contribution of this thesis is presented in this chapter. The model presented here is based on the SLIP model which was covered in Chapter 5 and the stiffness analysis of the half circular compliant leg which was covered in Chapter 6. The previous leg model was a straight leg model with constant stiffness. In the new model the leg length and the leg stiffness were derived as a function of the leg angle, considering the half circular leg geometry. Then these terms were replaced with the ones that were simply constants in the previous model. The simulation code had to be modified considerably, in order to be able to handle the new parameters and variables coming together with the half circular leg shape. The new model was verified with the realistic outputs from the simulations.

CHAPTER 7

CONCLUSION

In this thesis we have studied the half circular compliant legs of RHex in planar motion. In the first part, the kinematics of RHex was studied assuming rigid legs. Here the motivation was to see the effects of half circularity of the legs on the planar robot. The rest of the thesis was about modelling the compliance and the half circularity of the legs together. At the end, a single legged hopping system was simulated using the new leg model. The new leg model was developed considering the force-deflection relation for this special leg geometry and also taking the effects of rolling into account.

In the previous modelling studies, the half circular compliant leg was approximated as a linear spring with constant stiffness and constant rest length. We knew that we could model the leg more accurately if the actual leg geometry was taken into account. For this we studied the force-deflection relations for the half circular compliant leg. We derived the dynamic equations for a single legged hopping system and integrated the new relations into these dynamic equations. Then we needed a readily working simulation environment to test the new equations.

In a recent study, a single legged hopping system was simulated using the hybrid dynamic systems simulation method. This simulation environment was used for integrating our new relations and test the new leg model. In this thesis we explained the whole procedure in detail before presenting the simulation results. We made many simulations and tested the new model thoroughly in order to make sure that the model is valid and qualitatively realistic. In the last part of the thesis, we presented these simulations.

We were mostly curious about the effects of half circularity and rolling of the legs,

which could not be observed with the previous simpler models. The rolling causes the leg angle and the effective leg length to change at the same time. So even without considering compliance, the leg length should change during rolling, as a consequence of the leg geometry. Compliance is the second factor that effects the leg length, therefore the distance between the body and the leg-ground contact point. Calculating the leg length during dynamic motion was a challenge in this thesis, because these two effects had to be combined. The fact that the leg-ground contact point was also changing due to rolling was another important point. All these changes were integrated in the existing dynamic simulation of a simpler system: A spring loaded inverted pendulum (SLIP) system.

When studying the half circular compliant leg, we made an analysis using Castigliano's Theorem and derived the force-deflection relations. When implementing these relations into the existing simpler model, we had to make some assumptions and approximations. The angle of deflection was one of those approximations. The deflection was assumed to occur on the direction of the line connecting the hip point and the leg-ground contact point. This assumption was necessary for the sake of simplicity. The fact that the leg conserves its half circularity even when deflected was another important assumption. In fact, a half circular compliant element does not necessarily conserve the half circularity. But this assumption was necessary in order to apply the solution.

The simulations were realistic, and the results were mostly satisfying. When they were not, we were able to make guesses on the sources of inaccuracy. In a modelling study like this, one can always find better ways to make less approximations and to have a more accurate model. However the cost of having a perfect model of a real system is infinity. Approximations were inevitable in this model, too. More realistic behaviours can still be obtained by improving this model, with the cost of more calculational complexity.

7.1 Future Work

In this thesis we have developed a new model for the half circular compliant legs of RHex, and we compared the the new model with the previous models with simulations.

The model is shown to be qualitatively realistic, and reasonable results are obtained looking at many different outputs. The most important step towards validating this model is now comparing the results with the results of an actual experiment set up. Given the system parameters (i.e. the material properties, dimensions, etc.) and the initial conditions (i.e. the initial height, the initial horizontal speed, etc.), the results of the simulations should hold the results obtained from a similar physical system. This experiments can be done with a single legged hopper with one half circular compliant leg. The outputs of this system, which will be compared with those of the simulations can be the hopping height, step length, the changing leg radius, etc. Only the data taken from a physical test set up can tell if the new leg model is qualitatively more accurate than the previous and simpler straight leg model.

Some improvements can still be done on this new model. For example the assumptions made during the derivation of the dynamic equations can be revisited. Especially the conservation of the half circularity assumption can be replaced with an additional radius variable, resulting in an ellipsoid leg. In the real case, the leg is obviously not a perfect half circle any more, after the deflection. Also the direction of the ground reaction force can be discussed and corrected, by compromising other realistic assumptions.

If this model turns out to be accurate enough, then it can be used as a base for modelling more complex systems with half circular legs. Two or three legged planar systems can be modelled, or even a three dimensional model with more half circular compliant legs can be made.

REFERENCES

[1] M.H. Raibert, *Legged Robots that Balance*, MIT Press, 1986.

[2] U. Saranli, M. Buehler, and D. E. Koditschek, "RHex: A simple and highly mobile hexapod robot," *International Journal of Robotics Research*, vol. 20, no. 7, pp. 616–631, 2001.

[3] S. Burden, J. Clark, J. Weingarten, H. Komsuoglu, and D. Koditschek, "Heterogeneous leg stiffness and roll in dynamic running," in *Proceedings of the IEEE International Conference on Robotics and Automation*, 2007, vol. 1-10, pp. 4645–4652.

[4] S. Aoi, Y. Sato, and K. Tsuchiya, "Investigation of the effects on stability of foot rolling motion based on a simple walking model," in *Proceedings of the 2007 IEEE/RSJ International Conference on Intelligent Robots and Systems*, 2007, vol. 1-9, pp. 2993–2998.

[5] A. Seyfarth, H. Geyer, R. Blickhan, S. Lipfert, J. Rummel, Y. Minekawa, and F. Iida, "Running and walking with compliant legs," in *Proceedings of the Symposium on Fast Motions in Biomechanics and Robotics, 2005*, 2006, vol. 340, pp. 383–401.

[6] F. Hardarson, "Locomotion for difficult terrain," Tech. Rep. TRITA-MMK 1998:3, Dept. of Machine Design, Royal Institute of Technology, S-100 44 Stockholm, Sweden, 1998.

[7] S. M. Song and K. J. Waldron, *Machines That Walk: The Adaptive Suspension Vehicle*, MIT Press, 1988.

[8] J. D. Weingarten, G. A. D. Lopes, M. Buehler, R. E. Groff, and D. E. Koditschek, "Automated gait adaptation for legged robots," in *Proceedings of the IEEE International Conference on Robotics and Automation*, 2004, vol. 1- 5, pp. 2153–2158.

[9] G. C. Haynes and A. A. Rizzi, "Gaits and gait transitions for legged robots," in *Proceedings of the IEEE International Conference on Robotics and Automation*, 2006, vol. 1-10, pp. 1117–1122.

[10] J. Pratt and G. Pratt, "Intuitive control of a planar bipedal walking," in *Proceedings of the IEEE International Conference on Robotics and Automation*, 1998, vol. 1-4, pp. 2014–2021.

[11] S. H. Collins, M. Wisse, and A. Ruina, "A three-dimensional passive-dynamic walking robot with two legs and knees," *International Journal of Robotics Research*, vol. 20, no. 7, pp. 607–615, 2001.

[12] Y. Fukuoka, H. Kimura, and A. H. Cohen, "Adaptive dynamic walking of a quadruped robot on irregular terrain based on biological concepts," *International Journal of Robotics Research*, vol. 22, no. 3-4, pp. 187–202, 2003.

[13] R. Altendorfer, N. Moore, H. Komsuoglu, M. Buehler, H. B. Brown, D. McMordie, U. Saranli, R. Full, and D. E. Koditschek, "Rhex: A biologically inspired hexapod runner," *Autonomous Robots*, vol. 11, no. 3, pp. 207–213, 2001.

[14] M. Buehler, R. Battaglia, A. Cocosco, G. Hawker, J. Sarkis, and K. Yamazaki, "SCOUT: A simple quadruped that walks, climbs and runs," in *Proceedings of the IEEE International Conference on Robotics and Automation*, 1998, vol. 1-4, pp. 1707–1712.

[15] A. Saunders, D. I. Goldman, R. J. Full, and M. Buehler, "The RiSE climbing robot: Body and leg design," in *Proceedings of the Conference on Unmanned Systems Technology VIII*, 2006, vol. 6230, p. 23017.

[16] S. Hirose, K. Yoneda, K. Arai, and T. Ibe, "Design of a quadruped walking vehicle for dynamic walking and stair climbing," *Advanced Robotics*, vol. 9, no. 2, pp. 107–124, 1995.

[17] S. Talebi, M. Buehler, and E. Papadopoulos, "Towards dynamic step climbing for a quadruped robot with compliant legs," in *Proceedings of the 3rd International Conference on Climbing and Walking Robots (CLAWAR)*, 2000, pp. 441–446.

[18] E.Z. Moore, D. Campbell, F. Grimminger, and M. Buehler, "Reliable stair climbing in the simple hexapod 'RHex'," *Proceedings of the IEEE International Conference on Robotics and Automation*, pp. 2222–2227, 2002.

[19] J. G. Nichol, S. P. N. Singh, K. J. Waldron, L. R. Palmer, and D. E. Orin, "System design of a quadrupedal galloping machine," *International Journal of Robotics Research*, vol. 23, no. 10-11, pp. 1013–1027, 2004.

[20] M.H. Raibert, "Trotting, pacing and bounding by a quadruped robot," *Journal of Biomechanics*, vol. 23, no. Suppl. 1, pp. 79–98, 1990.

[21] G. Hawker and M. Buehler, "Quadruped trotting with passive knees - design, control, and experiments," in *Proceedings of the IEEE International Conference on Robotics and Automation*, 2000, pp. 3046–3051.

[22] D. Campbell and M. Buehler, "Preliminary bounding experiments in a dynamic hexapod," in *8th International Symposium on Experimental Robotics (ISER 02)*, 2003, vol. 5, pp. 612–621.

[23] I. Poulakakis, J. A. Smith, and M. Buehler, "Modeling and experiments of untethered quadrupedal running with a bounding gait: The Scout II robot," *International Journal of Robotics Research*, vol. 24, no. 4, pp. 239–256, 2005.

[24] T. McGeer, "Passive dynamic walking," *International Journal of Robotics Research*, vol. 9, no. 2, pp. 62–82, 1990.

[25] A. Goswami, "Postural stability of biped robots and the foot-rotation indicator (FRI) point," *International Journal of Robotics Research*, vol. 18, no. 6, pp. 523–533, 1999.

[26] C. Angle, "Genghis: A six-legged autonomous walking robot," May 1989, BSc Thesis in Electrical and Computer Science, MIT.

[27] S. N. Cubero, S. Walkington, and C. Danzi, "Design of a six-legged passenger carrying hybrid walking vehicle with four-wheel-drive capability," in *Proceedings of the 2nd International Conference on Climbing and Walking Robots (CLAWAR 99)*, 1999, pp. 361–372.

[28] J. Zhu, D. Sun, and S. K. Tso, "Development of a tracked climbing robot," *Journal of Intelligent & Robotic Systems*, vol. 35, no. 4, pp. 427–444, 2002.

[29] E. Tunstel, "Evolution of autonomous self-righting behaviors for articulated nanorovers," in *Proceedings of the ISAIRAS '99: 5th International Symposium On Artificial Intelligence, Robotics And Automation In Space*, 1999, vol. 440 of *ESA Special Publications*, pp. 341–346.

[30] R. A. Mann and J. Hagy, "Biomechanics of walking, running, and sprinting," *American Journal of Sports Medicine*, vol. 8, no. 5, pp. 345–350, 1980.

[31] D. A. Winter, "Biomechanics of human movement with applications to the study of human locomotion," *CRC Critical Reviews In Biomedical Engineering*, vol. 9, no. 4, pp. 287–314, 1984.

[32] R. J. Full, K. Autumn, J. I. Chung, and A. Ahn, "Rapid negotiation of rough terrain by the death-head cockroach," *American Zoologist*, , no. 38, pp. 81, 1998.

[33] C. T. Farley, J. Glasheen, and T. A. McMahon, "Running springs - speed and animal size," *Journal of Experimental Biology*, vol. 185, pp. 71–86, 1993.

[34] M. S. Fischer and H. F. Witte, "Evolution of vertebrate locomotory systems," in *CISM Course on Walking: Biological and Technological Aspects*, F. Pfeiffer and T. Zielinska, Eds., 2004, number 467 in CISM Courses and Lectures, pp. 51–79.

[35] P. Holmes, R. J. Full, D. Koditschek, and J. Guckenheimer, "The dynamics of legged locomotion: Models, analyses and challenges," *SIAM Review*, vol. 48, no. 2, pp. 207–304, 2006.

[36] A. D. Kuo, "Choosing your steps carefully - trade-offs between economy and versatility in dynamic walking bipedal robots," *IEEE Robotics & Automation Magazine*, vol. 14, no. 2, pp. 18–29, 2007.

[37] D. Winter, "The biomechanics and motor control of human gait, 2nd ed., waterloo. automatic recognition by gait," 1991.

[38] V. T. Inman, "Human locomotion (reprinted from can med assoc j, vol 94, pg 1047, 1966)," *Clinical Orthopaedics And Related Research*, , no. 288, pp. 3–9, 1993.

[39] D. M. Wilson, "Insect walking," *Annual Review of Entomology*, vol. 11, pp. 103–&, 1966.

[40] K. Pearson, "Control of walking," *Scientific American*, vol. 235, no. 6, pp. 72–&, 1976.

[41] T. A. McMahon, "The role of compliance in mammalian running gaits," *Journal of Experimental Biology*, vol. 115, no. MAR, pp. 263–282, 1985.

[42] D. F. Hoyt and C. R. Taylor, "Gait and the energetics of locomotion in horses," *Nature*, vol. 292, no. 5820, pp. 239–240, 1981.

[43] H. Cruse, "Coordination of leg movement in walking animals," in *Proceedings of the 1st International Conference on Simulation of the Adaptive Behavior: From Animals to Animats*, 1991, pp. 105–119.

[44] S. J. Wickler, D. F. Hoyt, E. A. Cogger, and G. Myers, "The energetics of the trot-gallop transition," *Journal of Experimental Biology*, vol. 206, no. 9, pp. 1557–1564, 2003.

[45] R. Blickhan, "The spring mass model for running and hopping," *Journal of Biomechanics*, vol. 22, no. 11-12, pp. 1217–1227, 1989.

[46] T. A. McMahon, "Mechanics of locomotion," *International Journal of Robotics Research*, vol. 3, no. 2, pp. 4–28, 1984.

[47] D. P. Ferris, M. Louie, and C. T. Farley, "Running in the real world: adjusting leg stiffness for different surfaces," *Proceedings of The Royal Society of London Series B - Biological Sciences*, vol. 265, no. 1400, pp. 989–994, 1998.

[48] T. A. McMahon and G. C. Cheng, "The mechanics of running - how does stiffness couple with speed," *Journal of Biomechanics*, vol. 23, no. Suppl. 1, pp. 65–78, 1990.

[49] R. M. Alexander, "3 uses for springs in legged locomotion," *International Journal of Robotics Research*, vol. 9, no. 2, pp. 53–61, 1990.

[50] J. E. Clark and M. R. Cutkosky, "The effect of leg specialization in a biomimetic hexapedal running robot," *Journal of Dynamic Systems Measurement and Control - Transactions Of The Asme*, vol. 128, no. 1, pp. 26–35, 2006.

[51] P. G. Adamczyk, S. H. Collins, and A. D. Kuo, "The advantages of a rolling foot in human walking," *Journal of Experimental Biology*, vol. 209, no. 20, pp. 3953–3963, 2006.

[52] H. Cruse, "What mechanisms coordinate leg movement in walking arthropods," *Trends In Neurosciences*, vol. 13, no. 1, pp. 15–21, 1990.

[53] R. D. Beer, R. D. Quinn, H. J. Chiel, and R. E. Ritzmann, "Biologically inspired - what can we learn from insects?," *Communications of the ACM*, vol. 40, no. 3, pp. 31–38, 1997.

[54] K. S. Espenschied, R. D. Quinn, R. D. Beer, and H. J. Chiel, "Biologically based distributed control and local reflexes improve rough terrain locomotion in a hexapod robot," *Robotics and Autonomous Systems*, vol. 18, no. 1-2, pp. 59–64, 1996.

[55] F. Pfeiffer, J. Eltze, and H. J. Weidemann, "6-legged technical walking considering biological principles," *Robotics and Autonomous Systems*, vol. 14, no. 2-3, pp. 223–232, 1995.

[56] R. D. Quinn and R. E. Ritzmann, "Construction of a hexapod robot with cockroach kinematics benefits both robotics and biology," *Connection Science*, vol. 10, no. 3-4, pp. 239–254, 1998.

[57] C. P. Chou and B. Hannaford, "Measurement and modeling of mckibben pneumatic artificial muscles," *IEEE Transactions on Robotics And Automation*, vol. 12, no. 1, pp. 90–102, 1996.

[58] G. K. Klute, J. M. Czerniecki, and B. Hannaford, "Artificial muscles: Actuators for biorobotic systems," *International Journal of Robotics Research*, vol. 21, no. 4, pp. 295–309, 2002.

[59] D. A. Kingsley, R. D. Quinn, and R. E. Ritzmann, "A cockroach inspired robot with artificial muscles," in *Proceedings of the 2006 IEEE/RSJ International Conference on Intelligent Robots and Systems*, 2006, vol. 1-12, pp. 1837–1842.

[60] R. Niiyama, A. Nagakubo, and Y. Kuniyoshi, "Mowgli: A bipedal jumping and landing robot with an artificial musculoskeletal system," in *Proceedings of the IEEE International Conference on Robotics and Automation*, 2007, vol. 1-10, pp. 2546–2551.

[61] J. McKendry, B. Brown, E. R. Westervelt, and J. P. Schmiedeler, "Kinematic design and dynamic analysis of a planar biped robot mechanically coordinated by a single degree of freedom," in *Proceedings of the IEEE International Conference on Robotics and Automation*, 2007, pp. 1875–1880.

[62] M. Buehler, "RePaC design and control - cheap and fast autonomous runners," in *Proceedings of the 4th International Conference on Climbing and Walking Robots (CLAWAR)*, 2001, pp. 579–585.

[63] D. Papadopoulos and M. Buehler, "Stable running in a quadruped robot with compliant legs," in *Proceedings of the IEEE International Conference on Robotics and Automation*, 2000, pp. 444–449.

[64] J. A. Smith and I. Poulakakis, "Rotary gallop in the untethered quadrupedal robot Scout II," in *Proceedings of the IEEE/RSJ International Conference on Intelligent Robots and Systems*, 2004.

[65] B. G. A. Lambrecht, A. D. Horchler, and R. D. Quinn, "A small, insect-inspired robot that runs and jumps," in *Proceedings of the IEEE International Conference on Robotics and Automation*, 2005, vol. 1-4, pp. 1240–1245.

[66] F. Asano and Z. W. Luo, "The effect of semicircular feet on energy dissipation by heel-strike in dynamic biped locomotion," in *Proceedings of the IEEE International Conference on Robotics and Automation*, 2007, vol. 1-10, pp. 3976–3981.

[67] K. D. Farrell, C. Chevallereau, and E. R. Westervelt, "Energetic effects of adding springs at the passive ankles of a walking biped robot," in *Proceedings of the IEEE International Conference on Robotics and Automation*, 2007, vol. 1-10, pp. 3591–3596.

[68] M. Gunther and R. Blickhan, "Joint stiffness of the ankle and the knee in running," *Journal of Biomechanics*, vol. 35, no. 11, pp. 1459–1474, 2002.

[69] K. Autumn, M. Buehler, M. Cutkosky, R. Fearing, R. J. Full, D. Goldman, R. Groff, W. Provancher, A. A. Rizzi, U. Saranli, A. Saunders, and D. E. Koditschek, "Robotics in scansorial environments," in *Proceedings of the Conference on Unmanned Ground Vehicle Technology VII*, 2005, vol. 5804, pp. 291–302.

[70] M. DeLasa and M. Buehler, "Dynamic compliant walking of a quadruped robot preliminary experiments," in *Proceedings of the 3rd International Conference on Climbing and Walking Robots (CLAWAR 2000)*, 2000, pp. 393–398.

[71] S. Talebi, I. Poulakakis, E. Papadopoulos, and M. Buehler, "Quadruped robot running with a bounding gait," in *Proceedings of the 7th International Symposium on Experimental Robotics, 2000*, 2001, vol. 271, pp. 281–289.

[72] D. McMordie and M. Buehler, "Towards pronking with a hexapod robot," *4th International Conference on Climbing and Walking Robots*, pp. 659–666, 2001.

[73] S. M. Song and T. Y. Ye, "Gait planning for legged robots," in *Proceedings of the 11th World Congress In Mechanism And Machine Science*, 2004, vol. 1-5, pp. 1832–1837.

[74] U. Saranli, M. Buehler, and D.E. Koditschek, "Design, modeling and preliminary control of a compliant hexapod robot," in *Proceedings of the IEEE International Conference on Robotics and Automation*, 2000, vol. 3, pp. 2589–2596.

[75] K. Galloway, J.E. Clark, and D.E. Koditschek, "Design of a tunable stiffness composite leg for dynamic locomotion," 2009.

[76] J. Jun and J.E. Clark, "Dynamic stability of variable stiffness running," in *Proceedings of the IEEE International Conference on Robotics and Automation*, 2009.

[77] H. M. Herr and T. A. McMahon, "A galloping horse model," *International Journal of Robotics Research*, vol. 20, no. 1, pp. 26–37, 2001.

[78] E. P. Hanavan, "A mathematical model of the human body," in *Behavioral Sciences Laboratory, Wright-Paterson Air Force*, 1964, pp. 64–102.

[79] C. L. Vaughan, B. L. Davis, and J. C. O' Connor, *Dynamics of Human Gait*, Kiboho Publishers, 1992.

[80] R. J. Full and D. E. Koditschek, "Templates and anchors: Neuromechanical hypotheses of legged locomotion on land," *Journal of Experimental Biology*, vol. 202, no. 23, pp. 3325–3332, 1999.

[81] R. Blickhan and R. J. Full, "Similarity in multilegged locomotion - bounding like a monopode," *Journal Of Comparative Physiology*, vol. 173, no. 5, pp. 509–517, 1993.

[82] R. M. Ghigliazza, R. Altendorfer, P. Holmes, and D. E. Koditschek, "A simply stabilized running model," *SIAM Review*, vol. 47, no. 3, pp. 519–549, 2005.

[83] H. Geyer, A. Seyfarth, and R. Blickhan, "Spring-mass running: simple approximate solution and application to gait stability," *Journal of Theoretical Biology*, vol. 232, no. 3, pp. 315–328, 2005.

[84] J. Seipel and P. Holmes, "Three-dimensional translational dynamics and stability of multi-legged runners," *International Journal of Robotics Research*, vol. 25, no. 9, pp. 889–902, 2006.

[85] M.H. Raibert and J. K. Hodgins, "Animation of dynamic legged locomotion," in *Proceedings of the Conference of the Special Interest Group on Graphics of the Association for Computer Machinery (SIGGRAPH '91)*, 1991, vol. 25, pp. 349–358.

[86] Michael McKenna and David Zeltzer, "Dynamic simulation of autonomous legged locomotion," in *Proceedings of the 17th Annual Conference on Computer Graphics and Interactive Techniques (SIGGRAPH '90)*, New York, NY, USA, 1990, pp. 29–38, ACM.

[87] R. Balasubramanian, A. A. Rizzi, and M. T. Mason, "Toward legless locomotion control," in *Proceedings of the IEEE/RSJ International Conference on Intelligent Robots and Systems*, 2006, vol. 1-12, pp. 5594–5599.

[88] J. Schmiedeler, R. Siston, and K. Waldron, "The significance of leg mass in modeling quadrupedal running gaits," in *Proceedings of the 14th Symposium on Theory and Practice of Robots and Manipulators*, 2002, number 438, pp. 481–488.

[89] U. Saranli and D. E. Koditschek, "Back flips with a hexapedal robot," in *Proceedings of the 19th IEEE International Conference on Robotics and Automation*, 2002, vol. I-IV, pp. 2209–2215.

[90] A. Greenfield, U. Saranli, and A. A. Rizzi, "Solving models of controlled dynamic planar rigid-body systems with frictional contact," *International Journal of Robotics Research*, vol. 24, no. 11, pp. 911–931, 2005.

[91] R. Altendorfer, U. Saranli, H. Komsuoglu, D. Koditschek, H. B. Brown, M. Buehler, N. Moore, D. McMordie, and R. Full, "Evidence for spring loaded inverted pendulum running in a hexapod robot," in *Proceedings of the 7th International Symposium on Experimental Robotics*, 2001, vol. 271, pp. 291–302.

[92] U. Saranli and D. E. Koditschek, "Template based control of hexapedal running," in *Proceedings of the 20th IEEE International Conference on Robotics and Automation*, 2003, vol. 1-3, pp. 1374–1379.

[93] Ege Sayginer, Tulay Akbey, Yigit Yazicioglu, and Afsar Saranli, "Task oriented kinematic analysis for a legged robot with half-circular leg morphology," in *Proceedings of the IEEE international Conference on Robotics and Automation*, 2009, pp. 1771–1776.

[94] K. C. Galloway, J. E. Clark, and D. E. Koditschek, "Design of a multi-directional variable stiffness leg for dynamic running," in *Proceedings of the ASME International Mechanical Engineering Congress and Exposition*, 2007, vol. 10, pp. 73–80.

[95] M. Ankarali, "Control of hexapedal pronking through a dynamically embedded spring loaded inverted pendulum template," M.S. thesis, Middle East Technical University, Ankara, Turkey, 2010.

[96] U. Saranli, *Dynamic Locomotion with a Hexapod Robot*, Ph.D. thesis, University of Michigan, 2002.

[97] A. Sato and M. Buehler, "A planar hopping robot with one actuator: Design, simulation and experimental results," in *Proceedings of the International Conference on Intelligent Robots and Systems*, 2004, vol. 4, pp. 3540–3545.

[98] J. E. Shigley and C. R. Mischke, *Mechanical Engineering Design*, McGraw-Hill, 5th edition, 1989.